UNITED NATIONS EDUCATIONAL, SCIENTIFIC AND CULTURAL ORGANIZATION
INTERNATIONAL CENTRE FOR THEORETICAL PHYSICS
I.C.T.P., P.O. BOX 586, 34100 TRIESTE, ITALY, CABLE: CENTRATOM TRIESTE

SMR.769 - 4

WORKSHOP ON "NON-LINEAR ELECTROMAGNETIC INTERACTIONS IN SEMICONDUCTORS"

1 - 10 AUGUST 1994

"Excitations, Responses and Backactions in Nonlinear Photo-excitation Processes of low-dimensional semiconductors"

A. SHIMIZU
Institute of Physics
University of Tokyo
3-8-1-Komaba, Meguru-Ku
Tokyo 153
JAPAN

These are preliminary lecture notes, intended only for distribution to participants

Excitations, responses, and backactions in nonlinear photo-excitation processes of low-dimensional semiconductors

Akira Shimizu

Institute of Physics, University of Tokyo

3-8-1 Komaba, Meguro-ku, Tokyo 153, Japan

Phone: Japan(81)-3-5454-6532 Fax: Japan(81)-3-3467-1281

e-mail: shmz@ASone.c.u-tokyo.ac.jp, smz@tansei.cc.u-tokyo.ac.jp

Nonlinear responses of low-dimensional semiconductors to optical fields have been attracting much attention. I will talk about some of our work in this field.

I will first discuss two-photon absorption spectra, laying emphasis on roles of quasi-low-dimensional excitons. I will show that the two-photon spectroscopy is much more sensitive probe of the dimensionality than the one-photon spectroscopy, and that dimensional crossover effect occurs when the confinement size varies across the exciton diameter. Both theory and experiment (on quantum wells and quantum wires) will be presented.

Most nonlinear optical responses, including the two-photon absorption, can be understood without quantization of electromagnetic fields. In contrast, the second topic of the lecture is a new direction of research, in which quantum nature of electromagnetic fields plays the essential role. I will show that an electron interferometer composed of quantum wires works as a quantum non-demolition photodetector, which measures the photon number without changing it. Both backaction and error of the measurement, as well as their physical origins, will be discussed.

This interesting photodetector leads us to reconsider what happens to the electromagnetic fields in nonlinear photo-excitation processes. The third topic discusses this subject by analyzing the generation of THz electric pulses through "virtual" photo-excitation of a dc-biased multiple quantum well structure. I will show that the photon frequency is subject to an extra red shift in addition to the usual self-phase modulation, whereas the photon number is conserved. The extra red shift occurs because of the coupling of the exciton system to the external circuit, and thus depends on the imppedance of the external circuit. This example reminds us that in some circumstances not only a quantum system under consideration but also "external" classical systems join in the game of determining the state of the quantum system.

Two-photon absorption in quantum-well structures near half the direct band gap

Akira Shimizu
Canon Research Center, 5-1, Morinosato-Wakamiya, Atsugi, Kanagawa 243-01, Japan
(Received 26 April 1989)

Two-photon absorption (TPA) of quantum-well structures is theoretically discussed with quasi-two-dimensional exciton effects included. The simple theory agrees with recent experimental results which show strongly anisotropic TPA spectra reflecting subband quantization. The TPA spectra in a static electric field normal to the quantum-well layers are also discussed. Substantial changes in the spectra are predicted.

Optical nonlinearities of quantum-well structures (QWS's) show a wealth of phenomena which have not been observed in bulk crystals. Most of the work, however, has been focused on the nonlinearities near the band gap.[1] Optical nonlinearities of QWS's with the photon energies close to half the band-gap energy[2,3] are interesting not only because they provide a powerful tool for the study of electronic structures but also because they may open up new applications. A pioneering experimental work has recently been performed by Tai *et al.*[3] on the two-photon absorption (TPA) spectra of GaAs/Al_x-$Ga_{1-x}As$ QWS's. They found that the TPA spectra are strongly anisotropic in QWS's reflecting the subband quantization, which is much different from the TPA spectra of bulk crystals. A part of their results can be explained by the theories of Spector[4] and Pasquarello and Quattropani.[5] However, those theories did not take account of exciton effects, while the experimental results indicate strong effects of quasi-two-dimensional (Q2D) excitons. The exciton effects have been discussed only qualitatively by Tai *et al.*[3] to explain their experimental results.

The purpose of the present paper is threefold. The first is to present a simple theory of TPA of Q2D exciton systems. The theory requires neither a complicated interaction Hamiltonian[5] nor the sum over all subband functions,[4,5] and thus is easy to apply to complicated systems. The second is to use this theory to explain the experimental results on TPA spectra of Tai *et al.*[3] Although the basic physics of our results is the same as that of their qualitative discussion, we shall give a more rigorous discussion. The third is to predict TPA spectra of QWS's in a static electric field normal to the quantum-well (QW) layers. Optical nonlinearities due to the lowest-lying $1S$ exciton have previously been discussed by the present author.[2] Here we will discuss the whole spectra of the TPA which has not been investigated previously.

First of all, we present a simple theory of TPA of Q2D exciton systems, which is based on successful theories for *bulk* crystals.[6,7] A basic formula for the two-photon transition rate W per unit time per unit volume has been given in many pieces of literature [see, e.g., Eqs. (2.1)–(2.3) of Ref. 6]. When the photon energies $\hbar\omega_1$ and $\hbar\omega_2$ are both close to half the band-gap energy E_G, and if the exciton binding energy is much smaller than E_G (as in GaAs), the energy denominator $E_\nu-\hbar\omega_j$ can be approximated by $E_G/2$, where E_ν is the energy of a many-body intermediate state (measured from the ground-state energy) and $j=1,2$. Mahan showed that resulting errors are indeed negligible.[6] Then, the summation over the intermediate states becomes trivial ($\sum|\nu\rangle\langle\nu|=1$) and we obtain (taking crystal volume $=1$)

$$W=\frac{2\pi}{\hbar}\sum_f|V_{fg}|^2S_f(\hbar\omega_1+\hbar\omega_2)\,, \tag{1}$$

$$V_{fg}\approx\frac{2e^2}{m^2c^2E_G}A_1A_2\langle f|[(\hat{\varepsilon}_1\cdot\mathbf{p})(\hat{\varepsilon}_2\cdot\mathbf{p})+(\hat{\varepsilon}_2\cdot\mathbf{p})(\hat{\varepsilon}_1\cdot\mathbf{p})]|g\rangle\,, \tag{2}$$

where $|g\rangle$ denotes the ground state, S_f is a line-shape function for a final state $|f\rangle$, m is the free-electron mass, A_j and $\hat{\varepsilon}_j$ are, respectively, the vector potential and polarization vector of ω_j photon, and $\mathbf{p}$ represents the (many-body) momentum operator. When the well thickness L_z is smaller than the three-dimensional (3D) exciton diameter, the wave function of a Q2D exciton with zero center-of-mass motion wave vector is well approximated by[1]

$$\phi_\nu^{\alpha\beta}(\mathbf{r}_e,\mathbf{r}_h)=\frac{v_0}{\sqrt{S}}\sum_{i,j}U_\nu^{\alpha\beta}(\mathbf{R}_{i\parallel}-\mathbf{R}_{j\parallel})\phi_c^\alpha(Z_i)\phi_v^{\beta*}(Z_j)\times w_c(\mathbf{r}_e-\mathbf{R}_i)w_v^*(\mathbf{r}_h-\mathbf{R}_j)\,, \tag{3}$$

where v_0 is the unit-cell volume, S is the QW area, w_c and w_v are Wannier functions of the conduction band c and the valence band v ($=$hh for the heavy hole, lh for the light hole), respectively, $\mathbf{R}_i=(\mathbf{R}_{i\parallel},Z_i)$ denotes a lattice-site vector (the z axis is taken normal to the QW layers), $\phi_b^\alpha(z)$ is the αth-subband envelope function of band b ($=c,v$), and $U_\nu^{\alpha\beta}(\mathbf{r}_e-\mathbf{r}_h)$ is the envelope function of the 2D exciton associated with subbands α (of electron) and β (of hole), with relative motion quantum number ν. For $E<E_G$, $\nu=n,m$ ($n=1,2,\ldots$, $|m|<n$), and for $E\geq E_G$, $\nu=\mathbf{k}_\parallel,m$. Analytic expressions for U_ν have been given by Shinada and Sugano.[8] Note that we define n according to recent convention, i.e., the present $n=n$ (Ref. 8) $+1$. For example, the lowest state for each pair of subbands is the $1S$ ($n=1$, $m=0$) state given by

$$U_{1S}^{\alpha\beta}=(8/\pi a_{\alpha\beta}^2)^{1/2}\exp(-2|\mathbf{r}_\parallel|/a_{\alpha\beta})\,, \tag{4}$$

where $\mathbf{r}_\parallel=\mathbf{r}_e-\mathbf{r}_h$ is the 2D relative-coordinate vector, and $a_{\alpha\beta}$ is, which for an ideal 2D system would be equal to the

3D effective Bohr radius,[8] treated here as a variational parameter.[1,2] The exciton energy $E_{1S}^{\alpha\beta}$ is also determined variationally. We shall assume that $U_\nu^{\alpha\beta}$ and $E_\nu^{\alpha\beta}$ are given by those for the 2D exciton[8] with the effective Bohr radius replaced by $a_{\alpha\beta}$ and the effective Rydberg energy replaced by $(E_G^{\alpha\beta}-E_{1S}^{\alpha\beta})/4$, respectively, where $E_G^{\alpha\beta}\equiv E_G+\varepsilon_c^\alpha+\varepsilon_v^\beta$ is the quantized band-gap energy with ε_c^α and ε_v^β being subband energies.

Let us assume the direct allowed gap as in GaAs. Inserting Eq. (3) into Eqs. (1) and (2), and considering the twofold degeneracy due to spin, one finds for $\hat{\boldsymbol{\varepsilon}}_1=\hat{\boldsymbol{\varepsilon}}_2\parallel\hat{\mathbf{z}}$ [transverse-magnetic (TM) polarization],

$$W=K\sum_v|(c|p_z|v\hat{\mathbf{z}})|^2\left(\frac{m}{\mu_z^v}\right)^2\sum_{\alpha,\beta,\nu}|P_{\alpha\beta}|^2|U_\nu^{\alpha\beta}(\mathbf{r}_\parallel=0)|^2S_\nu^{\alpha\beta}(\hbar\omega_1+\hbar\omega_2)\,, \tag{5}$$

and for $\hat{\boldsymbol{\varepsilon}}_1=\hat{\boldsymbol{\varepsilon}}_2\perp\hat{\mathbf{z}}$ [transverse-electric (TE) polarization],

$$W=K\sum_v|(c|p_x|v\hat{\mathbf{z}})|^2\left(\frac{m}{\mu_\parallel^v}\right)^2\sum_{\alpha,\beta,\nu}|I_{\alpha\beta}|^2\left|\frac{\hbar}{i}\frac{\partial}{\partial x}U_\nu^{\alpha\beta}(\mathbf{r}_\parallel)\right|^2_{\mathbf{r}_\parallel=0}S_\nu^{\alpha\beta}(\hbar\omega_1+\hbar\omega_2)\,, \tag{6}$$

where μ_z^v and $\mu_\parallel^v$ are the reduced mass (of the electron and hole of band v) for the motion along $\hat{\mathbf{z}}$ and in xy plane, respectively, and

$$K=\frac{64\pi e^4A_1^2A_2^2}{\hbar m^4c^4E_G^2(L_z+L_B)}\,, \tag{7}$$

$$(c|\mathbf{p}|v\hat{\mathbf{z}})=\frac{1}{v_0}\int_{\text{cell}}d^3\rho\,u_c^*(\rho)\frac{\hbar}{i}\nabla u_{v\hat{\mathbf{z}}}(\rho)\,, \tag{8}$$

$$I_{\alpha\beta}=\int dz\,\phi_c^{\alpha*}(z)\phi_v^\beta(z)\,, \tag{9}$$

$$P_{\alpha\beta}=\int dz\,\phi_c^{\alpha*}(z)\frac{\hbar}{i}\frac{\partial}{\partial z}\phi_v^\beta(z)\,, \tag{10}$$

where L_B is the thickness of a barrier layer (this factor comes from the QW density[2]), and u_c and $u_{v\hat{\mathbf{z}}}$ are, respectively, the cell-periodic parts of the $\mathbf{k}\to 0$ Bloch functions of the electron and hole. In general, $u_{v\mathbf{k}}$ strongly depends on the direction of $\mathbf{k}$, i.e., $u_{v\mathbf{k}}\to u_{v\hat{\mathbf{k}}}$ as $\mathbf{k}\to 0$.[9] The Q2D exciton wave function is a highly anisotropic superposition of Bloch functions as seen from Eq. (3), so that only $u_{v\hat{\mathbf{k}}}$ for $\hat{\mathbf{k}}=\hat{\mathbf{z}}$ has appeared in the above equations. We define as usual $M^2\equiv|(c|p_i|v\hat{\mathbf{k}})|^2$ averaged over $\hat{\mathbf{k}}$. The band-to-band matrix elements in Eqs. (5) and (6) are then given by[7,9] $|(c|p_z|v\hat{\mathbf{z}})|^2=q_z^vM^2$ and $|(c|p_x|v\hat{\mathbf{z}})|^2=q_x^vM^2$, respectively, where $q_z^{\text{hh}}=0$, $q_z^{\text{lh}}=2$, $q_x^{\text{hh}}=\frac{3}{2}$, and $q_x^{\text{lh}}=\frac{1}{2}$. We shall assume M^2 constant for states of interest.

Using the results of Shinada and Sugano[8] for $|U_\nu(0)|^2\propto\delta_{m,0}$ and $|U_\nu'(0)|^2\propto\delta_{|m|,1}$, we finally obtain for TM polarization,

$$W=KM^2\sum_v q_z^v\left(\frac{m}{\mu_z^v}\right)^2\sum_{\alpha,\beta}|P_{\alpha\beta}|^2\begin{cases}\sum_n[\pi a_{\alpha\beta}^2(n-\frac{1}{2})^3]^{-1}S_n^{\alpha\beta} & (\hbar\omega_1+\hbar\omega_2<E_G^{\alpha\beta})\,,\\ \mu_\parallel^v e^{\pi/\lambda_{\alpha\beta}}/[2\pi\hbar^2\cosh(\pi/\lambda_{\alpha\beta})] & (\hbar\omega_1+\hbar\omega_2\geq E_G^{\alpha\beta})\,,\end{cases} \tag{11}$$

and for TE polarization, taking account of the twofold degeneracy of $m=\pm 1$,

$$W=KM^2\sum_v q_x^v\left(\frac{m}{\mu_\parallel^v}\right)^2\sum_{\alpha,\beta}|I_{\alpha\beta}|^2\left(\frac{\hbar}{a_{\alpha\beta}}\right)^2\begin{cases}\sum_{n\geq 2}2n(n-1)/[\pi a_{\alpha\beta}^2(n-\frac{1}{2})^5]S_n^{\alpha\beta} & (\hbar\omega_1+\hbar\omega_2<E_G^{\alpha\beta})\,,\\ \mu_\parallel^v(1+\lambda_{\alpha\beta}^2/4)e^{\pi/\lambda_{\alpha\beta}}/[\pi\hbar^2\cosh(\pi/\lambda_{\alpha\beta})] & (\hbar\omega_1+\hbar\omega_2\geq E_G^{\alpha\beta})\,,\end{cases} \tag{12}$$

where for $\hbar\omega_1+\hbar\omega_2\geq E_G^{\alpha\beta}$,

$$\lambda_{\alpha\beta}\equiv[(\hbar\omega_1+\hbar\omega_2-E_G^{\alpha\beta})/(\hbar^2/2\mu_\parallel^v a_{\alpha\beta}^2)]^{1/2}\,. \tag{13}$$

Equations (11)–(13) together with Eqs. (7), (9), and (10) complete the solution.

Physical meanings of Eqs. (5) and (6) are easy to understand.[3] For a two-photon transition from $|g\rangle$ to $|f\rangle$ to occur, two changes in parity *in the polarization direction* are needed as seen from Eq. (2). One parity change occurs in Bloch functions and has appeared as the factor $(c|\mathbf{p}|v\hat{\mathbf{z}})$. For TM polarization, the other parity change can occur only in subband functions (as $P_{\alpha\beta}$), and the factor $|U_\nu(0)|^2$ just describes enhancement of the transition can occur only in subband functions (as $P_{\alpha\beta}$), and the factor $|U_\nu(0)|^2$ just describes enhancement of the transition due to electron-hole correlation in xy plane. Consequently, the selection rule is $\alpha-\beta=$odd and $m=0$. For TE polarization, on the other hand, the parity change occurs in U_ν, and the factor $|I_{\alpha\beta}|^2$ just describes overlap of the electron and hole in z direction. Consequently, the selection rule is $\alpha-\beta=$even ≈ 0 and $|m|=1$. It is worth noting that the factors $U(0)$ and $U'(0)$ in Eqs. (5) and (6) also appear in the one-phonon absorption (OPA) coefficient for direct allowed and direct forbidden cases, respectively.[8] Thus, TPA spectra for TM (TE) polarization for each subband is similar to OPA spectra for direct allowed (forbidden) transitions.

The absorption edge is of special interest. For TM polarization, the TPA edge is at $\hbar\omega_1+\hbar\omega_2=E_{1S}^{\text{lh2}}$ (energy of the $1S$ exciton associated with the first electron and the

second light-hole subbands), at which W is given by

$$W=2KM^2\left(\frac{m}{\mu_z^{lh}}\right)^2|P_{c1lh2}|^2\frac{8}{\pi a_{c1lh2}^2}S_{1S}^{c1lh2}. \quad (14)$$

For TE polarization, the absorption edge is at $\hbar\omega_1+\hbar\omega_2=E_{2P}^{c1hh1}$, and

$$W=\tfrac{3}{2}KM^2\left(\frac{m}{\mu_{\parallel}^{hh}}\right)^2|I_{c1hh1}|^2\left(\frac{\hbar}{a_{c1hh1}}\right)^2 \times\frac{8}{\pi a_{c1hh1}^2}\frac{16}{243}S_{2P}^{c1hh1}. \quad (15)$$

Considering that $P_{\alpha\beta}\sim\hbar/L_z\sim\hbar/a_{\alpha\beta}$, one finds that the latter W is much smaller in magnitude than the former W. Considering also the smaller ($\sim\frac{1}{9}$) binding energy of $n=2$ 2D excitons as compared with $n=1$ 2D excitons, which results in broadened S_{2P}, the absorption edge for TE polarization would be smeared out in usual experimental situations. This situation is essentially the same as in bulk crystals, for which no distinct peaks can be found at the TPA edge of direct allowed gap.[6,7] By contrast, for TM polarization in QWS's, a rigid peak is expected at the TPA edge.

The complete spectra for the GaAs/$Al_{0.45}Ga_{0.55}$As QWS with $L_z=120$ Å are shown in Fig. 1, where contribution from each pair of subbands is individually plotted, so that the overall W is given by the sum of these contributions. The $1S$ exciton energies and Bohr radii have been variationally determined[2] and the subband functions have been numerically evaluated.[10] We have assumed standard values at room temperature (RT) for band parameters in the z direction,[11] and in the xy plane we took $\mu_{\parallel}^{hh}=0.07m$ and $\mu_{\parallel}^{lh}=0.06m$ according to Maan *et al.*[12] As for the line-shape functions, we have assumed in the figure δ functions for S_ν of discrete levels in order to indicate each contribution clearly. In actual QWS's, S_ν is a Gaussian-like function with the full width at half maximum Γ approximately given by $\Gamma\approx\Gamma_{ph}+\Gamma_{imp}$, where Γ_{ph} is due to phonons, whereas Γ_{imp} is due to QW imperfections.[1] The Γ_{ph} is related with the exciton binding energy and the electron-phonon interactions, the latter being nearly independent of 2D quantization.[1] Our variational calculation has confirmed the conjecture of Ref. 3 that the binding energies of $1S$ excitons associated with different subbands are approximately equal in magnitude. Consequently, Γ_{ph} is also expected to be nearly equal in magnitude among the $1S$ excitons, which is ≈ 3 meV at RT and ≈ 0 at low temperature (LT).[1] On the other hand, Γ_{imp} is proportional to subband energy;[13] we expect $\Gamma_{imp}\approx 12$ meV for the 2nd subband if $\Gamma_{imp}=3$ meV for the 1st sub-

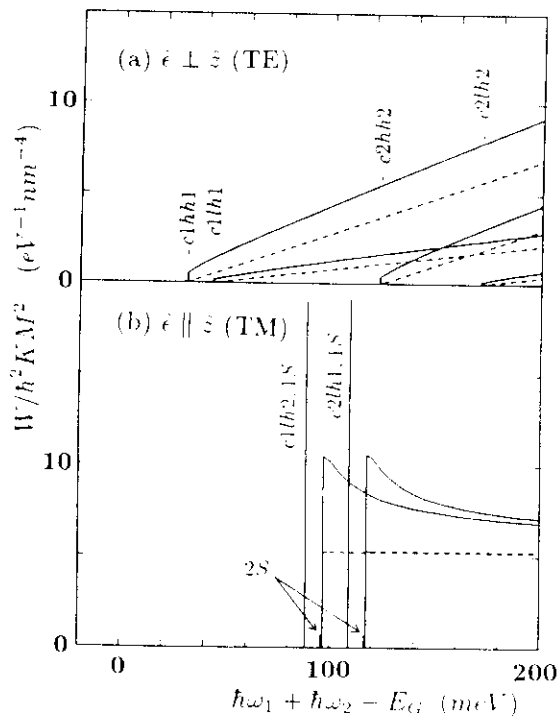

FIG. 1. TPA spectra of GaAs/Al_xGa_{1-x}As QWS ($L_z=120$ Å, $x=0.45$) (a) for TE polarization and (b) for TM polarization, with (solid curves) and without (dashed curves) exciton effects. Contribution from each pair of subbands is individually shown; e.g., the continuous spectrum the edge of which is indicated by $c1hh1$ is a contribution from the first electron and first heavy-hole subbands. The height of discrete spectra (δ functions) represents the integral height divided by 10 meV. Discrete spectra due to nP excitons for TE polarization are invisible in this scale.

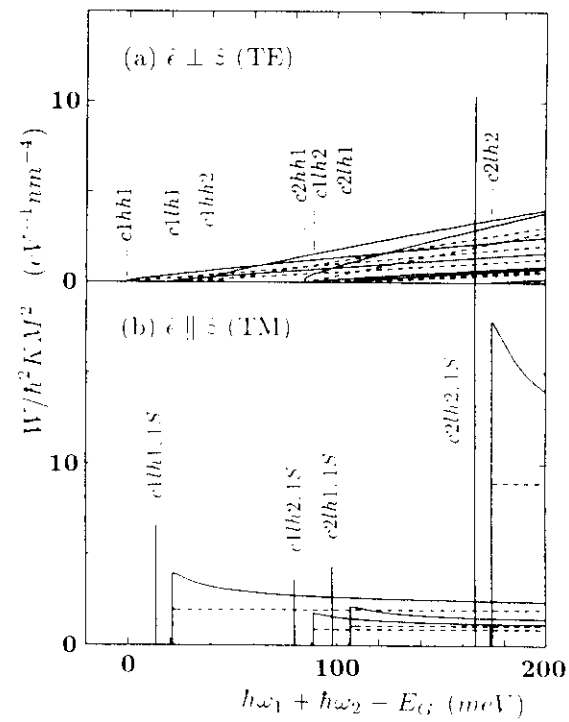

FIG. 2. TPA spectra of the same QWS as in Fig. 1 with a static electric field of 100 kV/cm applied normal to the QW layers. (a) for TE polarization and (b) for TM polarization, with (solid curves) and without (dashed curves) exciton effects. Contribution from each pair of subbands is individually shown. The height of discrete spectra (δ functions) represents the integral height divided by 10 meV. Continuous spectra due to the $c2hh2$ subbands for TE polarization are invisible in this scale at this particular field strength.

band. Therefore, for TM polarization, we expect 4 times (at LT) or 2–3 times (at RT) larger Γ for the TPA edge exciton (c1lh2, 1S) than Γ for the OPA edge exciton (c1lh1, 1S).

Another important effect of scatterings by phonons and QW imperfections is that it would destroy exciton correlation between an electron and a hole for excitons with large spatial extension of $U_\nu^{\alpha\beta}$. For continuum states (i.e., $E \geq E_G^{\alpha\beta}$), in particular, the spatial extension is large, so that the correlation seems to be destroyed for the QW samples used in Ref. 3. In that case, enhancement of W due to exciton effects disappear, and the resulting W is given by Eqs. (11) and (12) with $a_{\alpha\beta} \to \infty$, which correspond to the results of Ref. 5.[14] The results are plotted in Fig. 1 by dashed lines. These dashed lines together with discrete spectra agree with experiment.[3,15] For QWS's with better sample quality, or for QWS's of semiconductors with smaller Bohr radius, we do expect excitonic enhancement for continuum states.

Finally, we shall discuss what changes are expected in the TPA spectra if one applies a static electric field F normal to the QW layers, no experiments on which have yet been reported. Equations (1)–(13) remain valid in the presence of F. However, the selection rules for $\alpha - \beta$ are removed, since F causes parity mixing in subband functions. For example, the absorption edge for TM polarization occurs at E_{1S}^{c1lh1} at which W is given by Eq. (14) with the subband index "lh2" all replaced by "lh1". The resulting equation corresponds to a "momentum representation" of optical nonlinearities discussed in Ref. 2, in which the second- and third-order nonlinearities of this lowest-lying exciton have been discussed. The complete spectra for $F = 100$ kV/cm of the same QWS as in Fig. 1 are plotted in Fig. 2. In addition to the red shift due to the quantum-confined Stark effect,[16] substantial changes are seen. TPA peaks which are common with those in Fig. 1 become smaller because of loss in $|I_{\alpha\beta}|$ or $|P_{\alpha\beta}|$. On the other hand, TPA peaks due to excitons which were forbidden for $F = 0$ grow drastically. In particular, TPA for TM polarization due to the 1S exciton of c2lh2 becomes very strong, which is due to large P_{c2lh2} under this strong F. Considering effects of broadening, which is larger for higher subbands as discussed above, we may conclude that *actual* magnitude of TPA *just at the exciton peaks* are nearly equal between c1lh1 and c2lh2 excitons in Fig. 2(b). As for dependence of W on L_z or F, higher sensitivity on F for larger L_z can be easily speculated, as shown for the lowest exciton in Ref. 2. Quantitative discussions require detailed numerical calculations, which is beyond the scope of this short paper and thus will be described elsewhere.

The author thanks Dr. K. Tai for making his results available prior to publication. A part of numerical calculation has been performed with a computer program developed by K. Nakamura.

[1]For a review, see D. S. Chemla, D. A. B. Miller, and S. Schmitt-Rink, in *Optical Nonlinearities and Instabilities in Semiconductors*, edited by H. Haug (Academic, New York, 1988).

[2]A. Shimizu, Phys. Rev. Lett. **61**, 613 (1988); A. Shimizu and K. Nakamura, in *Proceedings of the Nineteenth International Conference on the Physics of Semiconductors, Warsaw, 1988* (Polish Academy of Sciences, Warsaw, 1988).

[3]K. Tai, A. Mysyrowicz, R. J. Fisher, R. E. Slusher, and A. Y. Cho, Phys. Rev. Lett. **62**, 1784 (1989).

[4]H. N. Spector, Phys. Rev. B **35**, 5876 (1987).

[5]A. Pasquarello and A. Quattropani, Phys. Rev. B **38**, 6206 (1988).

[6]G. D. Mahan, Phys. Rev. **170**, 825 (1968); C. C. Lee and H. Y. Fan, Phys. Rev. B **9**, 3502 (1974).

[7]Ch. Neumann, A. Nöthe, and N. O. Lipari, Phys. Rev. B **37**, 922 (1988).

[8]M. Shinada and S. Sugano, J. Phys. Soc. Jpn. **21**, 1936 (1966).

[9]M. Yamanishi and I. Suemune, Jpn. J. Appl. Phys. **23**, L35 (1984), and references therein.

[10]K. Nakamura, A. Shimizu, M. Koshiba, and K. Hayata, IEEE J. Quantum Electron. **QE-25**, 889 (1989).

[11]R. C. Miller, D. A. Kleinman, and A. C. Gossard, Phys. Rev. B **29**, 7085 (1984).

[12]J. C. Maan, G. Belle, A. Fasolino, M. Altarelli, and K. Ploog, Phys. Rev. B **30**, 2253 (1984).

[13]L. Goldstein, Y. Horikoshi, S. Tarucha, and H. Okamoto, Jpn. J. Appl. Phys. **22**, 1489 (1983).

[14]Note that we have achieved similar results as in Ref. 5, using, on the contrary to Ref. 5, the usual form of interaction $A \cdot p$. This is because we have performed (after the approximation for energy denominators) the complete (i.e., model-independent) summation over intermediate states to get Eq. (2).

[15]To get better agreement with the experiment, we have to take account of the energy dependence of $\mu_{\parallel}$ and M^2.

[16]See, e.g., D. A. B. Miller, J. S. Weiner, and D. S. Chemla, IEEE J. Quantum Electron. **QE-22**, 1816 (1986).

Two-photon absorption spectra of quasi-low-dimensional exciton systems

Akira Shimizu*
Quantum Wave Project, ERATO, JRDC, Keyaki-house 302, 4-3-24 Komaba, Meguro-ku, Tokyo 153, Japan

Tetsuo Ogawa
NTT Basic Research Laboratories, 3-9-11 Midori-cho, Musashino-shi, Tokyo 180, Japan

Hiroyuki Sakaki
Institute for Industrial Science, The University of Tokyo, Roppongi, Tokyo 106, Japan
(Received 27 December 1991)

We present a unified theory for two-photon absorption (TPA) spectra of Wannier excitons in a low-dimensional semiconductor of an arbitrary dimension $d=0$, 1, 2, and 3. It is found that the spectra strongly reflect the anisotropies of *both* the band structure *and* the quasi-d-dimensional exciton envelope functions. Therefore the low dimensionality can be sensitively detected by the TPA spectroscopy. This is in striking contrast to the one-photon absorption spectra, anisotropies of which cannot be taken as evidence of quantum confinements.

Stimulated by recent progresses in fabrication techniques of quasi-one-dimensional (Q1D) and quasi-zero-dimensional (Q0D) semiconductors, low-dimensional confinement effects of excitons have been attracting much attention. The confinement had been believed to be detected in experiments as optical anisotropies and/or blueshifts of one-photon absorption (OPA) spectra. However, Bauer and Sakaki[1] showed recently that these cannot be a proof of the confinement. Therefore another probe is being searched for to confirm experimentally the low dimensionality.

In this Brief Report, we develop a unified theory for two-photon absorption (TPA) spectra of semiconductors of an *arbitrary* dimension d ($=0,1,2,3$), while previous work discussed either 3D (bulk) (Ref. 2) or Q2D (Refs. 3–8) systems. The shape and anisotropies of the TPA spectra are found to depend drastically on d. Hence the dimensionality can be probed directly by TPA spectroscopy[9] with the help of the present unified theory.

Consider an undoped quasi-d-dimensional (QdD) semiconductor (or insulator), which consists of a d-dimensional well region surrounded by barrier regions. We take the x_ξ ($\xi=1,2,\ldots,d$) axes along the unconfined directions (denoted by the subscript $\|$), for which a normalization length is $L_\|$, and the x_ζ ($\zeta=d+1,d+2,\ldots,3$) axes along the confined directions (denoted by $\perp$), for which the well width is $L_\perp$. Accordingly, a position vector $\mathbf{r}$ is decomposed as $\mathbf{r}=(\mathbf{r}_\|,\mathbf{r}_\perp)=(\{x_\xi\},\{x_\zeta\})$. We assume a semiconductor with a one-photon-allowed direct band gap at the Γ point, which consists of a single conduction (c) band and one (the nondegenerate case) or two (the degenerate case) valence (v) band(s). In the degenerate case, the $(3-d)$-dimensional confinement lifts the degeneracy, and modified heavy-hole (hh) and light-hole (lh) bands are formed, so that the v-band parameters become anisotropic and d dependent. By contrast, in the nondegenerate case, they are isotropic (if isotropic for $d=3$) and d independent. Since we are most interested in QdD-exciton effects on the TPA spectra (rather than effects of bulk excitons confined in a QdD system), we assume that the lattice constant $< L_\perp <$ the exciton Bohr radius. In this case each QdD exciton can be assigned to a pair of c and v subbands, labeled by $\alpha\equiv\{\alpha_\zeta\}$ and $\beta\equiv\{\beta_\zeta\}$, respectively. The exciton envelope function for zero center-of-mass-motion wave number may be written as[5]

$$L_\|^{-d/2}U_\nu^{\alpha\beta}(\mathbf{r}_{e\|}-\mathbf{r}_{h\|})\phi_\alpha(\mathbf{r}_{e\perp})\phi_\beta^*(\mathbf{r}_{h\perp}) , \tag{1}$$

where $U_\nu^{\alpha\beta}$ represents the d-dimensional electron-hole (e-h) relative motion along the unconfined directions, which is specified by a quantum number(s) ν, and ϕ_α (ϕ_β) denotes a subband envelope function in the conduction (valence) band. The exciton has discrete spectra (bound states) when its energy $E_\nu^{\alpha\beta}<E_G(\alpha;\beta)$ and has a continuous spectra (unbound states) when $E_\nu^{\alpha\beta}\geq E_G(\alpha;\beta)$, where $E_G(\alpha;\beta)\equiv E_G+\varepsilon_\alpha+\varepsilon_\beta$ is the quantized band-gap energy, with ε_α (ε_β) the subband quantization energy of the c (v) band and E_G the bulk band-gap energy. Because of the finiteness of the spatial extensions of ϕ_α and ϕ_β, the $U_\nu^{\alpha\beta}$ deviates from those of the pure d-dimensional excitons when $d\leq 2$.[10,11] For $d=2$ we take account of the deviation by replacing the Bohr radius in the analytic form[12] of $U_\nu^{\alpha\beta}$ with a variationally determined value.[5] For $d=1$ we employ an analytic solution,[11] assuming a regularized e-h interaction. In both cases we here define "the principal quantum number" n as starting from 1, whereas n in Refs. 11 and 12 starts from 0. For $d=0$, $U_\nu^{\alpha\beta}=1$ because excitonic effects are weak under our assumption of small $L_\perp$.

Suppose that many identical QdD systems are arranged with a period of $L\equiv L_\perp+L_B$, where L_B is the barrier thickness, to constitute a $(3-d)$-dimensional array. We calculate the TPA rate $W_{\rm TPA}^{(d)}$ per unit time per unit volume of this array, as well as the OPA rate $W_{\rm OPA}^{(d)}$ for comparison. For an incident light beam of photon energy $\hbar\omega$, polarization vector $\hat{\boldsymbol{\epsilon}}$ and vector-potential amplitude A, the OPA rate is easily calculated as

$$W_{\mathrm{OPA}}^{(d)}=\frac{4\pi e^2|A|^2}{\hbar m_0^2 c^2 L^{3-d}}\sum_{v=\mathrm{hh,lh}}|(c|\hat{\epsilon}\cdot\mathbf{p}|v)_\perp|^2\sum_{\alpha,\beta}|\langle\phi_\alpha|\phi_\beta\rangle|^2\sum_\nu|U_\nu^{\alpha\beta}(\mathbf{r}_\parallel=0)|^2 S_\nu^{\alpha\beta}(\hbar\omega)\ , \tag{2}$$

where m_0 denotes the free-electron mass, $S_\nu^{\alpha\beta}$ a line-shape function of the $\alpha\beta\nu$ exciton, $(c|\hat{\epsilon}\cdot\mathbf{p}|v)_\perp$ the interband matrix element, with $\mathbf{p}$ the momentum operator, and $|v)_\perp$ is the Bloch function of the valence band when $\mathbf{k}$ approaches zero along the confinement directions.[5,13] Note that $\hat{\epsilon}$ dependence of $W_{\mathrm{OPA}}^{(d)}$ arises only from the interband matrix element. Therefore *anisotropies in the OPA spectra cannot be evidence of the low dimensionality.*

To calculate the TPA rate, we employ the same method as the previous theory for Q2D systems,[5] which agreed with experiment.[6] This method is valid when the photon energies $\hbar\omega_1$ and $\hbar\omega_2$ of incident light beams are both close to $\frac{1}{2}E_G$ and when the exciton binding energy is much smaller than E_G (as in GaAs).[2,5] For the incident light beams of vector-potential amplitudes A_1 and A_2, with a common polarization vector $\hat{\epsilon}$, we find the following general formulas for the TPA rate.

When $\hat{\epsilon}\|\hat{\mathbf{x}}_\zeta$ (a confined direction),

$$W_{\mathrm{TPA}}^{(d)}(\hat{\epsilon}\|\hat{\mathbf{x}}_\zeta)=\frac{64\pi\hbar e^4|A_1A_2|^2}{m_0^2c^4E_G^2}\sum_{v=\mathrm{hh,lh}}\frac{|(c|p_\zeta|v)_\perp|^2}{\mu_{v\perp}^2}G_v^{(d)}(\hat{\epsilon}\|\hat{\mathbf{x}}_\zeta)\ , \tag{3}$$

where $\mu_{v\perp}$ is the electron-hole reduced mass for the motion along the confined directions, p_ζ the $\hat{\mathbf{x}}_\zeta$ element of the momentum operator, and

$$G_v^{(d)}(\hat{\epsilon}\|\hat{\mathbf{x}}_\zeta)\equiv L^{d-3}\sum_{\alpha,\beta}\left|\left\langle\phi_\alpha\left|\frac{\partial}{\partial x_\zeta}\right|\phi_\beta\right\rangle\right|^2\sum_\nu|U_\nu^{\alpha\beta}(\mathbf{r}_\parallel=\mathbf{0})|^2S_\nu^{\alpha\beta}(\hbar\omega_1+\hbar\omega_2)\ . \tag{4}$$

Here the factor L^{d-3} comes from the density of the QdD systems, $(L_\perp/L)^{3-d}$, and the summation over ν can be performed for continuous states using the joint density of states. When penetration of the wave function into the barrier regions is small, ϕ_α and ϕ_β take decoupled forms such as $\phi_\alpha(\mathbf{r}_\perp)\simeq\prod_\zeta\phi_{\alpha_\zeta}(x_\zeta)$, where ϕ_{α_ζ}'s denote the subband envelope functions along the x_ζ axis. We then find the subband selection rules:

$$\alpha_\zeta-\beta_\zeta=\text{odd} \quad \text{for the polarization direction}\ , \tag{5a}$$

$$\alpha_{\zeta'}-\beta_{\zeta'}=\text{even}\simeq 0 \quad \text{for the other directions}\ . \tag{5b}$$

On the other hand, when $\hat{\epsilon}\|\hat{\mathbf{x}}_\xi$ (an unconfined direction),

$$W_{\mathrm{TPA}}^{(d)}(\hat{\epsilon}\|\hat{\mathbf{x}}_\xi)=\frac{64\pi\hbar e^4|A_1A_2|^2}{m_0^2c^4E_G^2}\sum_{v=\mathrm{hh,lh}}\frac{|(c|p_\xi|v)_\perp|^2}{\mu_{v\parallel}^2}G_v^{(d)}(\hat{\epsilon}\|\hat{\mathbf{x}}_\xi)\ , \tag{6}$$

where $\mu_{v\parallel}$ is the electron-hole reduced mass for the motion along the unconfined directions, p_ξ the $\hat{\mathbf{x}}_\xi$ element of the momentum operator, and

$$G_v^{(d)}(\hat{\epsilon}\|\hat{\mathbf{x}}_\xi)\equiv L^{d-3}\sum_{\alpha,\beta}|\langle\phi_\alpha|\phi_\beta\rangle|^2\sum_\nu\left|\frac{\partial}{\partial x_\xi}U_\nu^{\alpha\beta}(\mathbf{r}_\perp)\right|^2_{\mathbf{r}_\perp=0}S_\nu^{\alpha\beta}(\hbar\omega_1+\hbar\omega_2)\ . \tag{7}$$

The subband selection rule in this case becomes the same as Eq. (5b). We can also obtain the formula for the TPA rate *in the absence of excitonic effects* by making the substitution $U_\nu^{\alpha\beta}(\mathbf{r}_\perp)\to L_\perp^{-d/2}e^{i\mathbf{k}_\perp\cdot\mathbf{r}_\perp}$ in the above equations.

There appeared two factors in the summations in Eqs. (3) and (6): (i) $G_v^{(d)}(\hat{\epsilon})$, which may be called the "envelope-function part" because it is determined by the envelope functions only, and (ii) "the band part," which consists of the interband matrix element and the reduced mass. The TPA rate is found to depend strongly on the light-polarization direction through (i) the envelope-function part, which reflects strong anisotropies of the QdD-exciton envelope functions, and (ii), in the degenerate case, the band part. This is in striking contrast to the OPA rate [Eq. (2)], for which polarization dependence comes only from the interband matrix element. Even if the band structure is isotropic, the TPA spectra for $d=1$ and 2 exhibit drastic dependence on the light polarization through $G_v^{(d)}(\hat{\epsilon})$, unlike the OPA spectra. We will demonstrate this fact by plotting $G_v^{(d)}(\hat{\epsilon})$ below.

To do this we must specify a few band parameters such as effective masses, which themselves are functions of d for the degenerate case. However, to see the most fundamental features coming from the $G_v^{(d)}$ part, it is convenient to assume common band parameters for any d. (This is, of course, a good approximation for the nondegenerate case.) We here employ typical band parameters of the c and lh bands of a $GaAs/Al_{0.45}Ga_{0.55}As$ quantum well. For example,[4] we take $\mu_{\mathrm{lh}\parallel}=0.06m_0$ for any d. We also assume $L_\perp=L_B=90$ Å. Actual TPA spectra of a QdD structure can be obtained from our general formula once the band structure is known from, say, measurements of the OPA spectra. Note that in the degenerate case the actual spectra will be more complicated because of (i) modifications of the values of $G_v^{(d)}$ caused by the d dependence of the above band parameters, (ii) anisotropies and d dependences of the band part, and (iii) additional contributions from the hh band. For example, the c-lh interband matrix element for $\hat{\epsilon}\|\hat{\mathbf{x}}_\zeta$ is generally a few times larger than that for $\hat{\epsilon}\|\hat{\mathbf{x}}_\xi$,[5,10,13] so that the relative TPA

intensity for $\hat{\epsilon}\|\hat{\mathbf{x}}_\zeta$ will be a few times stronger than expected from the following figures. Keeping these things in mind, let us separately discuss characteristic features of the TPA spectra as a function of d.

(a) Three-dimensional case. When $d=3$ there is no "confinement direction," so that Eqs. (6) and (8) should be used for any polarization direction. Hence, if the bulk band structure is isotropic around the Γ point, the TPA spectra are also isotropic.[2] The $G_v^{(3)}$ in this case is shown in Fig. 1(a). Energies and lengths are, respectively, measured in units of an effective Rydberg energy $R_{\mathrm{lh}\|}\equiv\mu_{\mathrm{lh}\|}e^4/2\hbar^2\epsilon^2=5.2$ meV and an effective Bohr radius $a_{\mathrm{lh}\|}\equiv\epsilon\hbar^2/\mu_{\mathrm{lh}\|}e^2=110$ Å, where ϵ is a dielectric constant. The lowest absorption peak is the $2P$ exciton, whose oscillator strength is much smaller than those of the $n=1$ excitons observed for $d=1,2$.

(b) Quasi-zero-dimensional case. In the opposite case, $d=0$, an e-h pair is confined in all directions, so that Eqs. (3) and (4) should be used for any polarization direction, where the factor $\sum_\nu|U_\nu^{\alpha\beta}|^2$ should be dropped because excitonic effects are negligible as compared with strong effects of subband quantization (recall that we assume small $L_\perp$). The TPA spectra consist of discrete lines, each corresponding to a pair of subbands which satisfy the selection rules of Eq. (5), as shown in Fig. 1(b), where $G_v^{(0)}$ of a multiple-quantum-box structure is plotted. Note first that the vertical scale of this figure is expanded as compared with Fig. 1(a). This reflects the fact that the TPA intensity is as a whole weakened with lowering d, as seen more clearly from the plots of the $d=1$ and 2 cases discussed below, because the density of the well regions is decreased. The well density for the case of Fig. 1(b) is $(L_\perp/L)^3=\frac{1}{8}$, which results in an order-of-magnitude reduction. Nevertheless, it is seen that the TPA intensity at the lowest peak is much stronger than that at the lowest exciton peak in Fig. 1(a) of the bulk crystal.

(c) Quasi-two-dimensional case. When $d=2$ our general formulas reduce to those given in Ref. 5, as it should be, and the TPA spectra strongly depend on the polarization direction $\hat{\epsilon}$. For $\hat{\epsilon}\|\hat{\mathbf{x}}_\xi$ (an unconfined direction), the subband selection rule is Eq. (5b),[4-6] and the derivative of $U_\nu^{\alpha\beta}$ in Eq. (7) is nonzero only for $m=\pm1$ excitons (so-called P series),[5,6,12] as shown in Fig. 2(a). On the other hand, for $\hat{\epsilon}\|\hat{\mathbf{x}}_\zeta$ (the confined direction), the subband selection rule becomes Eq. (5a),[4-6] and $U_\nu^{\alpha\beta}$ in Eq. (4) is nonzero only for $m=0$ excitons (S series),[5,6,12] as plotted in Fig. 2(b). Note that the lowest exciton peak for $\hat{\epsilon}\|\hat{\mathbf{x}}_\zeta$ is much stronger than that of the bulk crystal, despite the decreased well density mentioned above.

(d) Quasi-one-dimensional case. These features become

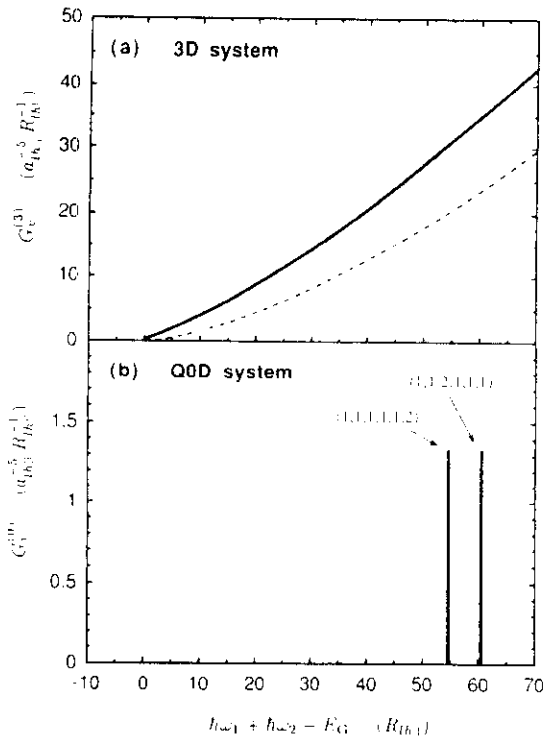

FIG. 1. Envelope-function part $G_v^{(d)}$ is plotted as a function of the sum of photon energies of incident light beams (a) for a bulk crystal and (b) for a multiple-quantum-box structure. The horizontal axis is scaled by the effective Rydberg energy R_{lh}. The vertical lines represent the discrete spectra, the height of which indicates the integrated TPA intensity divided by R_{lh}. In (b) each discrete line is assigned by $\{\alpha_\zeta;\beta_\zeta\}$, where $\{\alpha_\zeta\}$ and $\{\beta_\zeta\}$ denote the subband indices of the c and v bands, respectively. In this assignment $\hat{\epsilon}\|\hat{\mathbf{z}}$ is assumed. The dashed line in (a) represents $G_v^{(3)}$ in the absence of exciton effects.

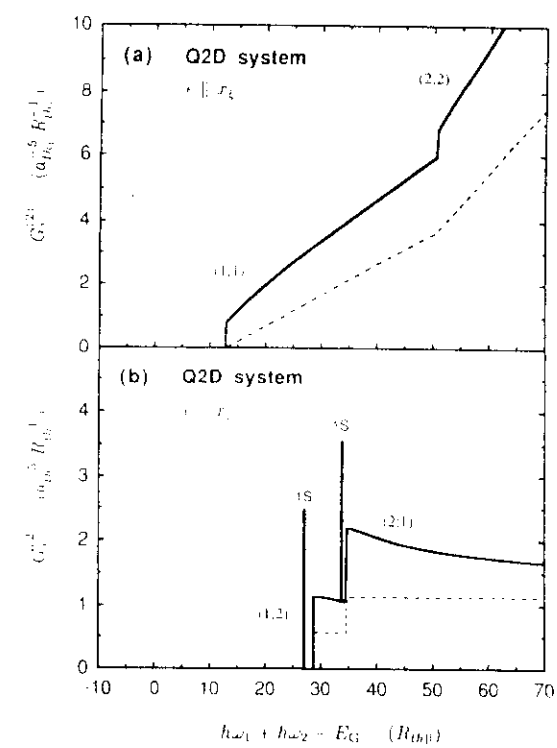

FIG. 2. Envelope-function part $G_v^{(2)}(\hat{\epsilon})$ of a multiple-quantum-well structure, for the light polarization $\hat{\epsilon}$ parallel to (a) an unconfined direction and (b) the confined direction. In (a) $2P$ exciton peaks are invisible in this scale, and quasicontinuous spectra just below the continuous ones are not shown. Origins of the TPA are shown by the subband indices $(\alpha;\beta)$ and the exciton quantum numbers n,m. The Q2D Bohr radius $a_\nu^{\alpha\beta}$ has been variationally determined for the $1S$ states for each subband pair, and $a_\nu^{\alpha\beta}\sim a_{1S}^{\alpha\beta}$ has been assumed for $\nu\neq1S$. The dashed lines represent $G_v^{(2)}$ in the absence of exciton effects.

more drastic when $d=1$ because the exciton binding energies become larger. For $\hat{\epsilon}\|\hat{\mathbf{x}}_\xi$ (the unconfined direction), the subband selection rule is Eq. (5b), and the derivative of $U_\nu^{\alpha\beta}$ in Eq. (7) was given in Ref. 11, which is nonzero only for odd-parity excitons. The $G_\nu^{(1)}(\hat{\epsilon}\|\hat{\mathbf{x}}_\xi)$ of a multiple-quantum-wire structure is plotted in Fig. 3(a). Here we have taken $z_0=0.12a_{\mathrm{1h}\|}$ for the value of the cutoff parameter, in accordance with $L_\perp=90$ Å.[11] On the other hand, for $\hat{\epsilon}\|\hat{\mathbf{x}}_\zeta$ (a confined direction), the subband selection rules become Eqs. (5a) and (5b), and $U_\nu^{\alpha\beta}$ in Eq. (4) was given in Ref. 11, which is nonzero only for even-parity excitons. The $G_\nu^{(1)}(\hat{\epsilon}\|\hat{\mathbf{x}}_\zeta)$ in this case is plotted in Fig. 3(b). Comparing these figures with Figs. 1(a) and 2, we see that the relative magnitude of the discrete spectra to the continuous spectra becomes larger for $d=1$. This is due to increased oscillator strengths for discrete states in Q1D systems.[11] In particular, a strong exciton peak can be observed even for $\hat{\epsilon}\|\hat{\mathbf{x}}_\xi$, in contrast to the cases of $d\geq 2$. If we look at the continuous spectra, it is interesting that exciton effects *enhance* the TPA for $\hat{\epsilon}\|\hat{\mathbf{x}}_\xi$ (the unconfined direction), whereas they *reduce* the TPA for $\hat{\epsilon}\|\hat{\mathbf{x}}_\zeta$ (a confined direction). By contrast, the TPA is always enhanced by exciton effects for $d\geq 2$ [see Figs. 1(a) and 2 and Refs. 2 and 5]. The reduction of the continuous TPA spectra of a direct-allowed-gap (two-photon-forbidden) quantum wire by exciton effects has the same origin as the reduction of the OPA of a direct-allowed-gap quantum wire, that is, an anomalously strong concentration of the oscillator strength on the lowest exciton state.[11] The enhancement, on the other hand, has the same origin as that of OPA of a direct-forbidden-gap quantum wire; an envelope function of the lowest odd-parity exciton has a large slope at $\mathbf{r}_\|=0$ because the *e-h* Coulomb attraction becomes more effective for $d=1$. In the case of the TPA of Q1D systems, one can observe *both* the reduction (for $\hat{\epsilon}\|\hat{\mathbf{x}}_\xi$) and enhancement (for $\hat{\epsilon}\|\hat{\mathbf{x}}_\zeta$) in the same sample simply by rotating the polarization direction.

We finally note that the strong TPA intensities at the lowest peaks in Figs. 1(b), 2(b), 3(a), and 3(b) indicate strong dispersions of the optical Kerr coefficient, which suggests possible applications to ultrafast nonlinear devices.[5,8]

In conclusion, we have developed a unified theory for TPA spectra of Wannier excitons in a low-dimensional semiconductor of an arbitrary dimension $d=0,1,2,3$. The spectra strongly reflect the anisotropies of *both* the band structure *and* the Q*d*D exciton envelopes. The TPA spectra give us a proof of the low-dimensional confinement of the electronic and excitonic states, which information cannot be obtained from the OPA spectra.

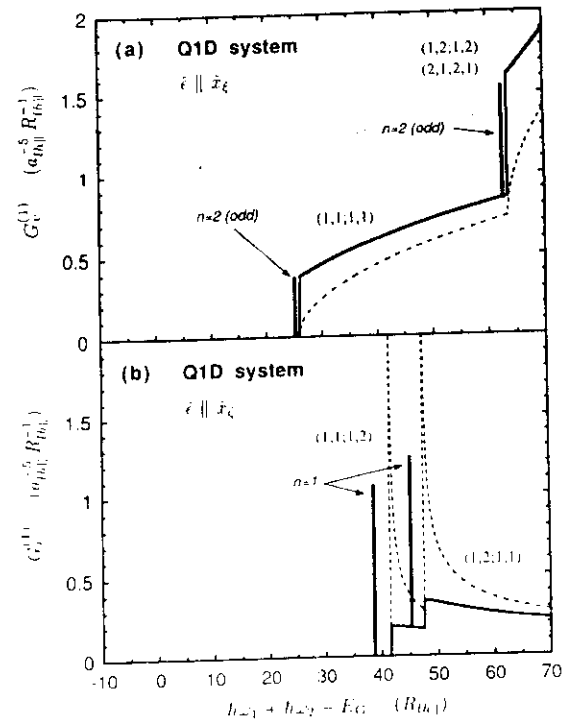

FIG. 3. Envelope-function part $G_\nu^{(1)}(\hat{\epsilon})$ of a multiple-quantum-wire structure, for the light polarization $\hat{\epsilon}$ parallel to (a) the unconfined direction and (b) a confined direction. In (b) discrete absorption lines due to the $n=2$ even excitons are invisible and quasicontinuous spectra just below the continuous ones are not shown. Origins of the TPA are shown by the subband indices $(\{\alpha_\zeta\};\{\beta_\zeta\})$ and the exciton quantum number n and parity. In (b) $\hat{\epsilon}\|\hat{\mathbf{z}}$ is assumed in this assignment. The dashed lines represent $G_\nu^{(1)}$ in the absence of exciton effects.

The authors thank T. Takagahara and H. Kanbe for discussions and K. Nakamura for supporting numerical computations.

*Present address: Institute of Physics, College of Arts and Sciences, The University of Tokyo, Komaba, Meguro-ku, Tokyo 153, Japan.

[1]G. E. W. Bauer and H. Sakaki, Surf. Sci. (to be published).
[2]G. D. Mahan, Phys. Rev. **170**, 825 (1968); C. C. Lee and H. Y. Fan, Phys. Rev. B **9**, 3502 (1974).
[3]D. Fröhlich, R. Wille, W. Schlapp, and G. Weimann, Phys. Rev. Lett. **61**, 1878 (1988); W. H. Knox, D. S. Chemla, D. A. B. Miller, J. B. Stark, and S. Schmitt-Rink, *ibid.* **62**, 1189 (1989).
[4]H. N. Spector, Phys. Rev. B **35**, 5876 (1987); A. Pasquarello and A. Quattropani, *ibid.* **38**, 6206 (1988).
[5]A. Shimizu, Phys. Rev. B **40**, 1403 (1989).
[6]K. Tai, A. Mysyrowicz, R. J. Fisher, R. E. Slusher, and A. Y. Cho, Phys. Rev. Lett. **62**, 1784 (1989); I. M. Catalano, A. Cingolani, R. Cingolani, M. Lepore, and K. Ploog, Phys. Rev. B **40**, 1312 (1989); Solid State Commun. **71**, 217 (1989).
[7]M. Nithisoontorn, K. Unterrainer, S. Michaelis, N. Sawaki, E. Gornik, and H. Kano, Phys. Rev. Lett. **62**, 3078 (1989).
[8]K. Fujii, A. Shimizu, J. Bergquist, and T. Sawada, Phys. Rev. Lett. **65**, 1808 (1990).
[9]Also, the exciton binding energy, band offset, and subband structures can be obtained from the TPA spectroscopy, as demonstrated in Ref. 6.
[10]D. A. B. Miller, J. S. Weiner, and D. S. Chemla, IEEE J. Quantum Electron. **QE-22**, 1816 (1986).
[11]T. Ogawa and T. Takagahara, Phys. Rev. B **43**, 14 325 (1991); **44**, 8138 (1991).
[12]M. Shinada and S. Sugano, J. Phys. Soc. Jpn. **21**, 1936 (1966).
[13]Y. Yamanishi and I. Suemune, Jpn. J. Appl. Phys. **23**, L35 (1984).

Dimensional crossover of excitons in one- and two-photon absorption processes

Tetsuo Ogawa
NTT Basic Research Laboratories, Midori-cho, Musashino-shi, Tokyo 180, Japan

Akira Shimizu
Institute of Physics, University of Tokyo, Komaba, Meguro-ku, Tokyo 153, Japan
(Received 10 March 1993)

We develop a theory of one- and two-photon absorptions (OPA and TPA) of Wannier excitons in the *intermediate regime*, where the dimensionality of the excitons is intermediate between one and two. We find that the TPA spectrum changes drastically with variations in the dimensionality, whereas the OPA spectrum keeps its qualitative nature. The theory explains the puzzling results of a recent experiment on the TPA spectrum of a quantum wire [R. Cingolani *et al.*, Phys. Rev. Lett. **69**, 1276 (1992)].

Following the many intensive studies on quasi-two-dimensional (Q2D) semiconductors (quantum wells) over the last two decades, optical properties of quasi-one-dimensional (Q1D) semiconductors (quantum wires) have recently been attracting much attention. However, most experimental work on quantum wires (QWR's) reported *linear* properties only, e.g., one-photon-absorption (OPA) spectra. Cingolani *et al.*[1] recently reported the first measurement of the two-photon-absorption (TPA) spectra, which is one of the most fundamental *nonlinear* properties[2] of a QWR. Since the experimental QWR sample was fabricated from a quantum well (QW), we shall take the z axis along the confinement direction of the QW, and the y axis along the lateral confinement direction, with the x axis being along the free motion. In the experiment,[1] the spectra were measured for two polarization directions: $\hat{\epsilon} \parallel \hat{x}$ and $\hat{\epsilon} \parallel \hat{y}$.

A theory of TPA in a QWR was first developed by Spector,[3] who neglected exciton effects. We recently developed a general theory, which is valid for semiconductors of arbitrary dimension $d = 0, 1, 2, 3$, that takes exciton effects into account.[4] Both theories predict that the TPA spectrum for $\hat{\epsilon} \parallel \hat{x}$ would be much more smeared and broadened than that for $\hat{\epsilon} \parallel \hat{y}$. However, the experiment in Ref. 1 reported puzzling results: (i) the observed TPA spectrum was indeed very anisotropic, (ii) but the strengths of the peaks were, on average, almost isotropic. This cannot be explained as the spectrum of a Q2D system either, because the spectrum of a Q2D system is isotropic in the xy plane, in contradiction to (i).

In this report we clarify the physical origin of the observed spectra. We note that the lateral width L_y of the QWR sample is several times $a_B^{(2)}$, where $a_B^{(d)}$ is the QdD-exciton Bohr radius and $a_B^{(1)} \lesssim a_B^{(2)} \lesssim a_B^{(3)}$ in general. Although this size of L_y does *not* violate the assumption of the nonexcitonic theory,[3] it *does* violate that of the excitonic theory,[4] which assumes either $L_y < a_B^{(1)}$ (Q1D regime) or $L_y \to \infty$ (Q2D regime). Hence, we here develop a theory of OPA and TPA of Wannier excitons *in the intermediate regime* ($L_y \gtrsim a_B^{(1)}$), where the dimensionality of the excitons (which we call Q1-2D excitons) is intermediate between one and two.

We first point out that although it has frequently been used in the literature, the model of Q2D excitons with a quantized center-of-mass motion (QCMM) does *not* explain the experimental results because the TPA spectrum of such excitons is almost isotropic in the xy plane, as we will show. By assuming a more realistic wave function, we will show that the TPA spectrum in the intermediate regime is very different from that for the Q1D or Q2D regime, and that it changes drastically with variations in L_y, i.e., in the dimensionality. In contrast, the OPA spectrum keeps its qualitative nature with variations in the dimensionality. Hence, besides explaining the experimental results, our theory shows that TPA spectroscopy is a much more sensitive probe of dimensionality than OPA spectroscopy.

We confine ourselves to an undoped QWR, whose well region is made of a semiconductor with a one-photon-allowed direct band gap of energy $E_{\rm gap}$. We assume, in accordance with the experiment,[1] that the photon energy $\hbar\omega \simeq \frac{1}{2}E_{\rm gap}$. The cross section of the QWR is assumed to be rectangular, $L_y \times L_z$.[5] Since we are interested in the crossover between $d = 1$ and $d = 2$, we vary L_y as a parameter, while L_z is fixed and small. That is, considering that energy is inversely proportional to the square of the length scale, we assume that

$$L_z^2 \ll L_y^2 \quad \text{and} \quad a^2 \ll L_z^2 \ll [a_B^{(2)}]^2, \tag{1}$$

where a is a lattice constant.[6] Typically, $a \simeq 5$ Å, $L_z \simeq 40$ Å, $a_B^{(2)} \simeq 100$ Å, and $L_y \gtrsim 3L_z$. In such a case, we must first diagonalize the $\mathbf{k}\cdot\mathbf{p}$ Hamiltonian taking into account the z-direction confinement. This causes the valence-band mixing, and Q2D subbands are formed. The cell-periodic part u of the Bloch functions (around the Γ point) is altered into a Q2D form, $u^{(2)}$. We then take account of the lateral (y) confinement and the exciton effect. Under condition (1), these effects cause no substantial change in u because energy separation between Q2D subbands is much larger than these perturbations (except when there is an accidental degeneracy in Q2D

valence subbands). That is, $u \simeq u^{(2)}$. On the other hand, these perturbations cause state mixing *within* each Q2D subband, or, more strictly speaking, mixing and correlation within each *pair* of Q2D conduction and valence subbands. As a result, envelope functions can be strongly altered into lower-dimensional excitonic forms. Therefore, we have a marginal situation that u's are of Q2D forms while the envelope functions are of lower-dimensional forms. This allows us to treat each pair of Q2D conduction and valence subbands *separately*, and the overall spectrum is just the sum over the pairs.

We first consider the hypothetical case in which a Q1-2D exciton is a Q2D exciton with a QCMM, which we call a Q2′D exciton. Its envelope function is

$$\Psi^{(2')}_{nmN}(\mathbf{r}_e,\mathbf{r}_h;[\alpha_z;\beta_z]) = G_N(Y)\,U^{(2)}_{nm}(x,y;[\alpha_z;\beta_z])\phi_{\alpha_z}(z_e)\,\phi_{\beta_z}(z_h), \quad (2)$$

where $\mathbf{r}_e = (x_e, y_e, z_e)$ is the position of an electron (e), $x = x_e - x_h$ is the relative coordinate of an electron and a hole (h), and $U^{(2)}_{nm}$ represents the relative motion of the Q2D exciton with two quantum numbers $n = 1, 2, \ldots$ and $m = 0, \pm 1, \ldots, \pm|n-1|$.[7–9] The QCMM is represented by a normalized function $G_N(Y)$ with a quantum number $N = 1, 2, \ldots$, where Y is the y coordinate of the center of mass. A subband envelope function in the α_zth conduction (β_zth valence) band is written as ϕ_{α_z} (ϕ_{β_z}). Since the summation over *all* intermediate states is essential to get the correct result for TPA, we perform, following Ref. 8, the complete summation by approximating off-resonant energy denominators as constant.

We find that the OPA or TPA rate, $W^{(2')}$, of a Q2′D exciton is simply given by[10]

$$W^{(2')} = \frac{1}{L_y}\left|\int G_N(Y)dY\right|^2 W^{(2)}\{2'\}, \quad (3)$$

where $W^{(2)}\{2'\}$ denotes the OPA or TPA rate obtained from $W^{(2)}$ of a Q2D exciton[8] by replacing its Q2D band parameters (effective masses and Bloch functions) with the corresponding Q2′D band parameters. We see that the selection rules are those for the Q2D excitons[8] and, additionally, $N = 1, 3, 5, \ldots$. More importantly, the polarization anisotropy in the xy plane can only come from a possible anisotropy of Q2′D effective masses (which results in an anisotropy in the Q2D envelope-function part[4]) and/or of Q2′D Bloch functions (which results in anisotropy in the interband matrix element M_{cv} in Ref. 4). However, as mentioned earlier, these Q2′D band parameters, under the condition (1), approximately equal the Q2D band parameters, which are isotropic in the xy plane. Therefore, when condition (1) is satisfied, the model of a Q2′D exciton (i.e., a Q2D exciton with a QCMM) does *not* lead to significant xy anisotropy in either the OPA or TPA spectrum. This means that the Q2′D model is wrong because strong anisotropies in the experiment[1] cannot be explained. This conclusion will also be supported below by a numerical calculation, which shows that the true exciton states significantly deviate from the Q2′D forms.

To find a more realistic wave function, we note that the QWR structure is invariant under $x \to -x$, and under $y \to -y$. This allows us to classify Q1-2D exciton states using corresponding parities, $\sigma_x = \pm 1$ and $\sigma_y = \pm 1$. We also note that the Q1D envelope function,

$$\Psi^{(1)}_{n\sigma}(\mathbf{r}_e,\mathbf{r}_h;[\alpha_y,\alpha_z;\beta_y,\beta_z]) = U^{(1)}_{n\sigma}(x;[\alpha_y,\alpha_z;\beta_y,\beta_z]) \times\phi_{\alpha_y}(y_e)\,\phi_{\beta_y}(y_h)\,\phi_{\alpha_z}(z_e)\,\phi_{\beta_z}(z_h), \quad (4)$$

also has definite parities of $\sigma_x = \sigma$ and $\sigma_y = (-1)^{\alpha_y+\beta_y}$. Here, $U^{(1)}_{n\sigma}$ represents the Q1D exciton relative motion,[11] which is specified by two quantum numbers: $n = 1, 2, \ldots$,[9] and $\sigma = \pm 1$ (even or odd), and ϕ_{α_y} and ϕ_{β_y} are the lateral-subband envelope functions. We will simply call $\{n = 1, \sigma = +1\}$ and $\{n = 2, \sigma = -1\}$ states "$1S^{(1)}$" and "$2P^{(1)}$" states, respectively. We can also arrange the Q2′D states of Eq. (2) to have definite parities $(\sigma_x\sigma_y)$, by taking a linear combination of $m = +|m|$ and $m = -|m|$ states. For example, linear combinations of $\{n = 2, m = \pm 1, N = 1\}$ states yield $\{n = 2, |m| = 1, N = 1\}$ states of $(\sigma_x\sigma_y) = (+-)$ and $(-+)$, which we will call $\{2P^{(2')}_y : N = 1\}$ and $\{2P^{(2')}_x : N = 1\}$ states, respectively. A schematic energy diagram of low-lying levels of the Q1D and Q2′D states is shown in Fig. 1, where $(\sigma_x\sigma_y)$ of each state is indicated.

We may approximate a Q1-2D envelope function of $(\sigma_x\sigma_y)$ parities by a linear combination of the Q1D and Q2D states of the same parities; that is,

$$\Psi^{(1-2)}_{\sigma_x\sigma_y} \simeq \sum{}' C^{(1)}\Psi^{(1)} + \sum{}' C^{(2')}\Psi^{(2')}, \quad (5)$$

where the sums are taken over the states of the same parities. Here, we have assumed that the band parameters can be approximated by the Q2D band parameters. This is justified under condition (1), as discussed earlier. To determine the superposition coefficients $C^{(1)}$ and $C^{(2')}$, we solve the matrix equation obtained by substituting Eq. (5) into the Schrödinger equation and taking the in-

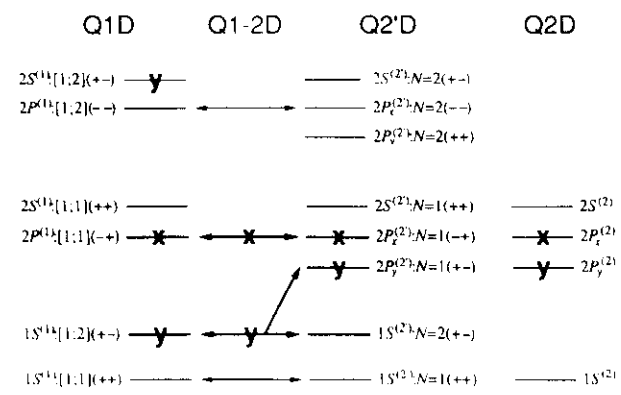

FIG. 1. Schematic level diagram of low-lying exciton states of Q1D, Q1-2D, Q2′D, and Q2D semiconductors. The z-subband indices $\alpha_z = \beta_z = 1$ are assumed and suppressed. The TPA activity is indicated by the bold letters **x** and **y**, corresponding to $\hat{\epsilon} \parallel \hat{x}$ and $\hat{\epsilon} \parallel \hat{y}$ polarizations, respectively.

ner product with each of $\Psi^{(1)}$ and $\Psi^{(2')}$. (A little care should be taken in doing this because $\Psi^{(1)}$ and $\Psi^{(2')}$ are *not* orthogonal.) Results will be given afterwards.

Using Eq. (5), the OPA and TPA rates $W^{(1-2)}$ can be evaluated in the same manner as $W^{(2')}$ [Eq. (3)]. We find that $W^{(1-2)}$ can be cast in the form

$$W^{(1-2)} \simeq \left|\sum{}' C^{(1)} w^{(1)}\{2\} + \sum{}' C^{(2')} w^{(2')}\{2\}\right|^2, \quad (6)$$

where $|w^{(1)}\{2\}|^2$ and $|w^{(2')}\{2\}|^2$ are the OPA or TPA rate of a Q1D exciton[4] and of a Q2'D exciton in Eq. (3), respectively, and in both of them, the band parameters are replaced with the Q2D band parameters.

An immediate conclusion of Eq. (6) is that the OPA spectrum of the Q1-2D excitons, under condition (1), is almost isotropic in the xy plane. This is because, in the case of OPA, $w^{(1)}_{\rm OPA}\{2\}$ and $w^{(2')}_{\rm OPA}\{2\}$ are totally isotropic (although $w^{(1)}_{\rm OPA}$ would have been slightly anisotropic if the Q1D band parameters had been used), as seen from Eq. (2) of Ref. 4 and Eq. (3). For example, at the OPA edge, both $w^{(1)}_{\rm OPA}$ and $w^{(2')}_{\rm OPA}$ exhibit a strong peak due to $\{1S^{(1)}:[1;1]\}$ and $\{1S^{(2')}:N=1\}$ components, respectively (see Fig. 1), a superposition of which will approximate the lowest Q1-2D exciton state. Since both components are isotropic in the xy plane, the Q1-2D OPA spectrum $W^{(1-2)}_{\rm OPA}$ also becomes isotropic. Moreover, we see that the OPA oscillator strength varies only slowly as a function of L_y. This is because, besides the oscillator strengths of both components varying slowly, both the strengths at the same value of L_y are of the same order of magnitude; hence the total oscillator strength becomes insensitive to the state mixing of Eq. (5). As a result, the OPA spectrum in the intermediate regime becomes similar to the Q2D spectrum, i.e., we can observe neither significant anisotropy nor sharp dependence on L_y. Therefore, the OPA spectroscopy is a poor probe of the dimensionality in this regime.[12]

The situation is very different for the TPA spectrum, which varies drastically, in both anisotropy and oscillator strength, as a function of L_y. The strong dependence of the xy anisotropy on L_y appears because, in the case of TPA, $w^{(1)}_{\rm TPA}\{2\}$ becomes strongly anisotropic (through the anisotropic envelope-function part[4]) whereas $w^{(2')}_{\rm TPA}\{2\}$ is isotropic. Therefore, the TPA spectrum becomes very anisotropic for small L_y (for which $C^{(1)}$'s become large), and almost isotropic for large L_y (where $C^{(2')}$'s become dominant).

To see this explicitly, let us examine the spectrum at the TPA edge, which is of particular interest because it is most sensitively detected by experiments. Henceforth, we assume that $\hat{\epsilon}$ is in the xy plane (in accordance with the experimental configuration[1]) and that $\alpha_z = \beta_z = 1$ (because this is the lowest z-subband pair which is responsible for the TPA spectrum for such polarization), and these z-subband indices will be suppressed.

Let us first summarize the edge spectra of the Q1D and Q2'D excitons. In the Q1D case,[4] the TPA edge spectrum for $\hat{\epsilon} \parallel \hat{x}$ is composed of $2P^{(1)}$ excitons of $[\alpha_y;\beta_y] = [1;1]$ subband pairs, whereas that for $\hat{\epsilon} \parallel \hat{y}$ is composed of $1S^{(1)}$ excitons of $[1;2]$ subband pairs. In Fig. 1 these states are indicated by the bold letters **x** and **y**, which denote that the state contributes to the TPA spectrum for $\hat{\epsilon} \parallel \hat{x}$ and for $\hat{\epsilon} \parallel \hat{y}$, respectively. In the Q2'D case—Eq. (3) with the help of Ref. 8— on the other hand, the TPA edge spectrum for $\hat{\epsilon} \parallel \hat{x}$ is composed of the $2P^{(2')}_x$ excitons of the $N = 1$ QCMM subband, whereas that for $\hat{\epsilon} \parallel \hat{y}$ is composed of $2P^{(2')}_y$ excitons of the same QCMM subband. These states, as well as the corresponding Q2D states for reference, are indicated in Fig. 1 by **x** or **y**.

We now turn to the Q1-2D spectrum, which is our main interest. We note that a hybridization of Eq. (5) occurs between states with similar energies. Hence, to a first approximation, the Q1-2D excitons can be obtained by the superposition indicated by the arrows in Fig. 1. For example, the Q1-2D exciton of the lowest energy of $(\sigma_x\sigma_y) = (-+)$ parities would be a linear combination of the $\{2P^{(2')}_x : N = 1\}$ Q2'D exciton and the $\{2P^{(1)} : [1;1]\}$ Q1D exciton. Since both components have **x** activity, with oscillator strengths of similar magnitude, this state exhibits a TPA peak only for $\hat{\epsilon} \parallel \hat{x}$, whose strength varies slowly with L_y, as will be shown in Fig. 3. On the other hand, the lowest exciton of $(+-)$ parities would be a linear combination of the $\{1S^{(1)} : [1;2]\}$ exciton (with **y** activity), the $\{1S^{(2')}:N=2\}$ exciton (no activity), and the $\{2P^{(2')}_y:N=1\}$ exciton (**y** activity) (see Fig. 1). In contrast to the $(-+)$ state, this $(+-)$ state exhibits a TPA peak only for $\hat{\epsilon} \parallel \hat{y}$. As a result, the total spectrum exhibits a strong xy anisotropy (as regards the energy positions of the TPA peaks), in agreement with the experiment.[1]

To fully interpret the puzzling experimental results, we must also explain why the strengths of the observed TPA peaks are, on an average, almost isotropic. For this purpose, we performed numerical calculations, assuming

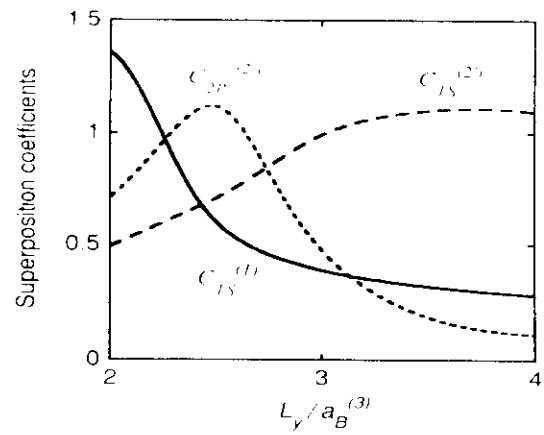

FIG. 2. The superposition coefficients for the lowest $(+-)$ state (see Fig. 1) are plotted as a function of L_y. The solid ($C^{(1)}_{1S}$), dotted ($C^{(2')}_{2P_y}$), and dashed ($C^{(2')}_{1S}$) curves represent the coefficients of the components of the $\{1S^{(1)}:[1;2]\}$, $\{2P^{(2')}_y:N=1\}$, and $\{1S^{(2')}:N=2\}$ excitons, respectively.

12

typical values of $\mu/M = 0.15$, $\mu/m_h = 0.2$, $a_B^{(2)}/a_B^{(3)} = 0.8$, and $L_z/a_B^{(3)} = 1.0$, where μ, M, and m_h denote the reduced, center of mass, and hole masses, respectively. The result for the lowest $(+-)$ exciton is shown in Figs. 2 and 3. Figure 2 clearly demonstrates that as L_y is increased (by only a factor of 2) the character of the lowest $(+-)$ state changes drastically from the $\{1S^{(1)} : [1;2]\}$ exciton (with y activity) to the $\{1S^{(2')} : N = 2\}$ exciton (no activity). As a result, the oscillator strength (Fig. 3) decreases rapidly from a large Q1D value toward zero. In particular, at $L_y/a_B^{(3)} \simeq 3$, which corresponds to the QWR sample of Ref. 1, the strength of the lowest $(+-)$ state for $\hat{\epsilon} \parallel \hat{y}$ becomes comparable to that of the lowest $(-+)$ exciton for $\hat{\epsilon} \parallel \hat{x}$, which is indicated by the dashed line in Fig. 3. Consequently, the TPA spectrum becomes almost *isotropic* in peak strength, and, as discussed above, very *anisotropic* in peak positions, in complete agreement with the experiment.[1] Figure 3 also shows that the TPA spectrum rapidly approaches a totally isotropic spectrum (in both energy positions and strengths of peaks) for larger L_y [because the $(+-)$ state loses its strength], and, for smaller L_y, a totally anisotropic spectrum [because the $(+-)$ peak becomes much stronger than the $(-+)$ peak]. Therefore, TPA spectroscopy is a much more sensitive probe of the dimensionality than OPA spectroscopy.

Although the above discussions concern quantum wires, it should be noted that similar crossover effects will also occur in quantum wells and quantum boxes when they are not small enough. Moreover, imperfections in their structures (such as wall roughness) can induce a similar effect because it causes state mixing. These effects will distort the pure QdD TPA spectrum of Refs. 4 and 8, depending on the nature of a sample, while the OPA spectrum will be almost unchanged. This may explain variations in the observed TPA spectra of QW's.[2] Lastly, we stress that our argument relies completely on the excitonic effects. In fact, if we had ignored the e-h Coulomb attraction, the length scale $a_B^{(d)}$ would not have appeared, and no qualitative change would have resulted when L_y varied.

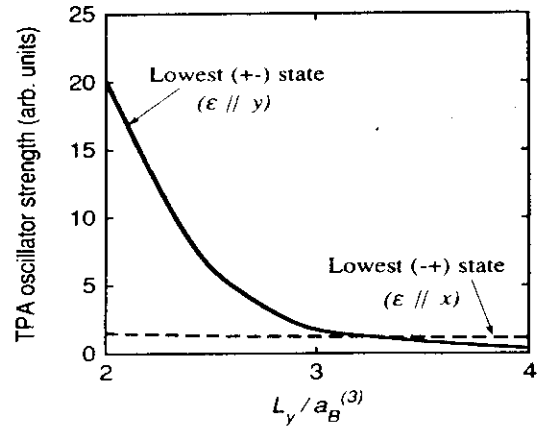

FIG. 3. The TPA oscillator strengths of the lowest $(+-)$ state for $\hat{\epsilon} \parallel \hat{y}$ and of the lowest $(-+)$ state for $\hat{\epsilon} \parallel \hat{x}$ are plotted as a function of L_y by the solid and dashed curves, respectively.

The authors thank R. Cingolani, H. Sakaki, and D. Heitmann for fruitful discussions.

[1] R. Cingolani *et al.*, Phys. Rev. Lett. **69**, 1276 (1992).

[2] Experimental work on the TPA of quantum wells for $\hbar\omega \simeq \frac{1}{2}E_{\rm gap}$ includes K. Tai *et al.*, Phys. Rev. Lett. **62**, 1784 (1989); M. Nithisoontorn *et al.*, *ibid.* **62**, 3078 (1989); K. Fujii *et al.*, *ibid.* **65**, 1808 (1990); I. M. Catalano *et al.*, Solid State Commun. **71**, 217 (1989); Phys. Rev. B **41**, 12 937 (1990).

[3] H. N. Spector, Phys. Rev. B **35**, 5876 (1987).

[4] A. Shimizu, T. Ogawa, and H. Sakaki, Phys. Rev. B **45**, 11 338 (1992).

[5] Although we assume infinite-height barriers and a rectangular shape for the cross section, essential results apply to any QWR that has inversion symmetry on a mesoscopic scale. Inversion symmetry on an atomic scale is not assumed.

[6] Although the last inequality $L_z^2 \ll [a_B^{(2)}]^2$ is not satisfied for the QWR of Ref. 1, it does not alter the conclusions on the xy anisotropy, so it is irrelevant to the comparison of the present theory with the experiment.

[7] M. Shinada and S. Sugano, J. Phys. Soc. Jpn. **21**, 1936 (1966).

[8] A. Shimizu, Phys. Rev. B **40**, 1403 (1989).

[9] The quantum numbers are chosen to start from 1, unlike the notations in Refs. 7 and 11.

[10] One might wonder why a term including a derivative of G_N does not appear in the TPA rate. Intuitively, this is because such a term should be proportional to the square of the integral $\int [dG_N(Y)/dY]dY$, which is zero since it just gives the difference between two boundary values of G_N, both of which are zero.

[11] T. Ogawa and T. Takagahara, Phys. Rev. B **44**, 8138 (1991); **43**, 14 325 (1991).

[12] Another reason for the noneffectiveness of OPA spectroscopy as a dimensional probe was discussed in G. E. W. Bauer and H. Sakaki, Surf. Sci. **267**, 442 (1992).

Electric-Field-Induced Changes in the Two-Photon Absorption Spectrum of Multiple-Quantum-Well Structures

Kazuhito Fujii, Akira Shimizu,[a] Johan Bergquist, and Takeshi Sawada
Canon Research Center, 5-1, Morinosato-Wakamiya, Atsugi, Kanagawa 243-01, Japan
(Received 11 June 1990)

We have measured two-photon absorption spectra of quantum-well structures *in static electric fields* for photon energies close to *half* the band-gap energy, and found drastic static-field-induced changes in the spectra. Our experimental results agree with a theory based upon an infinite-level model, the validity of which was previously established at zero bias, except that a field-induced growth of the two-photon absorption peak at *half* the lowest light-hole exciton energy is more drastic than the theoretical prediction. At high bias fields the peak height approaches a large value predicted by another simplified theory based upon a two-level model.

PACS numbers: 78.65.Fa, 42.65.−k, 71.35.+z

Two-photon absorption (TPA) of quantum-well structures (QWSs) is a subject of growing interest.[1-8] In particular, intensive studies have been devoted to the TPA spectra of QWSs near the TPA edge, i.e., for the photon energy $\hbar\omega \approx E_G/2$.[3-8] When the incident light is polarized in the plane normal to the confinement direction, $\hat{\epsilon} \perp \hat{z}$, rather smooth TPA spectra, which are not much different from those of the bulk crystal, were predicted by theories which did not consider excitonic effects.[6,7] If the excitonic effects are included, one may expect from the selection rule nP exciton peaks.[3-5] Their oscillator strengths are, however, shown to be very small (as compared with $1S$ exciton peaks which appear in the $\hat{\epsilon} \| \hat{z}$ spectra).[3,8] In agreement with theory,[8] Tai *et al.*[3] observed only a tail due to a $2P$ exciton, and Nithisoontorn *et al.*[4] observed only shoulders attributable to $2P$ excitons. On the other hand, when the incident light is polarized parallel to the confinement direction, $\hat{\epsilon} \| \hat{z}$, the TPA spectra become much different from those of the bulk crystal, reflecting subband quantization.[3,6-8] In particular, strong $1S$ exciton peaks, followed by steplike continuums, were observed by Tai *et al.*,[3] in agreement with theory.[8] In addition to these TPA spectra for *nonbiased* QWSs, the theory[8] also investigated the TPA spectra *in the presence of external static electric fields* ($\| \hat{z}$), and predicted drastic changes in the $\hat{\epsilon} \| \hat{z}$ spectra, which are caused by parity mixing in subband wave functions. In this Letter, we present the first experimental results for these drastic field-induced changes in the TPA spectra of QWSs.[2,9]

The experimental setup and the sample structure are shown in Fig. 1. Difference-frequency light pulses of 6 ns duration were generated from a Q-switched Nd-doped yttrium-aluminum-garnet and a dye laser. The tuning range is 1.45–1.75 μm. The energy per pulse is about 6 mJ, and its pulse-to-pulse fluctuation is about 20%. The light pulses were attenuated and were coupled into a sample of ridge-type waveguide using a 20× objective lens. The coupling efficiency was about 5%. At the output from the waveguide, the propagation beam was separated from scattered light using a 100× objective lens and a pinhole. The experimental arrangement allows either the $\hat{\epsilon} \perp \hat{z}$ or $\hat{\epsilon} \| \hat{z}$ polarization configuration. Moreover, because of the two-dimensional confinement of the light field, we can avoid self-focusing effects and surface effects, so that values of the TPA coefficient α_2 can be estimated more accurately than in conventional experiments. The samples consist of an undoped GaAs/$Al_{0.4}Ga_{0.6}As$ multiple-quantum-well (MQW) core region embedded in $Al_{0.4}Ga_{0.6}As$ cladding regions. We employed a p-i-n structure to apply static electric fields to the MQW region, perpendicularly to the QW layers. To avoid possible absorption changes in the waveguide due to carrier-density changes caused by the electric fields, the MQW region as well as portions of the cladding layers are undoped. All measurements were performed *at room temperature*.

We have measured the beam intensities I_{in} and I_{out} at the input and output, respectively, using Ge photodiodes of 0.5 ns rise time and a boxcar integrator. We have also measured the induced photocurrent J, using a transimpedance amplifier.[10] Light attenuation due to nonlinear

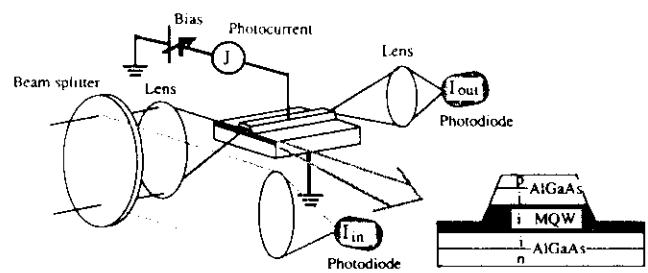

FIG. 1. Experimental setup and sample descriptions. The ridge width and length are 3 and 500 μm, respectively. The thickness of the MQW layer (75 periods of 100-Å-GaAs/62-Å-$Al_{0.4}Ga_{0.6}As$) and the i-$Al_{0.4}Ga_{0.6}As$ layers are about 1.2 and 0.4 μm, respectively.

14

processes was less than several percent for propagation-beam intensity less than 6 MW/cm^2. The duration of one photocurrent pulse was 6 ns, which is just the duration of one light pulse.[10] Figure 2 shows the light-intensity (I) dependence of the photocurrent. As it should be, the quadratic dependence of J upon I ($J/I \propto \alpha_0 + \alpha_2 I$) holds quite well. The magnitude of the TPA coefficient α_2 at each wavelength is estimated from the relation of J/I_{out} vs I_{out} (as shown in Fig. 2) and also from the relation of I_{out}/I_{in} vs I_{in}.[11] In the latter estimate, to get a sufficient signal-to-noise ratio, we have estimated $\alpha_2(V) - \alpha_2(0)$ rather than $\alpha_2(V)$ itself. Since $\alpha_2(0)$ for $\hat{\epsilon} \| \hat{z}$ vanishes at wavelengths longer than twice the lh2-c1;1S exciton wavelength[3,6,7] (lh denotes light hole; c, conduction), we can deduce $\alpha_2(V)$ itself in such wavelength regions, and we have compared it with that deduced from the photocurrent measurement. They are consistent if we take account of the bias-voltage dependence of η, the quantum efficiency of converting photogenerated carriers into currents, and linear scattering or absorption due to photogenerated free carriers.[11,12] We have also confirmed that all samples processed from the same epitaxial wafer showed almost the same TPA spectra.

Let us first look at the TPA spectra for $\hat{\epsilon} \perp \hat{z}$ polarization. According to Ref. 8, α_2 of the exciton, which has the relative-motion quantum number ν and is composed of the αth conduction subband and the βth heavy-hole (hh) or light-hole (lh) subband, is given by, for $\hat{\epsilon} \perp \hat{z}$,

$$\alpha_2 \propto q_x^{\nu} |I_{\alpha\beta}/\mu_{\parallel}^{\nu}|^2 |\hbar U_{\nu}^{\alpha\beta'}(0)|^2 S_{\nu}^{\alpha\beta}, \quad (1)$$

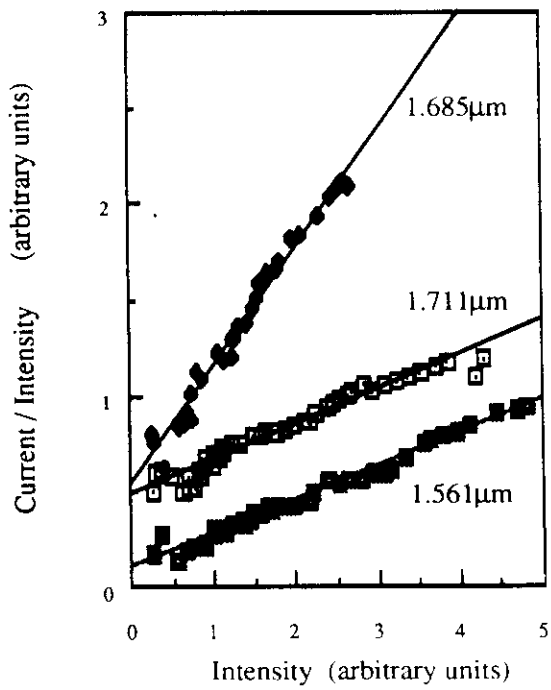

FIG. 2. Photocurrent divided by the light intensity plotted against the light intensity, for three different wavelengths.

where ν = hh or lh, $q_x^{hh} = \frac{3}{2}$, $q_x^{lh} = \frac{1}{2}$, $I_{\alpha\beta}$ is the overlap integral between the subband envelope functions, $\mu_{\parallel}^{\nu}$ is the reduced mass for the motion in the QW plane, $\hbar$ is Planck's constant divided by 2π, $U_{\nu}^{\alpha\beta'}(0)$ is the first derivative of the in-plane envelope function at $r_{\parallel} = 0$, and $S_{\nu}^{\alpha\beta}$ is a line-shape function. The validity of the theory was previously established at zero bias.[3,4,8] Since the theory does not assume any symmetries for QWSs, we expect that it is also valid at finite bias fields F.[8] For discrete states ($\nu = n,m$), $U_{nm}^{\alpha\beta'}(0)$ is nonzero only for nP excitons. However, we do not expect any distinct spectral structures in our experiment because the nP excitons are unstable at room temperature. As for continuous spectra ($\nu = k_{\parallel},m$), $|U_{k_{\parallel}m}^{\alpha\beta'}(0)|$ increases monotonically with energy. Hence, we expect smooth, monotonically increasing spectra.[8] Since the in-plane envelope function (characterized by the Bohr radius of the exciton) is not very sensitive to F,[13] the main F dependence of α_2 comes from the factor $I_{\alpha\beta}$ and the quantum-confined Stark shifts[14] of the exciton energies.[8] This situation is similar to one-photon absorption (OPA).[14] The experimental result for the TPA photocurrent spectra in the presence of a bias field of $F \approx 80$ kV/cm (which was estimated from the bias voltage $V = 15.5$ V) is shown in Fig. 3. In agreement with the theory, the spectra are smooth and no clear peaks are seen at the wavelengths of half the Stark-shifted energies of the lowest heavy-hole (hh1-c1;1S) and the lowest light-hole (lh1-c1;1S) excitons. On the other hand, we do not understand why the TPA photocurrent decreases at shorter wavelengths, whereas the theory predicts a monotonic increase.[8] One possible reason for the discrepancy is that some recombination channel might open at shorter wavelengths.[5]

Let us next investigate the TPA spectra for $\hat{\epsilon} \| \hat{z}$ polar-

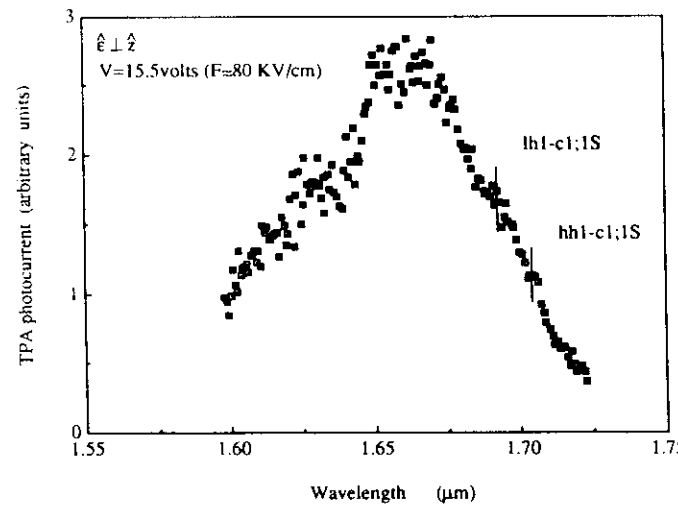

FIG. 3. Photocurrent spectra for the light polarized parallel to the QW layers, at the applied voltage of 15.5 V. The vertical lines indicate twice the wavelengths of the hh1-c1;1S and lh1-c1;1S excitons which are determined from the one-photon absorption spectra.

15

ization. According to theory,[8]

$$\alpha_2 \propto q_z^{\nu}|P_{\alpha\beta}/\mu_z^{\nu}|^2|U_{\nu}^{\alpha\beta}(0)|^2 S_{\nu}^{\alpha\beta}, \quad (2)$$

where $q_z^{hh}=0$, $q_z^{lh}=2$, $P_{\alpha\beta}$ is the momentum matrix element between the subband envelope functions, μ_z^{ν} is the reduced mass for the z-direction motion, and $U_{\nu}^{\alpha\beta}(0)$ is the in-plane envelope function at $r_{\parallel}=0$. For discrete states, $U_{nm}^{\alpha\beta}(0)$ is nonzero only for nS excitons. At room temperature, we expect strong peaks only for $1S$ excitons, because among nS excitons they are the only ones which have large binding energies as well as strong oscillator strengths.[8] As for continuous states, $|U_{k_{\nu}m}^{\alpha\beta}(0)|$ is almost constant independent of energy. Hence, we expect steplike spectra[7] along with the strong $1S$ exciton peaks.[3,8] The main F dependence of α_2 comes from the factor $P_{\alpha\beta}$ and the quantum-confined Stark shifts.[8] The experimental result for the spectra of $\alpha_2(V)-\alpha_2(0)$ is shown in Fig. 4, where the spectra for wavelengths longer than about 1.66 μm are equal to $\alpha_2(V)$ itself, because $\alpha_2(0)=0$ there.[3,6-8] In agreement with theory,[8] we have observed growth and redshifts of the peak of the lowest light-hole (lh1-c1;1S) excitons, which vanishes at zero bias.[3,8] To confirm that the observed peak indeed corresponds to the lh1-c1;1S exciton, we compared *half* the wavelength of the lowest peak with the lh1-c1;1S exciton wavelength determined from the OPA spectra. At each bias voltage they agreed quite well, which confirms our attribution.

In order to investigate α_2 at shorter wavelengths, where $\alpha_2(0)\neq 0$, let us look at photocurrent spectra (Fig. 5). In this case, we must keep in mind that $\eta(V)$, the quantum efficiency of converting carriers into currents, is smaller for lower applied voltages V. Hence, let us look at the spectrum at the highest voltage ($V=15.5$ V) represented by solid circles. In addition to the lh1-c1;1S exciton peak, two peaks are clearly observed at shorter wavelengths. On the basis of Eq. (2) and simple calculations of the energy-level structure, we attribute the peaks to the lh2-c1;1S and lh1-c2;1S excitons, which were also observed in the zero-bias spectra.[3] On the other hand, the smallness of the TPA photocurrent for shorter wavelengths (≤ 1.55 μm) could not be explained within the framework of Eq. (2). As in the case of $\hat{\epsilon}\perp\hat{z}$ spectra, one possible reason for the discrepancy is some recombination channel for shorter wavelengths.[5]

We finally make quantitative comparison with theory. Let us estimate the magnitude of α_2 at the lowest-energy peak (lh1-c1;1S) induced by the bias field of 80 kV/cm. We assume that the time-integrated photocurrent is equal to the quantum efficiency $\eta(V)$ times the number of carriers generated by TPA. Then, we obtain $\alpha_2 \simeq 0.07/\eta(V)$ cm/MW. Considering that $\eta<1$ and that absorption saturation might have occurred, we conclude that $\alpha_2 > 0.07$ cm/MW. This peak value of α_2 *at the TPA edge* is comparable with α_2 ($\simeq 0.03$ cm/MW)[15] of bulk GaAs crystals *at shorter wavelengths* (deep inside the TPA spectra), and is an order of magnitude larger than the theoretical prediction.[8,16] It is interesting that the observed value is close to that predicted by another simplified theory[13] based upon a two-level model. It suggests that a crossover occurred from an infinite-level-model-like behavior at zero bias to a two-level-model-like one at high bias voltages. Although we do not understand at present why this happened, it has a significant meaning in applications, because the large peak of $\alpha_2(V)$ *at the TPA edge* gives rise to a large peak of $\mathrm{Re}\chi^{(3)}$ *just below* the TPA edge. Such a large peak is absent in the bulk crystal.[17] Since MQWSs are "ultra-transparent" in this energy region[8,13] (because both OPA and TPA are absent, and also because the TPA tail is much sharper than that of bulk crystals) and the response time τ of the nonlinearity is ultrafast, we can obtain a large figure of merit $\chi^{(3)}/(\alpha_0+\alpha_2 I)\tau$ in biased MQWSs *even at room temperature*.

The present experiment has been performed using the Quantel laser system in the Research Institute for Polymers and Textiles (Tsukuba, Japan). We thank Dr. H.

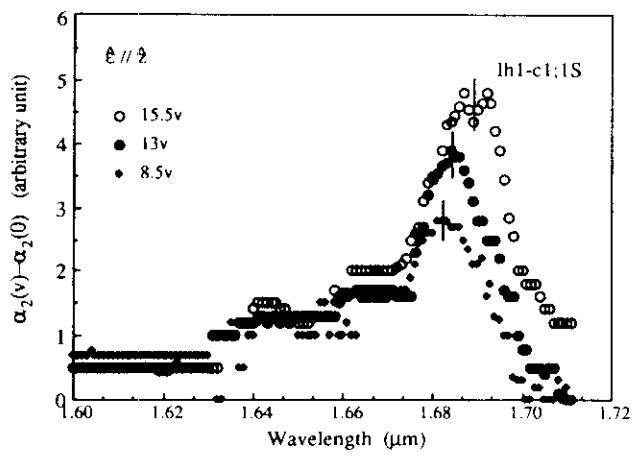

FIG. 4. Spectra of $\alpha_2(V)-\alpha_2(0)$ determined from the transmission measurements, at three different bias voltages. The light is polarized perpendicularly to the layers.

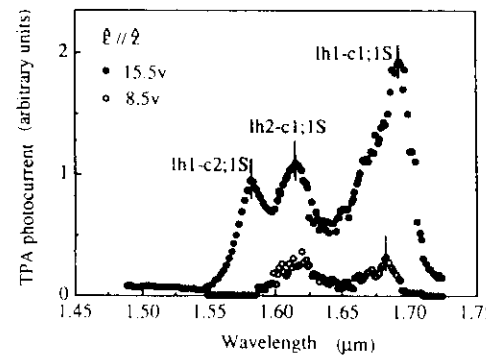

FIG. 5. Photocurrent spectra for the light polarized perpendicularly to the QW layers, at two different bias voltages.

16

Nakanishi and Dr. H. Matsuda for their support and helpful discussions. We also thank Professor M. Yamanishi, Professor A. Nakamura, Professor H. Sakaki, and Dr. Y. Handa for discussions, and S. Ikeda, K. Kaneko, and M. Hasegawa for the sample preparation.

---

[a]Present address: Sakaki Quantum Wave Project, Exploratory Research for Advanced Technology (ERATO) Program, Research Development Corporation of Japan, Keyaki House 302, 4-3-24, Komaba, Meguro-ku, Tokyo 153, Japan.

[1]D. Fröhlich, R. Wille, W. Schlapp, and G. Weimann, Phys. Rev. Lett. **61**, 1878 (1988).

[2]W. H. Knox, D. S. Chemla, D. A. B. Miller, J. B. Stark, and S. Schmitt-Rink, Phys. Rev. Lett. **62**, 1189 (1989). In their experiment, TPA for a voltage-applied QWS was measured at a photon energy which is close to E_G, where no distinct field-induced changes are expected for the TPA spectra.

[3]K. Tai, A. Mysyrowicz, R. J. Fisher, R. E. Slusher, and A. Y. Cho, Phys. Rev. Lett. **62**, 1784 (1989).

[4]M. Nithisoontorn, K. Unterrainer, S. Michaelis, N. Sawaki, E. Gornik, and H. Kano, Phys. Rev. Lett. **62**, 3078 (1989). They measured combined spectra, rather than pure TPA spectra, of TPA and the absorption of the second-harmonic wave (SHW). $1S$ exciton peaks in their results are due to the SHW.

[5]I. M. Catalano, A. Cingolani, M. Lepore, R. Cingolani, and K. Ploog, Phys. Rev. B **41**, 12937 (1990).

[6]H. N. Spector, Phys. Rev. B **35**, 5876 (1987).

[7]A. Pasquarello and A. Quattropani, Phys. Rev. B **38**, 6206 (1988).

[8]A. Shimizu, Phys. Rev. B **40**, 1403 (1989).

[9]A part of this work was previously presented: K. Fujii, A.Shimizu, J. Bergquist, and T. Sawada, in *Postdeadline Papers of the Seventeenth International Quantum Electronics Conference, Anaheim, May 1990* (Optical Society of America, Washington, DC, 1990), Paper No. QPDP-15.

[10]Since our measurements were performed at room temperature, photogenerated carriers in quantum wells can easily flow across the MQWS under high bias fields, as explicitly demonstrated by Okuda *et al.* [M. Okuda *et al.*, IEEE J. Quantum Electron. (to be published); M. Okuda (private communication)].

[11]K. Fujii, A. Shimizu, J. Bergquist, and T. Sawada (unpublished).

[12]H. C. Casey, Jr., and M. B. Panish, *Heterostructure Lasers* (Academic, New York, 1978), Pt. A, p. 174.

[13]A. Shimizu and K. Nakamura, in *Proceedings of the Nineteenth International Conference on the Physics of Semiconductors, Warsaw, 1988,* edited by W. Zawadzky (Polish Academy of Sciences, Warsaw, 1988); A. Shimizu, Phys. Rev. Lett. **61**, 613 (1988).

[14]D. A. B. Miller, J. S. Weiner, and D. S. Chemla, IEEE J. Quantum Electron. **22**, 1816 (1986).

[15]J. H. Bechtel and W. L. Smith, Phys. Rev. B **13**, 3515 (1976).

[16]We do *not* think that this discrepancy is due to some enhancement of TPA by deep impurities (or defects) which work as intermediate states, for the following reasons. (i) Since the deep-impurity states must be insensitive to F, not only $\alpha_2(V)$ but also $\alpha_2(0)$ has to be equally enhanced, so that the data of Fig. 5 are approximately proportional to the intrinsic $\alpha_2(V)-\alpha_2(0)$. We also note that α_2 at the lh2-c1;$1S$ peak has to be equally enhanced, because reported energy distributions of deep impurities are much broader than the separation of the two excitons. In that case, large *negative* values of $\alpha_2(V)-\alpha_2(0)$ should be observed around the wavelength of the $F=0$ lh2-c1;$1S$ exciton peak ($\sim 1.62\ \mu$m), because $P_{\alpha\beta}$ for that exciton is largely reduced by the electric field (see Ref. 8). However, we did *not* observe the negative values. (ii) Our samples showed *strong* photoluminescence at 77 K with the narrow full width of ~ 2 meV. This indicates that our sample quality is not much worse than those of Refs. 3 and 4 which did not observe any effects of deep impurities.

[17]G. D. Mahan, Phys. Rev. **170**, 825 (1968); C. C. Lee and H. Y. Fan, Phys. Rev. B **9**, 3502 (1974).

Two-Photon Absorption in GaAs Quantum Wires

R. Cingolani,[a] M. Lepore, R. Tommasi, and I. M. Catalano
Unità GNEQP-Dipartimento di Fisica, Università di Bari, Via Amendola 173, 70110 Bari, Italy

H. Lage, D. Heitmann, and K. Ploog
Max-Planck-Institut für Festkörperforschung, Heisenbergstrasse 1, D7000-Stuttgart 80, Federal Republic of Germany

A. Shimizu and H. Sakaki
Quantum Wave Project, Research Development Corporation of Japan, Keyaki-house 302, 4-3-24 Konaba, Tokyo 153, Japan

T. Ogawa
NTT Basic Research Laboratories, Musashino-Shi, Tokyo, Japan
(Received 26 December 1991)

We have investigated the polarization-dependent two-photon absorption in GaAs/AlGaAs quantum wires. The anisotropic selection rules of the multiphoton absorption process are exploited to study the one-dimensional $2p$ exciton states and the transitions between quantum wire subbands of different quantum numbers ($\Delta n_y \neq 0$ selection rule). The deviations from the selection rules derived for the strict one-dimensional case are discussed, and depend on the actual quasi-one-dimensional character of the excitonic wave functions.

PACS numbers: 78.65.Fa, 42.65.−k

The nonlinear optical properties of low-dimensional semiconductors have attracted great interest in the last few years. In particular, two-photon absorption (TPA) has been investigated in detail in two-dimensional (2D) semiconductor quantum wells, both experimentally and theoretically, to elucidate the impact of the reduced dimensionality on the nonlinear absorption processes [1]. Currently, interest has turned to systems with even lower dimensionality, like 1D quantum wires and 0D quantum dots (for a review see Ref. [2]). The optical properties of undoped low-dimensional systems are strongly governed by excitonic effects. An interesting aspect of TPA is that it gives direct access to excited excitonic states having a significantly larger excitonic radius ($2p$ states). It is therefore expected that the influence of lateral confinement is stronger on these excited $2p$ states than on the excitonic ground state, i.e., the $1s$ exciton. A special situation should occur when the width of the lateral confinement is in between the extension of the $1s$ and $2p$ states. In this Letter we report an experimental study of TPA in GaAs/AlGaAs quantum wires. We find a strong quantum confinement effect on the $2p$ exciton states, significantly enhanced with respect to that on the $1s$ states observed in conventional photoluminescence excitation spectroscopy (PLE). The TPA curves show rich excitation spectra with a strong polarization dependence, in agreement with theoretical predictions [3,4]. In fact, we find that optical transitions between quantum wire states with the same quantum numbers ($\Delta n_y = 0$) are allowed when the polarization direction of the exciting beam (ϵ) is perpendicular to the wire quantization direction (y), whereas $\Delta n_y = \pm 1$ transitions are dominant in the $\epsilon \| y$ geometry. These peculiar selection rules allow us to discriminate between true one-dimensional and quasi-two-dimensional excitonic states which are involved as the final states of different linear and nonlinear absorption processes.

The investigated quantum wire array has been fabricated by holographic patterning and subsequent reactive ion etching of a molecular-beam-epitaxy-grown multiple-quantum-well heterostructure. The quantum well structure consisted of 25 GaAs wells of width $L_z = 103$ Å and $Al_{0.34}Ga_{0.66}As$ barriers of width $L_{bz} = 148$ Å grown on top of a 1-μm-thick $Al_{0.34}Ga_{0.66}As$ cladding layer providing optical confinement of the luminescence (throughout the paper the indices z and y indicate the confinement directions of the quantum well and of the quantum wire, respectively). The processed quantum well structure resulted in a regular array of quantum wires with 280-nm periodicity and a crystalline wire width $L_y = 60 \pm 5$ nm as determined by the analysis of high-resolution x-ray diffraction spectra. Details on the structural and linear optical properties of the sample are reported in Ref. [5] and Refs. [6,7], respectively. The nonlinear absorption has been studied by measuring the two-photon-absorption-induced photoluminescence excitation spectra (TPA-PLE) at 10 K for different polarization directions of the exciting laser beam. The detection energy was set at the fundamental quantum wire exciton state ($E_{11}^{1s} = 1.554$ eV), independently measured by linear PLE spectroscopy, and by scanning the exciting photon energy in the transparency region of the crystal. The laser source was a two-stage amplified dye laser pumped by the second harmonic of a Nd:YAG laser, operating at 10 Hz repetition frequency and with 9 nsec pulse duration. The dye-laser radiation was frequency converted in the infrared by a low-pressure H_2 Raman cell. The output beam could be tuned in the spectral range $0.75\ \text{eV} < \hbar\omega < 0.82$ eV with tuning accuracy of the laser dye of about 2 Å and with maximum power density of the or-

der of 10 MW cm^{-2} after focusing. The emitted radiation was detected by a 0.5-m double monochromator equipped with a 60ER photomultiplier tube and the exciting beam was monitored by a fast-response photodiode. Both signals were sent to a digital oscilloscope for further processing. To reduce the effects of fluctuations in the input beam intensity, the ratio of the photomultiplier signal to the second power of the monitor signal was used. Moreover, the quadratic behavior of the detected luminescence signal versus excitation intensity was checked at each experimental point and several measurement runs were carried out at all exciting wavelengths. With the adopted experimental conditions the signal-to-noise ratio was of the order of 200:1. In Fig. 1 we show the typical intensity dependence of the nonlinear luminescence induced by the absorption of two photons of energy $\hbar\omega = 0.795$ eV ($2\hbar\omega = 1.590$ eV) and $\hbar\omega = 0.805$ eV ($2\hbar\omega = 1.610$ eV) versus the laser power density. Much care has been taken to reduce and test the influence of the inhomogeneity of the power distribution across the exciting laser section. The experimental points exhibit the expected quadratic behavior as shown by the comparison with the quadratic regression curves (solid lines in Fig. 1). The slope-2 curves fit the experimental data points within 3% at all wavelengths. The experimental TPA-PLE spectra at $T = 10$ K in the $\epsilon \perp y$ and $\epsilon \parallel y$ configurations are shown in Fig. 2 together with the linear PLE.

Before entering into a detailed discussion of the TPA-PLE data we briefly summarize the results of the linear spectroscopy under low and high excitation intensity. As a result of the relatively large width of the investigated quantum wires, which amounts approximately to 4 times

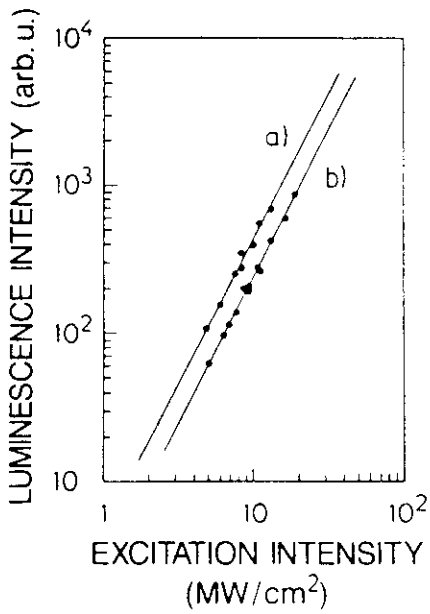

FIG. 1. Logarithmic plot of the intensity dependence of the photoluminescence induced by two-photon absorption at energy (a) $2\hbar\omega = 1.590$ eV and (b) $2\hbar\omega = 1.610$ eV, respectively, versus the laser power density in the $\epsilon \perp z$ configuration. The straight lines are the best-fit quadratic regression curves to the experimental points. Curves fit all data points within $\pm 3\%$.

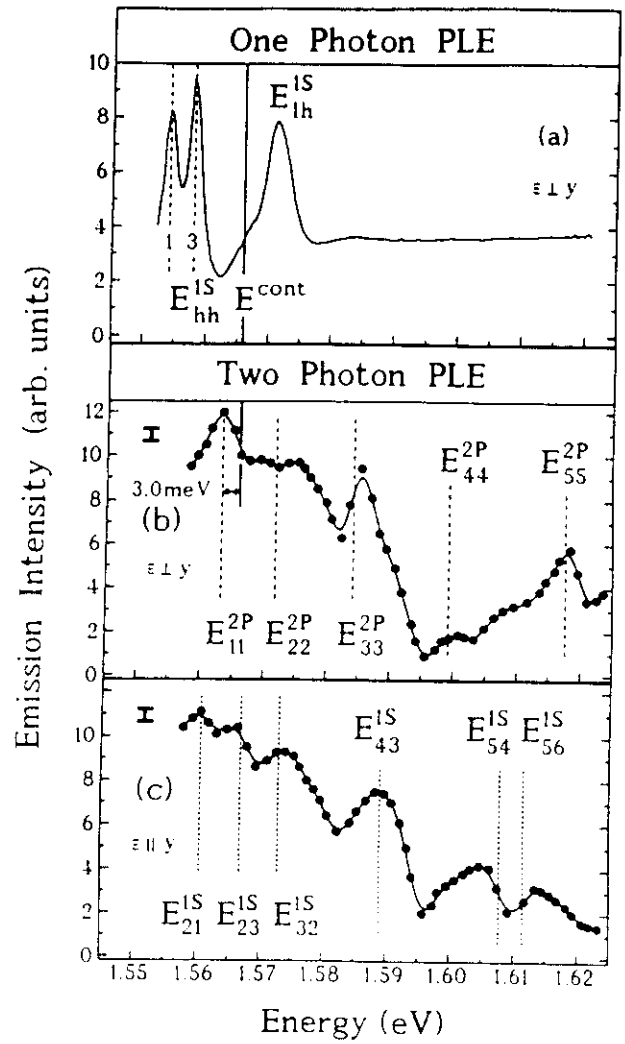

FIG. 2. (a) Linear photoluminescence excitation (PLE) spectrum of the quantum wire array at $T = 10$ K. The detection energy was set at the low-energy tail of the fundamental quantum wire exciton state (around 1.552 eV). E^{cont} indicates the energy of the exciton continuum. (b) Two-photon-absorption-induced photoluminescence excitation spectrum (TPA-PLE) of the quantum wires measured in the $\epsilon \perp y$ configuration at $T = 10$ K. The vertical lines indicate the calculated energy positions of the $2p$ exciton states associated with $\Delta n_y = 0$ transitions ($E^{2P}_{n_y,n_y}$ transitions). The 3.0-meV splitting indicates the estimated binding energy of the $2p$ excited state of the $n_y = 1$ exciton in the quantum wire. The vertical error bar deriving from signal-to-noise ratio and slope-2 regression on experimental points is indicated. The horizontal error bar coincides with the solid dots (the tuning accuracy was 2 Å). (c) The same as (b) but in the $\epsilon \parallel y$ configuration. The vertical lines indicate the calculated energy positions of the $1s$ exciton states associated with $\Delta n_y = \pm 1$ transitions ($E^{1S}_{n_y,n_y \pm 1}$). For both TPA spectra the detection energy was set at around 1.554 eV.

13

the bulk exciton Bohr radius (a_0), the quantum effects induced by the lateral confinement (y direction) are expected to be different under different excitation conditions. It has been shown that 1D intersubband transitions can be clearly resolved under high-excitation conditions in stationary [6] and time-resolved photoluminescence experiments [7]. Comparison of PL spectra with Kohn-Luttinger-type calculations taking into account the complex valence-band structure in the wires [8] allowed us to identify intersubband recombination processes involving quantum wire subbands with quantum numbers as high as $n_y = 5$ and the selection rule $\Delta n_y = 0$ [6,7]. In particular, the confinement energies of the 1D valence subbands were taken from Ref. [8] for a GaAs wire with $L_y = 60$ nm and $L_z = 10$ nm, whereas the confinement energies of the conduction subbands were calculated by the square-well model assuming infinite height of the potential barrier. However, when the optical properties are dominated by excitonic effects, as is the case under low-excitation conditions, the quantum size effects induced by the lateral confinement appear to be different. It was pointed out in Ref. [9] that in the rather wide quantum wires of our experiment the lateral confinement leads to a quantization of the excitonic center-of-mass motion, which leaves the internal structure of the exciton (i.e., the wave function of the *relative* motion of the electron and hole) unchanged and therefore 2D-like. The center-of-mass motion quantization manifests itself in the split heavy-hole exciton peaks of Fig. 2(a), which are quantized states of the translational motion of the $1s$ heavy-hole exciton. Therefore the linear PLE profile of Fig. 2(a) still maintains some 2D character (including a sharp light-hole exciton resonance around 1.574 eV) and does not exhibit pure 1D states. The results of these experiments demonstrated that quantum size effects are differently pronounced under different experimental conditions. In fact, depending on the wire width L_y one can find one-dimensional excitons if $L_y < a_0$ and two-dimensional excitons if $L_y \gg a_0$. In our sample we have roughly $L_y \approx 4a_0$; hence, $1s$ excitons behave almost like 2D excitons, while $2p$ excitons, having a larger extent of the relative motion, should exhibit an almost 1D character (with transition energies close to the 1D intersubband transitions observed in the high-excitation-intensity photoluminescence spectra of Refs. [6,7]).

Due to the complementary selection rules, two-photon spectroscopy offers the unique possibility to access directly $2p$ excitonic states. Since the diameter of the $2p$ excited states is enlarged by a factor of 4 (valid for 3D excitons) in comparison with $1s$ excitons, these states should be effectively quantized and therefore exhibit a true one-dimensional character. This should enable us to observe 1D excitonic states in the TPA-PLE spectra. In order to use the familiar classification of 2D excitons for 1D excitons also, we will label states of even parity by "s" and of odd parity by "p" [10]. This allows us to classify one- and two-dimensional excitonic states without changing notation. Furthermore, it leads to identical selection rules for 1D and 2D systems with respect to the confined and unconfined directions. Inspection of experimental TPA spectra in the $\epsilon \perp y$ and $\epsilon \| y$ configurations reveals a clear difference with respect to the linear PLE spectrum [Fig. 2(a)]. In addition, the TPA-PLE line shapes are different depending on the relative orientation of the laser polarization vector with respect to the quantum wire lateral quantization direction. Such an anisotropy is theoretically predicted by the theory for quasi-one-dimensional systems [3,4]. In particular, in the $\epsilon \perp y$ geometry it is expected that the matrix elements of the TPA process do not vanish for transitions involving quantum wire states with the same quantum numbers (selection rule $\Delta n_y = 0$). Conversely, in the $\epsilon \| y$ geometry only intersubband transitions with $\Delta n_y = \pm 1, \pm 3, \ldots$ are allowed. In addition, if excitons are included in the 1D theory of two-photon absorption [4], it results that only $2p$ exciton states related to $\Delta n_y = 0$ transitions are allowed as final states of the TPA process in the $\epsilon \perp y$ configuration. On the contrary, $1s$ exciton states are allowed in the $\epsilon \| y$ geometry for $\Delta n_y \neq 0$ transitions. These additional constraints result from the requirements of parity conservation in the two-photon-absorption process. In the light of these theoretical arguments we can interpret the experimental spectra of Figs. 2(b) and 2(c).

In the $\epsilon \perp y$ configuration [Fig. 2(b)] we observe five structures whose relative energy splittings are the same as those observed for the $\Delta n_y = 0$ transitions in the time-resolved [6] and in the stationary luminescence spectra [7] under the high-photoexcitation condition, i.e., they directly reflect the 1D subband spacing. Furthermore, the first resonance of the TPA-PLE spectrum in Fig. 2(b) is about 3 meV below the onset of the continuum in Fig. 2(a). This confirms that indeed $2p$ excitonic states are observed. The estimated binding energy of 3 meV for $2p$ state is additionally in good agreement with that predicted for a perfectly quantized 1D exciton. In fact, such a $2p$ exciton follows the normal 3D hydrogenic series [10] that gives for its binding energy a value of about 4 meV in GaAs quantum wires. The spectral positions of the higher-energy transitions [which are indicated by dashed lines in Fig. 2(b)] have been obtained by adding the 1D subband spacing of Ref. [6] to the transitions labeled E_{11}^{2p}. The coincidence strongly supports our assumption that the observed resonances are related to one-dimensional excitonic transitions. Therefore, we conclude that the TPA-PLE peaks of Fig. 2(b) are related to $2p$ excited states of the 1D excitons associated with $\Delta n_y = 0$ transitions, in agreement with the theoretical expectations.

In the $\epsilon \| y$ configuration the TPA-PLE spectrum appears to be even more structured, and exhibits several transitions. The vertical lines of Fig. 2(c) represent the energy positions of the $1s$ exciton states associated with $\Delta n_y = \pm 1$ transitions in the quantum wire. These are calculated by adding the net confinement energies of the

1D conduction and valence subbands to the E_{11}^{1s} exciton energy (i.e., the detection energy). Comparison of these calculated transitions with the experimental data points reveals reasonable agreement. This demonstrates that in this configuration $1s$ states with $\Delta n_y = \pm 1$ are allowed, in agreement with the theory. However, the TPA-PLE spectrum of Fig. 2(c) exhibits rather broad peaks in this configuration, which requires further comment. In fact, the TPA selection rules employed for the interpretation of the presented nonlinear absorption data have been derived by a strict one-dimensional model [3,4], which obviously should be modified to treat the intermediate regime of quasi-one-dimensional excitons where $L_y \simeq 4a_0$. Under these conditions departures from the selection rules valid for the strictly 1D systems are expected due to the residual 2D character of the exciton wave functions. In particular, one should consider either pure 1D exciton states (both $1s$ and $2p$ states) or 2D excitons with quantized center-of-mass motion as final states of the multiphoton absorption process. A linear combination of the wave functions of these two different excitons can be used to represent a realistic form of the quasi-1D exciton wave function. Additional broadenings are expected in the TPA spectra due to this superposition, which qualitatively explains the observed broad structures in the TPA-PLE spectrum of Fig. 2(c). A detailed discussion of these preliminary theoretical results will be reported elsewhere.

In conclusion, we have reported the first study of two-photon absorption in GaAs quantum wires. Our experiment provides evidence for the strongly anisotropic selection rules of the interband two-photon absorption related to the reduced dimensionality of the system. Further, we have observed the excited $2p$ excitonic states and several $\Delta n_y = \pm 1$ transitions in these one-dimensional structures. Finally, the mixed 1D and 2D confinements of the excitonic states in wide quantum wires have been discussed with relevance to the peculiar nonlinear absorption selection rules.

This work has been supported by the National Research Council of Italy and by the Bundesministerium für Forschung und Technologie of the Federal Republic of Germany.

---

[a]Permanent address: Dipartimento Scienza dei Materiali, Università di Lecce, Via Arnesano, 73100 Lecce, Italy.

[1] For an updated review, see R. Cingolani and K. Ploog, Adv. Phys. **40**, 535 (1991).

[2] K. Kash, J. Lumin. **46**, 69 (1990).

[3] H. N. Spector, Phys. Rev. B **35**, 5876 (1987).

[4] A. Shimizu, T. Ogawa, and H. Sakaki, in Proceedings of the Ninth International Conference on Electronic Properties of Two Dimensional Systems (EP2DS-9), Nara, Japan [Surf. Sci. (to be published)]; Phys. Rev. B **45**, 11 338 (1992).

[5] L. Tapfer, G. C. LaRocca, H. Lage, R. Cingolani, P. Grambow, D. Heitmann, A. Fisher, and K. Ploog, Surf. Sci. **267**, 227 (1992).

[6] R. Cingolani, H. Lage, L. Tapfer, H. Kalt, D. Heitmann, and K. Ploog, Phys. Rev. Lett. **67**, 891 (1991).

[7] R. Cingolani, H. Lage, H. Kalt, L. Tapfer, D. Heitmann, and K. Ploog, Semicond. Sci. Technol. **7**, B287 (1992).

[8] U. Bockelmann and G. Bastard, Europhys. Lett. **15**, 215 (1991).

[9] H. Lage, D. Heitmann, R. Cingolani, P. Grambow, and K. Ploog, Phys. Rev. B **44**, 6550 (1991).

[10] A 4-meV binding energy of the $2p$ exciton state for a perfectly 1D GaAs quantum wire is expected from the theoretical results of R. Loudon, Am. J. Phys. **27**, 649 (1959); and T. Ogawa and T. Takagahara, Phys. Rev. B **44**, 8138 (1991). On the other hand, the binding energy of the $2p$ exciton state in a 10-nm GaAs quantum well is expected to be 1.5 meV [see R. Greene, K. K. Bajai, and D. E. Phelps, Phys. Rev. B **29**, 1807 (1984)]. Our experimental result is in between these two values. This is reasonable taking into account the experimental error of ± 1 meV on the energy axis and the accuracy in the determination of the continuum energy (E^{cont}).

PHYSICAL REVIEW B VOLUME 42, NUMBER 14 15 NOVEMBER 1990-I

Absorption-free modulation of electron-interference currents by optical fields using intersubband virtual transitions

Akira Shimizu,* Kazuhito Fujii, and Masahiro Okuda
Canon Research Center, 5-1 Morinosato-wakamiya, Atsugi, Kanagawa 243-01, Japan

Masamichi Yamanishi
Department of Physical Electronics, Faculty of Engineering, Hiroshima University, Shitami, Saijocho, Higashi-hiroshima 724, Japan
(Received 25 June 1990)

We propose to modulate quantum interference currents in a semiconductor electron interferometer by optical fields using intersubband virtual transitions, in which the optical fields are subject to no absorptions despite a high modulation efficiency. The electron-light interaction is more direct and efficient than those of previous proposals, and moreover, extra transitions, which could cause absorptions and/or destroy the electron coherence, are almost perfectly suppressed.

It has recently become possible to observe quantum interference currents in small-size ("mesoscopic") metal or semiconductor structures.[1] Most previous work treated modulation of the interference currents either by *static* magnetic or by *static* electric fields (or potentials).[1] A possibility of modulation of the interference currents by *time-dependent* fields (such as optical fields) was first considered by one of the authors (M.Y.).[2] He proposed to drive an electrostatic Aharonov-Bohm (AB) device by a dc voltage generated by optical "virtual" excitations (i.e., optical rectification). The most remarkable point may be that the interference currents can be modulated *without* light absorption. Although in that scheme electron-light interactions are rather indirect ones (i.e., the light field does not interact directly with electrons in the AB device), he recently proposed another scheme in which electrons interact with photoexcited "virtual" excitons through an exchange interaction.[3]

In general terms, these ideas are summarized as follows. Although it is applicable to any time-dependent field, we call the field "optical field" and call the associated quanta "photons" for convenience. Consider the absorption spectra of an electron system in an "optical field." If the "photon" energy lies within a gap of the absorption spectra, the optical field is subject to no absorptions. However, it does *not* mean absence of effects of the optical field upon the electron system. Electron wave functions are slightly deformed by perturbations of an electron-field interaction. By expanding the deformed wave functions in terms of unperturbed eigenfunctions, we can interpret that electrons are *coherently* excited with small amplitudes to excited states.[4] These coherent excitations are sometimes called "virtual excitations."[4] In contrast, when the photon absorptions occur, parts of electrons are *incoherently* excited to excited states, which are called real excitations. The basic idea is use of the slight deformation of electron wave functions induced by virtual excitations. Although the wave-function deformations are, in general, small (less than a few percent, typically), they can have strong effects on electron-interference currents, because a small wave-number change caused by the small wave-function deformation can lead to a large phase shift as an electron travels a distance long compared to its wavelength. As a result, electron-interference currents can be modulated drastically by optical fields without absorptions. From a view point of applications, the total system works as an "absorption-free detector" of the field intensity, because the magnitude of the electron-interference currents varies as a function of the field intensity. This type of device has wide potential applications.[2,3] In particular, it has been recently pointed out that well-designed absorption-free photodetectors work as quantum nondemolition photodetectors.[5]

At first sight, the absorption-free property may look to be inconsistent with a fundamental requirement of quantum mechanics: any measurement must accompany dissipations. In our case, the dissipations *do* occur in classical systems of external apparatus (including contact regions which work as electron reservoirs) which are used to measure the interference currents. However, the dissipations do *not* cause dissipations *in the optical fields* if the measuring apparatus are decoupled from the optical fields, and if the apparatus are *only* coupled with electrons which have *finished* interactions with the optical fields.[5,6] This last point is of particular importance, although it has not been stressed before. In fact, it can be shown[6] that dissipations (absorptions) of the optical fields would occur when the electrons interacting with the optical fields are *simultaneously* coupled with a classical dissipative system, such as a resistor and a transmission line. That is, "virtual excitations" are *not* necessarily free from dissipations of the optical fields.[6]

In this Rapid Communication, we propose a scheme[7] for the absorption-free optical modulation of electron-interference currents, in which electron-light interactions are more direct and efficient than those[2,3] previously proposed, and, more importantly, extra transitions, which could cause photon absorptions and/or could destroy electron coherence, are almost perfectly suppressed. The basic idea is the use of the optical Stark effects of intersubband virtual transitions.[8] Figure 1 shows schematic absorption spectra of a doped quantum-well (QW) struc-

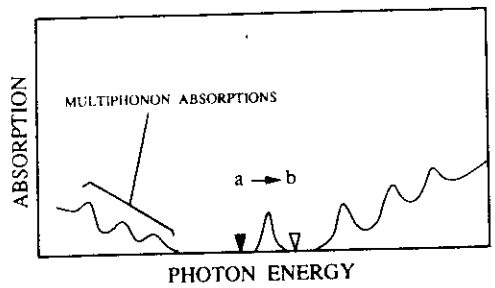

FIG. 1. Schematic absorption spectra of a doped narrow quantum well for the light polarized perpendicularly to the layers. The absorption is negligibly small if the photon energy is just below (as indicated by the solid triangle) or just above (as the open triangle) the absorption peak of the transitions from the first to the second subbands, $a \rightarrow b$. Multiphonon absorptions occur for lower photon energies, while for higher photon energies the absorption spectra approach those of the free-carrier absorptions of a bulk crystal.

ture for the photon energies $\hbar\omega$ in the range of intersubband transition energies.[9] The light is assumed to be polarized perpendicularly to the QW layers. We set the photon energy as

$$\hbar\omega = \varepsilon_b - \varepsilon_a - \Delta , \tag{1}$$

where ε_a and ε_b are the first (a) and second (b) subband energies, and Δ is called the detuning energy. Absorptions and/or scatterings of the light fields are absent if $\hbar\omega \gg$ optical phonon energies and if $|\Delta| > \Gamma$, the width of the $a \rightarrow b$ transitions. Main origins of Γ at low temperatures are QW imperfections and nonparabolicities.[9] Owing to recent rapid progresses in crystal growth techniques, the broadening due to the former has already been greatly suppressed,[10] and is expected to become negligible in the near future.[10] In that case, Γ is almost due to the nonparabolicities which make transition energies different for different values of transverse (parallel to the QW layers) wave numbers. For thin QW's as we will assume below, this Γ may become as large as 10 meV. However, it should be noted that in contrast to other broadening mechanisms this broadening does *not* degrade the device proposed below, because only the states at the Fermi level carry currents and the width of each of the states is much smaller than Γ. Their contributions in the absorption spectra appear at the lower-energy edge of the $a \rightarrow b$ absorption peak. All we have to do is to replace $\varepsilon_b - \varepsilon_a$ in Eq. (1) by this lower energy.

There are many reasons for using intersubband virtual transitions rather than interband ones: (i) Extra transitions, such as interband transitions and free-carrier scatterings, are almost perfectly suppressed. In contrast, if one used interband transitions, the light not only would induce interband virtual transitions but also would interact directly with conduction electrons. This could cause photon absorptions and/or could destroy electron coherence. (ii) The transition dipole moment is very large,[9] which leads to smaller light intensity to modulate currents. (iii) Electron density can be made very high because it is unnecessary to maintain excitons as in Ref. 3. As a result, a large Fermi velocity v_F is obtained, which leads to a high operation speed, a long coherence length ($l_\phi = v_F \tau_\phi$), and a high monochromaticity ($\delta k/k_F \sim k_B T/\varepsilon_F$) of electron waves.[1] (iv) It is possible to make Δ negative as well as positive, as seen from Fig. 1. Consequently, as explained below, the optical fields need not be focused upon a very small spot as in previous work,[2,3] and also the optical Stark shifts of two arms can be utilized constructively [see Eq. (10) below]. (v) The operation wavelength is compatible with ultralow-loss optical communications.[11]

Figure 2 shows the proposed structure. This is based upon the electrostatic AB effect device proposed by Datta *et al.*[12] To modulate interference currents, they utilized a change in electrostatic potential, whereas we utilize the optical Stark shifts of subband levels induced by optical fields,[8] as explained below. Two quantum-well wires (QWW's) *of different well widths*, the narrow (N) and the wide (W) ones, constitute an AB geometry. The ring should be made within the coherence length l_ϕ of electrons, which is of the order of 10 μm at 1 K.[1] For simplicity we further assume that the electrons move ballistically,[1] although the interference may also occur in the diffusive case.[1] We also assume that the confining potential in the y direction is common for the two QWW's, so that they have the same eigenfunction $\phi_\nu(y)$ and eigenenergy ε_ν. For the z direction, we denote the lowest-subband energy and wave function in N or W by $\varepsilon_a^{N,W}$ and $\phi_a^{N,W}(z)$, respectively, and the second-subband energy by $\varepsilon_b^{N,W}$. By appropriately designing the widths and alloy compositions of the wells, we can easily make the subband energies to satisfy the relations

$$\varepsilon_a^N = \varepsilon_a^W \equiv \varepsilon_a , \tag{2}$$

$$\varepsilon_b^W - \varepsilon_a^W < \hbar\omega < \varepsilon_b^N - \varepsilon_a^N . \tag{3}$$

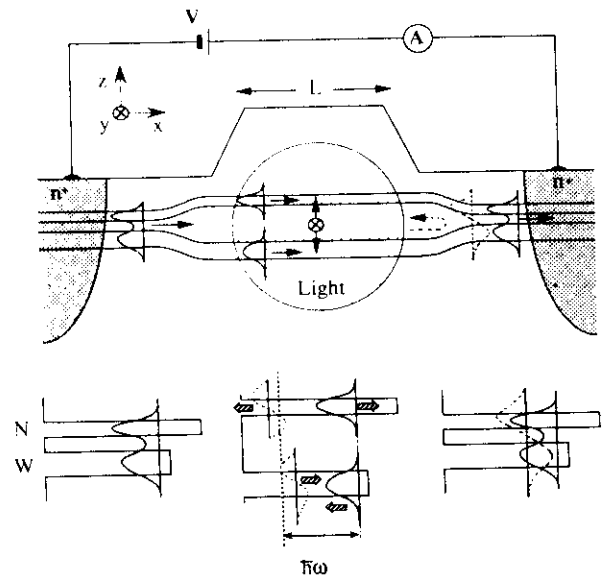

FIG. 2. Schematic diagram of the proposed structure. The large circle represents the cross section of the light beam. The electrons at the Fermi level flow from left to right. The band diagrams and eigenfunctions in the left, middle, and right regions are shown in the lower side. In the middle band diagram, the arrows indicate the directions of the optical Stark shifts of the subband energies.

In the coupling regions lying between the ring and the contact regions, the lowest subband state is given by

$$\phi_S = (\phi_a^N + \phi_a^W)/\sqrt{2}. \quad (4)$$

At temperatures lower than the energy separation between this state and the second-subband state, an electron which is injected from the left-contact region into the left-coupling region is in this ϕ_S state.[12] Despite the difference in the well widths of N and W, the weights of ϕ_a^N and ϕ_a^W are equal in ϕ_S, as in Eq. (4), owing to the relation (2). Hence, as an electron proceeds to the ring region, its wave function will just be halved into two parts: $e^{ikx}\phi_y(y)\phi_a^N(z)/\sqrt{2}$ and $e^{ikx}\phi_y(y)\phi_a^W(z)/\sqrt{2}$, where k is the wave number of the motion in the x direction and is related with the Fermi energy ε_F by

$$\varepsilon_F = \hbar^2 k^2/2m^* + \varepsilon_y + \varepsilon_a, \quad (5)$$

with m^* being the effective mass. In the center region (we call it the interaction region) of the ring region, a z-polarized optical beam propagating in the y direction is shown. In this interaction region, $\varepsilon_a^{N,W}$ is slightly changed due to the optical Stark effect by[8]

$$\Delta\varepsilon_a^{N,W} = -|\mu_{N,W}\mathcal{E}|^2/\Delta_{N,W}, \quad (6)$$

where $\mu_{N,W}$ is the $\phi_a^{N,W} \rightarrow \phi_b^{N,W}$ transition dipole moment,[8,9] $\mathcal{E}$ is the electric-field amplitude of the optical field, and $\Delta_{N,W}$ is the detuning energy. As a result of the above optical Stark shift of $\varepsilon_a^{N,W}$, the wave number k is also changed in the interaction region according to Eq. (5) by

$$\Delta k_{N,W} = (k^2 + 2m^*\Delta\varepsilon_a^{N,W}/\hbar^2)^{1/2} - k. \quad (7)$$

After the electron passes through the interaction region, the two parts of its wave function in the two QWW's acquire the relative phase difference given by

$$\Delta\theta = (\Delta k_N - \Delta k_W)L + \Delta\theta_0, \quad (8)$$

where L is the length of the interaction region (i.e., the width of the optical beam) and $\Delta\theta_0$ is an offset phase difference caused by possible difference in the path lengths along the two QWW's. While entering the right-coupling region, only the in-phase part of the wave function can go into the coupling region.[12] Hence, if we neglect multiple reflections for simplicity, the conductance G between the two contact regions varies as[12]

$$G \propto \cos^2(\Delta\theta/2). \quad (9)$$

Since $\Delta\theta$ is a function of the light intensity I ($\propto|\mathcal{E}|^2$) as seen from Eqs. (6)–(8), G varies with I. To get larger $\Delta\theta$ for a given value of I, it is particularly effective to make Δ_N and Δ_W different in signs; $\Delta_N > 0$ and $\Delta_W < 0$. (This is possible for intersubband virtual transitions.) In that case, the directions of the optical Stark shifts in the two QWW's become opposite, as indicated by the arrows in Fig. 2, and consequently the two QWW's contribute *constructively* to $\Delta\theta$ in Eq. (8):

$$\Delta k_N - \Delta k_W = |\Delta k_N| + |\Delta k_W|. \quad (10)$$

If we assume GaAs/AlAs QWW's of about 40-Å well thickness, the photon wavelength λ becomes about 2.8 μm, which is compatible with ultralow-loss optical communications.[11] We also assume the beam width $L \sim \lambda/$(refractive index) ~ 1 μm, the detuning energies $\Delta_N \approx -\Delta_W = 10$ meV, and the electron density $\sim 10^6$ cm^{-1}. Then, G is modulated over 50% at the light intensity of $I \simeq 2$ MW/cm^2, which intensity is an order of magnitude smaller than those of previously proposed structures.[2,3] Since the beam area is 1 μm^2, the light power is only 20 mW, and its fraction hitting upon the QWW's is as small as about 0.2 mW.

In the above discussions, we have assumed that the light-induced level shifts are due to the *pure* optical Stark shifts as observed in simple atomic systems. In other words, many-body effects, which were important in the case of Ref. 3, have been assumed to be unimportant in our case of intersubband virtual transitions. Although this was experimentally confirmed in an *undoped* QW,[8] no experiments have been performed for *doped* QW's or QWW's. We evaluated many-body corrections using a simple theory and found that they are indeed very small for intersubband *virtual* excitations in *thin* QW's or QWW's.[13] This conclusion should be contrasted with the case of intersubband *real* excitations where many-body corrections to the subband energies are important.[9-13] Although the theoretical result[13] may need an experimental test, we note that Eqs. (7)–(9) are valid irrespective of origins of the level shifts. Hence, the currents can be modulated even if the many-body effects played a role.

We finally consider the feasibility of observing the proposed effect. The structure of Fig. 2 or of Ref. 12 has not been fabricated so far. However, we note that our proposed effect does not depend on the specific structure of the electron interferometer. That is, the absorption-free optical modulation of electron-interference current should be observable in any electron interferometers whose interference patterns are altered by intersubband virtual transitions. For example, the effect should also be observable in the resonant tunneling diode of Fig. 3 of Ref. 5, or in the electron interferometer of Ref. 14, in which the exact 1:1 branching ratio as well as the single mode transmission in an AB ring can be achieved by forming a ring-shaped electron path in a *straight* double-quantum-wire structure by control of wave functions by gate voltages.[14] Another possibility of observing the effect is to observe changes in magnetoresistance[15] in an AB ring structure caused by intersubband virtual transitions. Experiment on these possibilities is in progress.

In summary, we have proposed a scheme for an absorption-free optical modulation of electron-interference currents. The electron-light interaction is more direct and efficient than those previously proposed, and, more importantly, extra transitions, which could cause photon absorptions and/or could destroy electron coherence, are almost perfectly suppressed. Among structures ever proposed, the most efficient current modulation has been achieved.

We wish to thank Professor H. Sakaki for fruitful discussions.

*Present address: Sukaki Quantum Wave Project, Keyaki House 302, 4-3-24, Komaba, Meguro-ku, Tokyo 153, Japan.

[1]For reviews, see R. Webb and S. Washburn, Phys. Today **41** (12), 46 (1988); S. Datta, Superlatt. Microstruct. **6**, 83 (1989).

[2]M. Yamanishi, K. Kurosaki, Y. Osaka, and S. Datta, in *Proceedings of the Sixth International Conference Ultrafast Phenomena,* edited by T. Yajima *et al.* (Springer-Verlag, Berlin, 1988), p. 334.

[3]M. Yamanishi, Y. Osaka, and S. Ago, *International Conference on Quantum Electronics Technical Digest Series 1990* (Optical Society of America, Washington, DC, 1990), Vol. 8, p. 92.

[4]See, e.g., B. S. Wherrett, A. C. Walker, and F. A. P. Tooley, in *Optical Nonlinearities and Instabilities in Semiconductors,* edited by H. Haug (Academic, New York, 1988), Chap. 10, Sec. 2.

[5]A. Shimizu, *International Conference on Quantum Electronics Technical Digest Series 1990* (Ref. 3), Vol. 8, p. 96; A. Shimizu (unpublished).

[6]A. Shimizu and M. Yamanishi (unpublished).

[7]A part of this work was presented by A. Shimizu *et al.*, in *Proceedings of the Spring Meeting of the Physical Society of Japan, Abstracts* (Physical Society of Japan, Tokyo, 1990), Paper No. 30p-Z2.

[8]D. Fröhlich, R. Wille, W. Schlapp, and G. Weimann, Phys. Rev. Lett. **59**, 1748 (1987).

[9]L. C. West and S. J. Eglash, Appl. Phys. Lett. **46**, 1156 (1985); L. C. West, Ph.D. thesis, Stanford University, 1985.

[10]H. Sakaki, M. Tanaka, and J. Yoshino, Jpn. J. Appl. Phys. Pt. 2 **24**, L417 (1985); H. Sakaki (private communication).

[11]K. Mohammed *et al.*, Electron. Lett. **22**, 215 (1986).

[12]S. Datta, M. R. Melloch, S. Bandyopadhyay, and M. S. Lundstorm, Appl. Phys. Lett. **48**, 487 (1986).

[13]A. Shimizu and M. Yamanishi (unpublished).

[14]M. Okuda, K. Fujii, and A. Shimizu, in *Proceedings of the Autumn Meeting of the Japan Society of Applied Physics, Abstracts* (Japan Society of Applied Physics, Tokyo, 1990), Paper No. 27p-ZL16; Appl. Phys. Lett. (to be published).

[15]P. G. N. de Vegvar *et al.*, Phys. Rev. B **40**, 3491 (1989).

Quantum nondemolition measurement of a photon number using electron interferometers of semiconductor microstructures

Akira Shimizu*
Canon Research Center, 5-1 Morinosato-Wakamiya, Atsugi, Kanagawa 243-01, Japan
(Received 30 July 1990)

We discuss effects of *quantized* electromagnetic fields upon the electronic conduction in interferometers of semiconductor microstructures. An optical field in an arbitrary quantum state is assumed to hit the interferometer, and the time evolution of the coupled photon-electron system is evaluated. It is found that the interferometer works as a quantum nondemolition photodetector if the interferometer is designed such that the interaction is switched adiabatically.

Electronic conduction in microstructures of metals or semiconductors is a subject of growing interest.[1] Most previous works discussed effects of static magnetic or electric fields upon the electronic conduction.[1] A few works have appeared recently that discussed the conductance modulation by classical electromagnetic fields.[2] In this paper we discuss effects of *quantized* electromagnetic fields upon the electronic conduction in semiconductor interferometers of a "mesoscopic" size.[3] An optical field in an arbitrary quantum state, such as a number state or a coherent state, is assumed to hit the mesoscopic interferometer, and the time evolution of the coupled photon-electron system is evaluated. Various quantities, such as a quantum-mechanical noise in the electron-interference current, are given in closed forms. Most importantly, it is found that the interferometer works as a quantum nondemolition (QND) photodetector[4–7] if the interferometer is designed such that the interaction is switched adiabatically. That is, one can measure the photon number without "backactions" upon the photon number by measuring the electron-interference current. In contrast, ordinary measuring apparatus contaminate the observable of interest (the photon number) by backactions of the measurements.[4] Due to the specific natures of the electrons in semiconductor microstructures as probe quanta, the operation principle of the present QND scheme is different from any of the previously proposed ones.[4–7]

To contrast the present case with the case of classical optical fields,[2] and also to reduce mathematical complexities, we employ the structure of Fig. 1 as a model system, although experiment may be more easily performed in other structures, as mentioned later. Our structure is basically the one described in Ref. 2, except that the "electron mode converter" is employed and both of the quadrature components of the interference currents, J_- and J_-, are measured. This improvement has been made to avoid reflections of electrons back to the source region, and also, as explained later, to improve the signal-to-noise ratio (SNR) of the device. Two quantum-well wires (QWW's) of *different well widths*, the narrow (N) and the wide (W) ones, constitute an Aharonov-Bohm (AB) geometry. We assume that the size of the ring is small enough (~ 1 μm typically) for the electrons at the Fermi surface to move *ballistically* from the source to the drain regions. This can be realized in, say, high-quality GaAs/AlAs QWW's at low temperatures. An optical field polarized in the z direction propagates in the $+y$ direction, and is confined in the center region (which we call the interaction region) by an optical waveguide structure, where the optical field interacts with electrons in the QWW's. If the photon energy $\hbar\omega$ is slightly detuned from the intersubband transition energies, or, more rigorously, if the right-hand side (rhs) of Eq. (3) is small enough, the interaction induces only "virtual transitions" so that no photons are absorbed. The virtual transitions

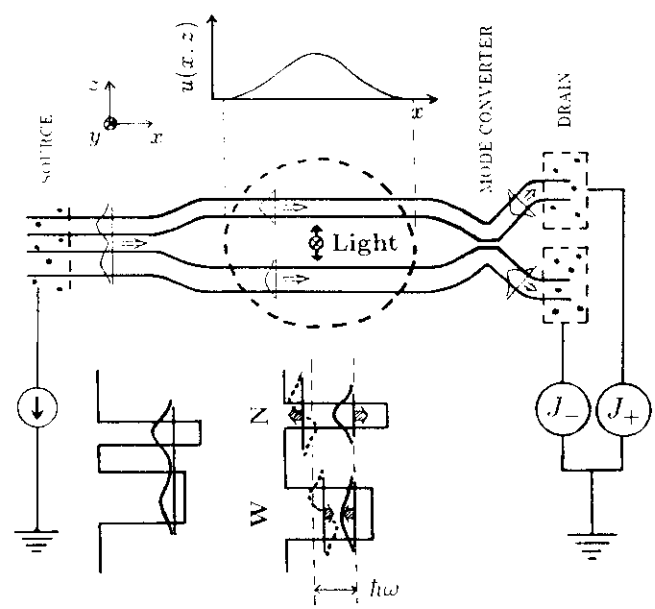

FIG. 1. Schematic structure of the quantum nondemolition photodetector used in the analysis. The optical field propagating in the $+y$ direction is confined in the center dotted region, with the transversal mode function $u(x,z)$, which is schematically shown in the upper side. The band diagrams and subband eigenfunctions in the source and center regions are shown in the lower side, where the arrows indicate the directions of the optical Stark shifts.

cause phase shifts in the electron wave functions, and thus give rise to changes in the electron-interference currents, from which we can deduce the photon number.

We will investigate the time evolution of the initial (i.e., prior to the interaction) photon state of the general form: $|\psi\rangle=\sum_n a_n|n\rangle$, where $|n\rangle$ is the number state, which is defined according to the following quantized optical electric field:[8]

$$\hat{\mathcal{E}}_z(\mathbf{r})=\left[\frac{2\pi\hbar\omega}{\epsilon L_y}\right]^{1/2}[\hat{a}u(x,z)e^{i\beta y}+\text{H.c.}]\ , \tag{1}$$

where ϵ is the dielectric constant, $\hat{a}$ is the photon annihilation operator, $u(x,z)$ is the normalized transversal mode function, β is the propagation constant, and L_y is a normalization length in the y direction. Electrons are supplied from the source region. We note that the wave function of each electron must be a wave packet of some finite length l. Previous experiments on a neutron source[9] and an electron source[10] suggest that the wave packet has a Gaussian-like envelope and that l is close to the length determined by the uncertainty principle. It is thus natural to consider that the electron wave function in our case also has the Gaussian envelope of the length $l\simeq v_F\tau_\phi'$, where v_F is the Fermi velocity and τ_ϕ' is the phase breaking time[1] *in the source region*. (τ_ϕ' would be shorter than that in the AB ring region). We can safely employ this assumption because our final results are independent of the length and detailed forms of the wave packet.[11] For the same reason, we will not write explicitly the Gaussian envelope function in the following equations. We will also drop in the equations the eigenenergies and eigenfunctions corresponding to the y-direction confinement, because they play no important roles.[11]

By appropriately designing the widths and alloy compositions of the wells, we can easily make the lowest subband energies of the two QWW's to satisfy $\epsilon_a^N=\epsilon_a^W\equiv\epsilon_a$. An electron wave packet emitted from the source region will be split into two, and its wave function with the Fermi energy of $\epsilon_F=\epsilon_a+\hbar^2k^2/2m^*$ becomes of the form[2]

$$|\Phi\rangle=(e^{ikx}|\varphi_a^N\rangle+e^{ikx}|\varphi_a^W\rangle)/\sqrt{2}\ , \tag{2}$$

where $\varphi_a^{N,W}(z)$ is the lowest-subband eigenfunctions of N or W. Hence, the initial state of the total system (electron plus optical field) is $|\Psi\rangle\equiv|\psi\rangle|\Phi\rangle$. We can analytically solve the time-dependent Schrödinger equation to obtain the time evolution of this initial state, using an adiabatic approximation (ADA) to separate the x and z coordinates of the electron, another ADA to treat pulsed optical fields, the rotating-wave approximation (RWA), and the Wentzel-Kramers-Brillouin (WKB) approximation.[11] The total resulting error is estimated to be $\sim 1\%$, which is dominated by the RWA. However, the RWA as well as the WKB approximation are irrelevant to the QND property of the device because the neglected terms cause *no* real transitions.[11] It is found that the error resulting from the two ADA's, which is related with destruction of photons, is given by[11]

$$\frac{\|\Psi-\Psi_{\text{ADA}}\|^2}{\|\Psi\|^2}\simeq\left|\frac{\gamma\sqrt{n}}{\Delta}\right|^2\left[\frac{\hbar}{\tau_I\Delta}\right]^2\ , \tag{3}$$

where τ_I is the characteristic time that it takes for the photon-electron interaction to switch, γ is the maximum value of $\gamma_q(x)$ [see Eq. (7)], and $|\Delta|\equiv\min(|\Delta_N|,|\Delta_W|)$ [see Eq. (6)]. This equation is the standard expression for the validity of the ADA in time-dependent problems, and thus demonstrates that our QND device relies upon the adiabatic switching of the interaction. τ_I is of the order of the shorter one of τ_t, the transit time of the electron through the interaction region, and the optical-pulse duration τ_p. Owing to the smooth profiles of the optical fields as a function of x and y, as described by $u(x,z)$ (see Fig. 1) and the optical-pulse shape, the collision of the electron moving in the $+x$ direction with the optical field becomes adiabatic with the switching time of τ_I. This should be contrasted with the situation of the Jaynes-Comming model,[8] where the collision occurs abruptly, resulting in the quantum Rabi flopping.[8] In the numerical example discussed below, $\tau_t\sim 1\ \mu\text{m}/v_F\sim 10$ ps for $v_F\sim 10^7$ cm/s, so that, if we assume $\tau_p\geq 10$ ps, the error due to the ADA's is estimated to be as small as 10^{-6}.

Because the full analysis is quite lengthy and complicated,[11] we will describe essential points only. As the electron proceeds to the interaction region, the electron and the photons will be coupled by the interaction, $H_I=-ez\hat{\mathcal{E}}_z(\mathbf{r})$. Since this interaction does not commute with $\hat{n}$, the photon number is *not* conserved *during the interaction*.[12] Each component $e^{ikx}|\varphi_a^q\rangle|n\rangle$ in $|\Psi\rangle$, where $q=N$ or W, evolves into the dressed state[8] of the form

$$\sqrt{k/K_k^q}\exp\left[i\int_0^x dx' K_k^q(x')\right]\times(\cos\theta_n^q|\varphi_a^q\rangle|n\rangle+\sin\theta_n^q|\varphi_b^q\rangle|n-1\rangle)\ , \tag{4}$$

where

$$\tan\theta_n^q(x)\approx\gamma_q(x)\sqrt{n}/\Delta_q\ , \tag{5}$$

$$\Delta_q\equiv(\epsilon_b^q-\epsilon_a^q)-\hbar\omega\ , \tag{6}$$

$$\gamma_q(x)\equiv\left[\frac{2\pi\hbar\omega}{\epsilon L_y}\right]^{1/2}u(x,z_q)\langle\varphi_b^q|-ez|\varphi_a^q\rangle\ . \tag{7}$$

Here, z_q denotes the z coordinate of the QWW q, and $K_k^q(x)$ is the local wave number, which is shifted from k due to the local (i.e., x-dependent) optical Stark shift.[8]

$$K_k^q(x)\approx k\left[1+\frac{\gamma_q(x)^2n/2\Delta_q}{\hbar^2k^2/2m^*}\right]\ . \tag{8}$$

When the electron further proceeds off the interaction region, the interaction is over and each component of $|\Psi\rangle$ *adiabatically* returns to its original form, but with a phase shift

$$\Psi'\rangle=\sum_n a_n e^{\ \ \ \ \ \ }|n\rangle(e^{i\theta_n^N}|\varphi_a^N\rangle+e^{i\theta_n^W}|\varphi_a^W\rangle)/\sqrt{2}\ , \tag{9}$$

where we have dropped the common factor $\exp(ikx-i\epsilon_Ft/\hbar)$, and the phase shifts are given by

$\theta_n^q \approx \zeta_q n$ plus *terms independent of* n, where ζ_q is the *effective coupling constant* given by

$$\zeta_q = \int_{-\infty}^{\infty} dx \frac{\gamma_q(x)^2/\Delta_q}{\hbar^2 k^2/2m^*} \frac{k}{2} . \tag{10}$$

The electron then enters the mode converter, which consists of the crossed QWW's and the thin barrier layer of 50% transmittance (see Fig. 1). Just as the 50% beam splitter for optical fields, the mode converter transforms the electron wave function in Eq. (9) into

$$|\Psi''\rangle = \sum_n a_n e^{-in\omega t} |n\rangle (C_{n,+}|\varphi_+\rangle + C_{n,-}|\varphi_-\rangle) , \tag{11}$$

where φ_+ and φ_- are eigenfunctions of the final two output channels, and, for $\sigma = \pm 1$,

$$C_{n\sigma} = (e^{i(\theta_n^N + \Delta\theta_0/2)} + \sigma e^{i(\theta_n^M - \Delta\theta_0/2)})/2 . \tag{12}$$

Here, $\Delta\theta_0$ is a phase that is determined by the structures of the mode converter. We finally measure the currents of the two output channels: $\hat{J}_\sigma = j_0 |\varphi_\sigma\rangle\langle\varphi_\sigma|$, where j_0 is a constant.

Based upon the above results for the system of optical field plus single electron, we next consider the actual case when many electrons at the Fermi surface travel from the source to the drain regions. To do this, we note that (i) there is no coherence between different electron wave packets emitted from the source region, and (ii) they do not overlap each other for a small source-drain current, such as the one we are treating. In this case, the calculations on the system of optical field plus N traveling electrons become straightforward.[11] Here, N is *not* the total number of electrons in the QWW's, but the number of electrons detected as interference currents during the measurement [see Eq. (17)]. Let us first consider how we can deduce the photon number from the measurements of $J_\pm$. In order to get the maximum sensitivity at $n=0$, let us design the device such that $\Delta\theta_0 = -\pi/2$. In this case, we can define the *readout variable* $\hat{n}_r$ by

$$\sin(g\hat{n}_r) \equiv \frac{\hat{J}_- - \hat{J}_+}{\hat{J}_- + \hat{J}_+} , \tag{13}$$

where $g = \zeta_N - \zeta_M$ is the overall effective coupling constant of the device, and the rhs is well defined because $[\hat{J}_-, \hat{J}_+] = 0$. It can be shown that

$$\langle \sin(g\hat{n}_r) \rangle = \langle \sin(g\hat{n}) \rangle_0 , \tag{14}$$

$$\langle [\delta \sin(g\hat{n}_r)]^2 \rangle = \langle [\delta \sin(g\hat{n})]^2 \rangle_0 + \langle \cos^2(g\hat{n}) \rangle_0 / N , \tag{15}$$

where $\langle \ \rangle_0 \equiv \langle \psi_0 | \ \ | \psi_0 \rangle$ denotes the average over the initial photon-number distribution. Equation (14) ensures that the device works as a photon-number counter. In particular, if $g\langle \hat{n} \rangle \ll 1$, it is reduced to $\langle \hat{n}_r \rangle = \langle \hat{n} \rangle_0$. On the other hand, Eq. (15) is reduced to $\langle \delta\hat{n}_r^2 \rangle = \langle \delta\hat{n}^2 \rangle_0 + \delta n_{\rm err}^2$, where $\delta n_{\rm err}^2$ is the *measurement error*[4-6] (or *quantum noise* in the measurement), which is given by

$$\delta n_{\rm err}^2 = 1/g^2 N . \tag{16}$$

Note that a similar expression for $\delta n_{\rm err}^2$ was obtained for the QND measurement based upon the optical Kerr effect,[5] although the operation principle of such a QND photodetector and that of the present one are very different (for example, in the former one n is conserved *throughout* the measurement[5]). This is because Eq. (16) reflects the general principle of quantum mechanics that many particles in the same state are needed to measure the phase of the particle's wave function. In our case, N is determined by the quantized conductance[1] $e^2/\pi\hbar$ and thus is given by

$$N = e\tau_p N_{\rm dev} V_{\rm SD}/\pi\hbar , \tag{17}$$

where τ_p is the optical-pulse duration or the detection period (in the case of cw optical fields), $V_{\rm SD}$ is the source-drain voltage, and we have assumed that an array of $N_{\rm dev}$ devices are used as a single photodetector. We can make N arbitrarily large by increasing $N_{\rm dev}$ or by confining the optical field in a cavity and thereby making τ_p long, as discussed later. Hence, $\delta n_{\rm err}^2$ can be made arbitrarily small: for example, we can realize $\delta n_{\rm err}^2 < \langle \delta\hat{n}^2 \rangle_0$ when $N > 1/g^2 \langle \delta\hat{n}^2 \rangle_0$. Note also that N itself fluctuates from measurement to measurement at a microscopic level, because the electron emissions from the source region are random processes. This fluctuation, however, is irrelevant to the above results because N is canceled between the numerator and the denominator on the rhs of Eq. (13). Hence, the SNR is better for the present structure than that of Ref. 2.

Let us next consider the final photon states. The final density operator traced over the electron coordinates is evaluated to be

$$\hat{\rho}_{\rm ph}'' = \sum_{n,m} a_m a_n^* e^{i(n-m)\omega t} |m\rangle\langle n| \times (\tfrac{1}{2} e^{i\zeta_N (m-n)} + \tfrac{1}{2} e^{i\zeta_M (m-n)})^N . \tag{18}$$

If the initial photon state is a number state ($a_n = \delta_{n,n_0}$), we can see that the photon wave function is unchanged by the measurement, which means an absence of backactions. For other initial states, the photon wave function must be reduced by measurement (even when it is a QND measurement).[5] However, Eq. (18) tells us that the final photon-number distribution *for the statistical ensemble* is $|a_n|^2$, which is just that of the initial photon state. In particular, $\langle \hat{n} \rangle = \langle \hat{n} \rangle_0$, $\langle \delta\hat{n}^2 \rangle = \langle \delta\hat{n}^2 \rangle_0$. This invariance of the distribution, together with the fact that $\delta n_{\rm err}^2$ can be made sufficiently small, are just those required for general QND measurements.[4-6] On the other hand, the phase of the photon state is randomized through the measurement.[4-7] To see this, we assume a coherent state for the initial state, and evaluate the fluctuation of the cosine operator.[5,11] Then, for $\langle n \rangle \gg 1$ and for $g^2 N \ll 1$, the phase fluctuation of the final photon state is evaluated to be $\langle \delta\phi^2 \rangle = \langle \delta\phi^2 \rangle_0 + \delta\phi_{\rm BA}^2$, where $\delta\phi_{\rm BA}$ is the *backaction phase noise*[1-4] given by

$$\delta\phi_{\rm BA}^2 \approx Ng^2/4 . \tag{19}$$

28

Note that the minimum uncertainty relationship[4-6] holds: $\delta n_{\rm err}^2 \delta\phi_{\rm BA}^2 \approx \frac{1}{4}$.

We finally consider a numerical example. For the same structural parameters as in Ref. 2, the readout [Eq. (14)], which increases with the light intensity I, reaches its maximum value 1 when $I = I_{\rm peak} \simeq 2$ MW/cm^2. If $\tau_p = 10$ ps, this corresponds to 10^6 photons. The resolution is determined by the measurement error, and is given by $I_{\rm peak}/\sqrt{N} \simeq 0.7$ kW/cm^2 for, say, $N = 10^7$. This corresponds to 300 photons, which is smaller than the quantum noise $\sqrt{n}$ of $n = 10^5$ coherent state. To realize $N = 10^7$, we may confine the optical field and thereby make τ_p long, or we may increase $N_{\rm dev}$. For the latter case, for example, we can estimate $N_{\rm dev}$ by noting that $V_{\rm SD}$ should be kept small.[13] When $V_{\rm SD} = 0.1$ mV, we obtain, from Eq. (17), $N_{\rm dev} = 2 \times 10^7$. If we assume a 20×10^6 array of the devices with a 200-Å period, the length of the array in the direction of light propagation is 2 cm, which is much shorter than the interaction length of QND photodetectors based on optical nonlinearities due to virtual transitions.[5,6] In actual experiments, one may measure a highly stabilized optical field in an open cavity,[14] where τ_p can be made large and thus the above large scale integration is unnecessary. Also, the electron interferometer of Fig. 1 can be replaced with other ones such as those proposed in Ref. 15 and Fig. 3 of Ref. 3, which are much easier to fabricate.

In summary, we have analyzed the collision between photons in an arbitrary quantum state, and electrons in a semiconductor microstructure, which constitutes an electron interferometer. By evaluating the time evolution of the coupled photon-electron system, we have shown that the interferometer works as a quantum nondemolition photodetector if it is designed such that the interaction is switched adiabatically. The measurement error $\delta n_{\rm err}$ decreases with N, the number of detected electrons as interference currents, in proportion to $1/\sqrt{N}$. A backaction of the measurement occurs as the increased phase noise $\delta\phi_{\rm BA} (\propto \sqrt{N})$ in the photon state. Here, $\delta n_{\rm err}$ and $\delta\phi_{\rm BA}$ satisfy the *minimum* uncertainty relationship; $\delta n_{\rm err}^2 \delta\phi_{\rm BA}^2 \approx \frac{1}{4}$. Owing to the high efficiency of the photon-electron interaction, the required length is typically as small as 2 cm to achieve $\delta n_{\rm err} < \sqrt{n}$ for $n = 10^5$.

Note added. After the submission of the present paper, there appeared two papers on QND photodetectors by M. Brune *et al.* [Phys. Rev. Lett. **65**, 976 (1990)] and by M. D. Levenson [Phys. Rev. A **42**, 2935 (1990)]. Their operation principles are, in a way, analogous to the present one.

The author acknowledges Professor M. Yamanishi (Hiroshima University), Dr. Y. Yamamoto (NTT), and Professor H. Sakaki (Tokyo University) for fruitful discussions.

---

*Present address: Quantum Wave Project, Research Development Corporation of Japan (JRDC), Keyaki House 302, 4-3-24 Komaba, Meguro-ku, Tokyo 153, Japan.

[1]For a review, see R. Webb and S. Washburn, Phys. Today **41** (12), 46 (1988).

[2]A. Shimizu, K. Fujii, M. Okuda, and M. Yamanishi, Phys. Rev. B **42**, 9248 (1990), and references therein.

[3]The basic idea of this work was previously discussed in A. Shimizu, *International Conference on Quantum Electronics: Technical Digest Series 1990* (Optical Society of America, Washington, D.C., 1990), Vol. 8, p. 96; A. Shimizu, *Abstracts of the Spring Meeting of the Physical Society of Japan* (Physical Society of Japan, Tokyo, 1990), paper no. 2aR7.

[4]V. B. Braginsky, Y. I. Vorontsov, and K. S. Thorne, Science **209**, 547 (1980); C. M. Caves, K. S. Thorne, R. W. P. Drever, V. D. Sandberg, and M. Zimmermann, Rev. Mod. Phys. **52**, 341 (1980).

[5]W. G. Unruh, Phys. Rev. D **18**, 1764 (1978); G. J. Milburn and D. F. Walls, Phys. Rev. A **28**, 2065 (1983); N. Imoto, H. A. Haus, Y. Yamamoto, *ibid.* **32**, 2287 (1985); M. D. Levenson, R. M. Shelby, M. Reid, and D. F. Walls, Phys. Rev. Lett. **57**, 2473 (1986).

[6]B. Yurke, J. Opt. Soc. Am. B **2**, 732 (1985); A. La Porta, R. E. Slusher, and B. Yurke, Phys. Rev. Lett. **62**, 28 (1989).

[7]K. Watanabe, H. Nakano, A. Honold, and Y. Yamamoto, Phys. Rev. Lett. **62**, 2257 (1989).

[8]P. Meystre and M. Sargent III, *Elements of Quantum Optics* (Springer-Verlag, Berlin, 1990).

[9]C. Dewdney *et al.*, Phys. Lett. **102A**, 291 (1984).

[10]H. Schmid (unpublished).

[11]A. Shimizu (unpublished).

[12]Although $[H_I, \hat{n}] = 0$ was claimed as a condition for QND measurements in Ref. 4, it is not a necessary condition as demonstrated by Refs. 6 and 7 and by the present work.

[13]The *central* energies of electron wave packets have a finite distribution with the width of $\sim eV_{\rm SD}$, or, at finite temperature, $\sim k_B T$. This distribution smears the interference currents and also causes additional noises in the currents. For this to be irrelevant, the width should be smaller than the difference of the optical Stark shifts in the two QWW's at $I = I_{\rm peak}$. In our example, this condition is well satisfied if $T < 1$ K and if $V_{\rm SD} < 0.1$ mV. Details will be described elsewhere.

[14]Y. Yamamoto *et al.* (unpublished).

[15]M. Okuda, K. Fujii, and A. Shimizu, Appl. Phys. Lett. **57**, 2231 (1990).

Invited talk to JRDC Int. Symp. Nanostructures & Quantum Effects, 1993
Proceedings, Springer-Verlag (1994)

Quantum Measurement and Fluctuations in Nanostructures

Akira Shimizu

Institute of Physics, University of Tokyo, Komaba, Tokyo 153, Japan
Electronic address: smz@tansei.cc.u-tokyo.ac.jp, Fax: (03) 3467-1281

Abstract. Measurement and fluctuations are closely related to each other in quantum mechanics. This fact is explicitly demonstrated in the case of a quantum non-demolition photodetector which is composed of a double quantum-wire electron interferometer.

1. Introduction

Recent rapid progress of studies on nanostructures is opening up possibilities of new measuring apparatus using nanostructures. For example, a tiny change of the electric charge in a nano-scale region can be detected through a single-electron-tunneling transistor [1]. Another example is a quantum-wire electron interferometer that works as a quantum non-demolition (QND) photodetector, which measures the photon number without absorbing photons [2]. The functions of these nanostructure devices are hardly accessible by conventional devices, thus make nanostructure devices very attractive.

On the other hand, these devices stimulate studies on a very basic problem of physics— what happens when you measure a quantum system? To discuss this problem the nanostructure devices are useful because they allow microscopic analysis of the measuring devices. As a result, we can clarify close relationships among the measurement error, backactions, and fluctuations. I here demonstrate these things by reviewing our studies on the quantum-wire QND photodetector.

2. Quantum-wire QND photodetector

A schematic diagram of the quantum non-demolition (QND) photodetector [2] is shown in Fig.1. Before going to the full analysis in the following sections, I here give an intuitive, semi-classical description [3] of the operation principle.

The device is composed of two quantum wires, N and W. The lowest subband energies (of the z-direction confinement) ϵ_a^N and ϵ_a^W of the wires are the same, but the second levels ϵ_b^N and ϵ_b^W are different. Electrons occupy the lowest levels only. A z-polarized light beam hits the dotted region. The photon energy $\hbar\omega$ is assumed to satisfy $\epsilon_b^W - \epsilon_a^W < \hbar\omega < \epsilon_b^N - \epsilon_a^N$, so that real excitation does not occur and no photons are absorbed. However, the electrons are

excited "virtually" [4], and the electron wavefunction undergoes a phase shift between its amplitudes in the two wires. Since the magnitude of the virtual excitation is proportional to the light intensity [4], so is the phase shift. This phase shift modulates the interference currents, J_+ and J_-. By measuring $J_\pm$, we can know the magnitude of the phase shift, from which we can know the light intensity. Since the light intensity is proportional to the photon number n, we can get information on n. We thus get to know n without photon absorption, i.e., without changing n; hence the name QND [5]. (More accurate definition of QND will be given in section 7.) In contrast, conventional photodetectors drastically alter the photon number by absorbing photons. Keeping this semi-classical argument in mind, let us proceed to a fully-quantum analysis.

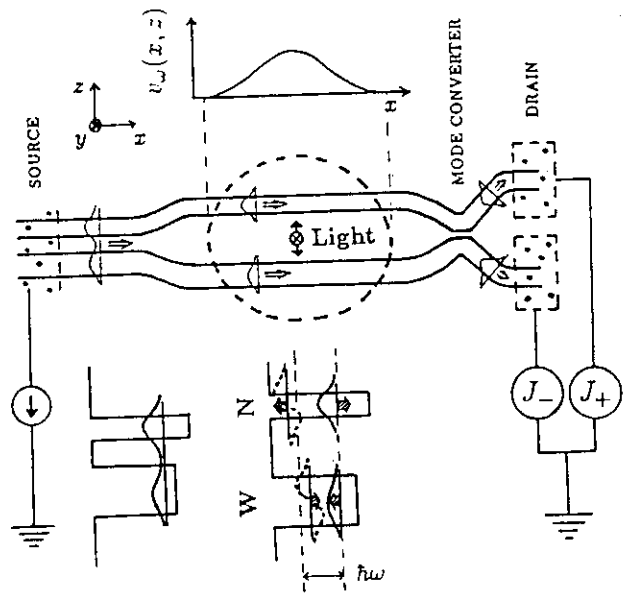

Fig. 1 A quantum non-demolition photodetector composed of a double-quantum wire electron interferometer. (Taken from [2])

3. Quantized light field for a waveguide mode

We assume that the measured light of frequency ω, plane polarized in the z direction, is confined in the x and z directions in a waveguide, propagating in the y direction with the propagation constant β_ω. A normalized mode function

$\mathbf{u}(\mathbf{r})$ then takes the form

$$\mathbf{u}(\mathbf{r}) = (0, 0, u(\mathbf{r})), \quad u(\mathbf{r}) = v_\omega(x, z) \exp(i\beta_\omega y)/\sqrt{L_y}. \tag{1}$$

Here, L_y is a normalization length, and $v_\omega(x, z)$ is the lateral mode function. $u(\mathbf{r})$ is normalized as [6]

$$\int \epsilon |u|^2 d^3\mathbf{r} = 1, \tag{2}$$

where ϵ is the dielectric constant. (The permeability is unity at the optical frequency.) The quantized optical electric field in this mode is expressed as [7]

$$\hat{\mathcal{E}}(\mathbf{r}, t) = \sqrt{2\pi\hbar\omega} \left[\hat{a}\mathbf{u}(\mathbf{r})e^{-i\omega t} + h.c.\right]. \tag{3}$$

The annihilation operator $\hat{a}$ thus defined is the one for a freely propagating waveguide mode. When mirrors are placed at $y = \pm L_y/2$, on the other hand, the measured light is confined in all directions, and $\mathbf{u}(\mathbf{r})$ is then given by a superposition of Eq. (1) with $\pm\beta_\omega$. Using such $\mathbf{u}(\mathbf{r})$ in Eq. (3), we obtain $\hat{a}$ for the confined mode [9], and $\hat{n} \equiv \hat{a}^\dagger\hat{a}$ then defines the photon number *in the confined mode* [7]. We can also treat the case where the measured light takes a wavepacket form, for which the "mode function" is given by a superposition of $\mathbf{u}(\mathbf{r})e^{-i\omega t}$ of Eq. (1) over a narrow range of ω. Replacing $\mathbf{u}(\mathbf{r})e^{-i\omega t}$ with this mode function in Eq. (3), we obtain $\hat{a}$ for the wavepacket mode [9], and $\hat{n} \equiv \hat{a}^\dagger\hat{a}$ then defines the photon number in the wavepacket [7]. In any case, the number state is defined by $\hat{n}|n\rangle = n|n\rangle$, with $n = 0, 1, 2, \ldots$, and any state vector of light in the mode of interest can be expressed as

$$|\psi_{ph}\rangle = \sum_n a_n |n\rangle, \tag{4}$$

which we assume for the state before the measurement.

Either of the above three cases can be treated in a similar manner in the following discussions. However, since equations become slightly complicated in the wavepacket case, we hereafter assume the former two cases.

4. Single quantum-wire structure

Before going to the full analysis, let us consider the simplified case where the light field interacts with a *single* electron which is confined in a *single* quantum-wire structure.

Assuming for simplicity that the confinement potential in the y direction is high enough, we can decompose the y dependence of the electron wavefunction; $\psi_{el}(\mathbf{r}, t) = \psi_{el}(x, z, t)Y(y)$. Hence, we hereafter drop the y-subband eigenfunction $Y(y)$ from equations.

The electron is emitted from the source region, which is in the thermal equilibrium (of zero temperature, for simplicity). Hence, no quantum coherence

exists between the electron and photons before they interact. To describe this fact, it is convenient to consider that the initial ($t = 0$) wavefunction of the electron takes a wavepacket form;

$$\psi_{el}(x, z, t = 0) = e^{ikz} G(x) \varphi_a(z). \tag{5}$$

Here, φ_a is the eigenfunction of the lowest level (which the electron is assumed to occupy) of the z subbands, and G is a localized function. When G does not change appreciably on the scale of the Fermi wavelength, the detailed form of $G(x)$ is irrelevant to the following results. We will therefore use the simplified notation like $|\psi_{el}\rangle = |\varphi_a\rangle$. Combining this with Eq. (4), we write for the initial state vector of the coupled photon-electron system as

$$|\Psi\rangle = |\psi_{ph}\rangle|\psi_{el}\rangle = \sum_n a_n |n\rangle|\varphi_a\rangle. \tag{6}$$

Our task is now to investigate its time evolution — I will present here only the *final* state, i.e., the state after the photon-electron collision.

Let us work in the Schrödinger picture, in which the optical electric-field operator $\hat{\mathcal{E}}(\mathbf{r})$ is given by $\hat{\mathcal{E}}(\mathbf{r}, t = 0)$ of Eq. (3). The Hamiltonian of the *coupled photon-electron system* is given by

$$H = H_{ph} + H_{el} + H_I, \quad H_I = -e\mathbf{r} \cdot \hat{\mathcal{E}}(\mathbf{r}), \tag{7}$$

where H_{ph} and H_{el} denote the free-photon and free-electron Hamiltonians, respectively, and H_I is the photon-electron interaction in the dipole approximation. Since $\mathbf{u}(\mathbf{r})$ varies on the scale of the photon wavelength, $\hat{\mathcal{E}}(\mathbf{r})$ does not vary appreciably on the scale of the electron Fermi wavelength. As a result, H_I induces only an "adiabatic change" in the state vector [2], and we can show that the final state is simply given by [2]

$$|\Psi'\rangle = \sum_n a_n e^{i\theta_n} |n\rangle|\varphi_a\rangle. \tag{8}$$

where

$$\theta_n = \zeta n + \text{terms independent of } n. \tag{9}$$

Here, ζ is an effective coupling constant which is a function of the structural parameters such as the effective mass m^* and the wire width:

$$\zeta = \frac{2\pi\hbar\omega |\langle\varphi_b|ez|\varphi_a\rangle|^2 / \Delta}{\hbar^2 k / m^*} \int_{-\infty}^{\infty} |u(x, y_0, z_0)|^2 dx, \tag{10}$$

where y_0, z_0 denote the center position of the wire (which extends along the x axis), and

$$\Delta \equiv \epsilon_b - \epsilon_a - \hbar\omega \tag{11}$$

is the detuning energy. (ϵ_a and ϵ_b are the first and the second subband energies.)

We see that *the final state acquires n-dependent phase shift*, θ_n. If we could measure θ_n we would be able to know the photon number n. However, for the *single* quantum-wire structure as we are assuming in this section, there is no way to measure θ_n. In the case of $a_n = \delta_{n,n_0}$, for example, θ_{n_0} is the *absolute* phase of the wavefunction, which is not a physical quantity, and thus is unable to observe. We therefore see that we could *not* measure n if we used a *single*-wire structure.

5. Double quantum-wire structure

We now turn to the case of Fig.1; a double-wire structure composed of narrow (N) and wide (W) quantum wires. As before, suppose that an electron wavepacket is emitted from the source. As it proceeds towards the positive x direction, the electron wave is split into two, and the state vector of the coupled photon-electron system becomes

$$|\Psi\rangle = |\psi_{ph}\rangle|\psi_{el}\rangle = \sum_n a_n|n\rangle(|\varphi_a^N\rangle + |\varphi_a^W\rangle)/\sqrt{2}, \tag{12}$$

where $\varphi_a^N(z)$ and $\varphi_a^W(z)$ denote the lowest-subband eigenfunctions of the N and W wires, respectively.

Similarly to Eq. (8), the final state is shown to be [2]

$$|\Psi'\rangle = \sum_n a_n|n\rangle(e^{i\theta_n^N}|\varphi_a^N\rangle + e^{i\theta_n^W}|\varphi_a^W\rangle)/\sqrt{2}. \tag{13}$$

where $\theta_n^{N,W} = \zeta_{N,W}\, n$ + terms independent of n. Here, ζ_N and ζ_W are the effective coupling constants of the N and W wires, respectively, which are given by Eq. (10) with $\phi_{a,b} \to \phi_{a,b}^{N,W}$, $\Delta \to \Delta_{N,W}$, and $y_0, z_0 \to y_0^{N,W}, z_0^{N,W}$.

Unlike the *absolute* phase in Eq. (8), we can measure the *relative* phase $\theta_n^N - \theta_n^W$ in Eq. (13) by the method described in the next section. The relative phase is given by

$$\theta_n^N - \theta_n^W = gn \tag{14}$$

where $g \equiv \zeta_N - \zeta_W$ is an overall effective coupling constant. Since the intersubband transition energy is higher in the N wire than in the W wire, the detuning energies have opposite signs: $\Delta_N > 0$, $\Delta_W < 0$, as seen from Eq. (11). This results in $\zeta_N > 0$, $\zeta_W < 0$, hence $g = |\zeta_N| + |\zeta_W| \neq 0$. (Typically, $\zeta_W \simeq -\zeta_N$, so that $g \simeq 2\zeta_N$.) Measurement of the relative phase thus provides us with the knowledge about n (see Eq. (17) below).

Since $\zeta_N \neq \zeta_W$ (i.e., $g \neq 0$) is essential to the above discussion, we also see that a *double*-wire structure composed of *identical* quantum wires would not work as a photodetector. Hence, the use of *double*-wire structure composed of *non-identical* wires is essential to the present QND photodetector.

6. Measurement of the relative phase

We can measure the relative phase $\theta_n^N - \theta_n^W$ in Eq. (13) by composing an electron interferometer. In Fig.1, a simple interferometer is employed: The two phase-shifted components of Eq. (13) is superposed at the "mode converter", which is composed of a thin barrier of 50 % transmittance. The mode converter plays the same role as the beam splitter does for the optical beam: the input electron waves are superposed, so that the state vector evolves into

$$|\Psi''\rangle = \sum_n a_n |n\rangle (C_{n+}|\varphi_+\rangle + C_{n-}|\varphi_-\rangle), \tag{15}$$

where $|\varphi_\pm\rangle$ are the traveling modes of the two output channels, and

$$C_{n\pm} = [e^{i(\theta_n^N + \theta_0)} \pm e^{i(\theta_n^W - \theta_0)}]/2. \tag{16}$$

Here, the additional phase angle θ_0 is a function of the structural parameters, such as the height and thickness of the barrier, of the mode converter.

We measure the intensities of the output electron waves as the interference currents, J_+ and J_-. Equations (15) and (16) yield

$$\langle J_\pm \rangle \propto \sum_n |a_n|^2 |C_{n\pm}|^2 = \frac{1}{2}\sum_n |a_n|^2 [1 \pm \cos(gn + \theta_0)] = \frac{1}{2}[1 \pm \langle \cos(gn + \theta_0) \rangle]. \tag{17}$$

When the mode converter is designed in such a way that $\theta_0 = -\pi/2$, for example, this relation yields $\langle J_+ \rangle - \langle J_- \rangle \propto \langle \sin gn \rangle$. We can therefore measure n by measuring $J_\pm$.

7. QND property

As we will see in section 9, we need *many* electrons to reduce the measurement error. The many-electron versions of Eqs. (12), (13) and (15) are obtained by taking their Slater determinant for the electron part. (Here, each electron state must of course be different in either of spin, or the center position of the wavepacket, etc.) Since we measure $J_\pm$ of such a many-electron state, the state vector after the measurement is "reduced" to an eigenstate of the many-electron $J_\pm$. (See also section 9.) For the reduced state vector, only the photon part is of our interest. When $N_\pm$ electrons are found in the $\pm$ channels, *the photon state after the measurement* is found to be

$$|\psi''_{ph}(N_+, N_-)\rangle = \left[P(N_+, N_-)/\binom{N}{N_+}\right]^{-1/2} \sum_n a_n (C_{n+})^{N_+} (C_{n-})^{N_-} |n\rangle, \tag{18}$$

where $P(N_+, N_-)$ is the probability of finding $N_\pm$ electrons in the $\pm$ channels (for a given $N = N_+ + N_-$), and is evaluated to be

$$P(N_+, N_-) = \binom{N}{N_+} \sum_n |a_n|^2 |C_{n+}|^{2N_+} |C_{n-}|^{2N_-}. \tag{19}$$

In other words, with the probability of $P(N_+, N_-)$ the post-measurement photon state becomes $|\psi''_{ph}(N_+, N_-)\rangle$. Let us confirm the QND property using these equations.

We first consider the case where the initial photon state is a number state; $|\psi_{ph}\rangle = |n_0\rangle$. Since $a_n = \delta_{n,n_0}$ in this case, we find from Eqs. (18) and (19) that $|\psi''_{ph}(N_+, N_-)\rangle = |n_0\rangle$. That is, when the pre-measurement photon state is a number state, the post-measurement state becomes the *same* number state — no change occurs by the measurement either in the photon number or in the state vector! Hence the name a QND photodetector [5].

We next consider the general case where the initial photon state is given by Eq. (4) with a_n being arbitrary. In this case, the *general* requirement of quantum mechanics *requires* some changes in the state vector. Otherwise, the uncertainty principle, for example, would be broken. (See the next section.) Therefore, even when you use a QND detector the state vector of the measured system must be changed [5, 2, 8]. Indeed, the post-measurement photon state, Eq. (18), is clearly different from the initial state. In particular, the photon-number distribution after the measurement is

$$|\langle n|\psi''_{ph}(N_+, N_-)\rangle|^2 = \frac{|a_n|^2 |C_{n+}|^{2N_+} |C_{n-}|^{2N_-}}{\sum_m |a_m|^2 |C_{m+}|^{2N_+} |C_{m-}|^{2N_-}}, \tag{20}$$

which is *different* from that before the measurement, $|\langle n|\psi_{ph}\rangle|^2 = |a_n|^2$.

However, the unique property of a QND detector can be seen by considering an *ensemble* of many equivalent systems [5, 2, 8] such an ensemble has been very frequently used (either explicitly or implicitly) in discussions on quantum physics [12]. *For each member* in the ensemble, the above equations can be applied. We can therefore calculate the density operator $\hat{\rho}$ of the ensemble as follows. Here, I will present the density operator traced over the electron degrees of freedom, $\hat{\rho}_{ph} = \mathrm{Tr}_{el}[\hat{\rho}]$, which is of our principal interest. Before the measurement, all members have the same state vector of Eq. (4), hence

$$\hat{\rho}_{ph} = \sum_{m,n} a_m a_n^* |m\rangle\langle n|. \tag{21}$$

and the photon-number distribution *over the ensemble*, $\mathrm{Prob}(n)$, is simply given by $\mathrm{Prob}(n) = |a_n|^2$. After the measurement, on the other hand, a member in the state of Eq. (18) is found in the ensemble with the probability of Eq. (19). Therefore, the photon density operator (for a given $N = N_+ + N_-$) becomes

$$\hat{\rho}''_{ph} = \sum_{N_+} P(N_+, N_-) |\psi''_{ph}(N_+, N_-)\rangle\langle\psi''_{ph}(N_+, N_-)|$$

$$= \sum_{n,m} a_m a_n^* |m\rangle\langle n| \left(\frac{1}{2}e^{i\zeta_N(m-n)} + \frac{1}{2}e^{i\zeta_W(m-n)}\right)^N \qquad (22)$$

and the distribution after the measurement is

$$\begin{aligned} \mathrm{Prob}''(n) &= \sum_{N_+} P(N_+, N_-)|\langle n|\psi''_{ph}(N_+, N_-)\rangle|^2 \\ &= \sum_{N_+} \binom{N}{N_+} |a_n|^2 |C_{n+}|^{2N_+} |C_{n-}|^{2N_-} \\ &= |a_n|^2(|C_{n+}|^2 + |C_{n-}|^2) = |a_n|^2, \end{aligned} \qquad (23)$$

where use has been made of Eqs. (16), (19) and (20). We thus find that *the photon-number distribution over the ensemble is unchanged.* In this sense the QND photodetector is said to cause no change in the "statistical distribution" of the photon number, or, to cause no "backaction" on the photon number [5, 2, 8]. In particular, we find from Eq. (23) that the final state has the same average and variance of n as the initial state:

$$\langle n\rangle_{final} = \langle n\rangle_{init}, \quad \langle \delta n^2\rangle_{final} = \langle \delta n^2\rangle_{init}. \qquad (24)$$

This is in a sharp contrast with conventional photodetectors, which drastically alter the photon-number distribution by absorbing photons.

Note that all the above results referred to either the initial or the final state. It can be shown that Prob(n) *does change during the measurement*, i.e., during the photon-electron collision [2, 8]. The absence of change is claimed *only for the post-measurement state*, and *this suffices to claim the QND property* [2, 8]. This is in a sharp contrast with previous QND photodetectors [5], which were claimed to cause no change of Prob(n) *throughout the measurement.* This fact demonstrates that the operation principle of the present QND photodetector is much different from the previous ones. We recently developed a general theory which clarifies the physics of various types of QND measurement [8].

8. Backaction noise generated by the measurement

We have seen that our QND photodetector causes no backaction on the *measured variable* — the photon number n, in the sense of Eqs. (23) and (24). On the other hand, we expect from the uncertainty principle that the detector *must* cause some backaction on the phase ϕ — the conjugate variable of n — of the photon field [5, 2].

To demonstrate this, we consider the case where the initial photon state is a coherent state $|\xi\rangle$, for which

$$a_n = e^{-|\xi|^2/2}\xi^n/\sqrt{n!}, \qquad (25)$$

3F

which yields $\langle n\rangle_{init} = \langle \delta n^2\rangle_{init} = |\xi|^2$, and the phase fluctuations are evaluated to be $\langle \delta\phi^2\rangle_{init} \simeq 1/4|\xi|^2$ for large $|\xi|$ [10]. (In the large-$|\xi|$ limit, in particular, both $\langle \delta n^2\rangle_{init}/(\langle n\rangle_{init})^2$ and $\langle \delta\phi^2\rangle_{init}$ tend to zero, and $|\xi\rangle$ approaches the classical state in which $\hat{a}$ in Eq. (3) is replaced with ξ [10].) It is convenient to introduce "quadrature variables," $\hat{a}_1$ and $\hat{a}_2$, which correspond to the amplitudes of the cosine and sine parts of the optical field [10];

$$\hat{a}_1 \equiv (\hat{a} + \hat{a}^\dagger)/2, \quad \hat{a}_2 \equiv (\hat{a} - \hat{a}^\dagger)/2i. \tag{26}$$

The above fluctuations in n and ϕ are translated into fluctuations of these variables as $\langle \delta a_1^2\rangle_{init} = \langle \delta a_2^2\rangle_{init} = 1/4$. Therefore, in the a_1-a_2 plane a coherent state can be represented as a circular "cloud" [10], which schematically visualizes the fluctuations, as shown in Fig. 2 (a). In this diagram, n corresponds to the square of the radial distance from the origin, and ϕ to the azimuthal angle [10]. Fluctuations in n and ϕ are therefore represented by the spread of the cloud in the radial and azimuthal directions, respectively.

It is instructive to consider first the case of *identical wires*, for which $\zeta_N = \zeta_W$ ($\equiv \zeta$). In this case Eqs. (22) and (25) yield

$$\hat{\rho}''_{ph} = \sum_{n,m} a_m a_n^* e^{iN\zeta(m-n)} |m\rangle\langle n| = |e^{iN\zeta}\xi\rangle\langle e^{iN\zeta}\xi|, \tag{27}$$

where, as before, N denotes the number of colliding electrons. Thus, the identical wires just induce the phase rotation in the parameter ξ, and the final photon state is the same coherent state as the initial state except for this unimportant phase rotation. This is illustrated in Fig. 2 (b) for the case of $N = 1$.

For non-identical wires, on the other hand, $\zeta_N \neq \zeta_W$, and $\hat{\rho}''_{ph}$ can no longer be factorized in such a simple form. In particular, off-diagonal terms, $\langle m|\hat{\rho}''_{ph}|n\rangle$ with $m \neq n$, are significantly reduced with increasing N. This leads to phase randomization because the quantum-mechanical phase is a measure of the off-diagonal coherence. In fact, we can show for large $|\xi|$ that [2]

$$\langle \delta\phi^2\rangle_{final} = \langle \delta\phi^2\rangle_{init} + \delta\phi^2_{BA}, \quad \delta\phi^2_{BA} \simeq Ng^2/4, \tag{28}$$

where, as before, $g \equiv \zeta_N - \zeta_W$. The physical origin of this backaction noise, $\delta\phi^2_{BA}$, is sketched in Fig. 2 (c)-(f), where for simplicity $\zeta_N = -\zeta_W$ ($\equiv \zeta$) is assumed. When one electron collides with the photons, the electron amplitudes in the two wires simultaneously cause rotations of angles $\zeta_N = \zeta$ and $\zeta_W = -\zeta$, as shown in Fig. 2 (c). As a result, the photon state is split into two clouds. When one more electron joins the game, each cloud is again split into two, and the photon state becomes as Fig. 2 (d). Similarly, we get Fig. 2 (e) for $N = 3$, and finally Fig. 2 (f) for large N. This banana-like state is a graphical representation of $\hat{\rho}''_{ph}$, Eq. (22). As compared with the initial state (a), we see that the final state (f) indeed has larger phase fluctuations (which correspond to the azimuthal distribution), while the magnitude of the photon-number fluctuations (the radial distribution) remains the same. Comparison

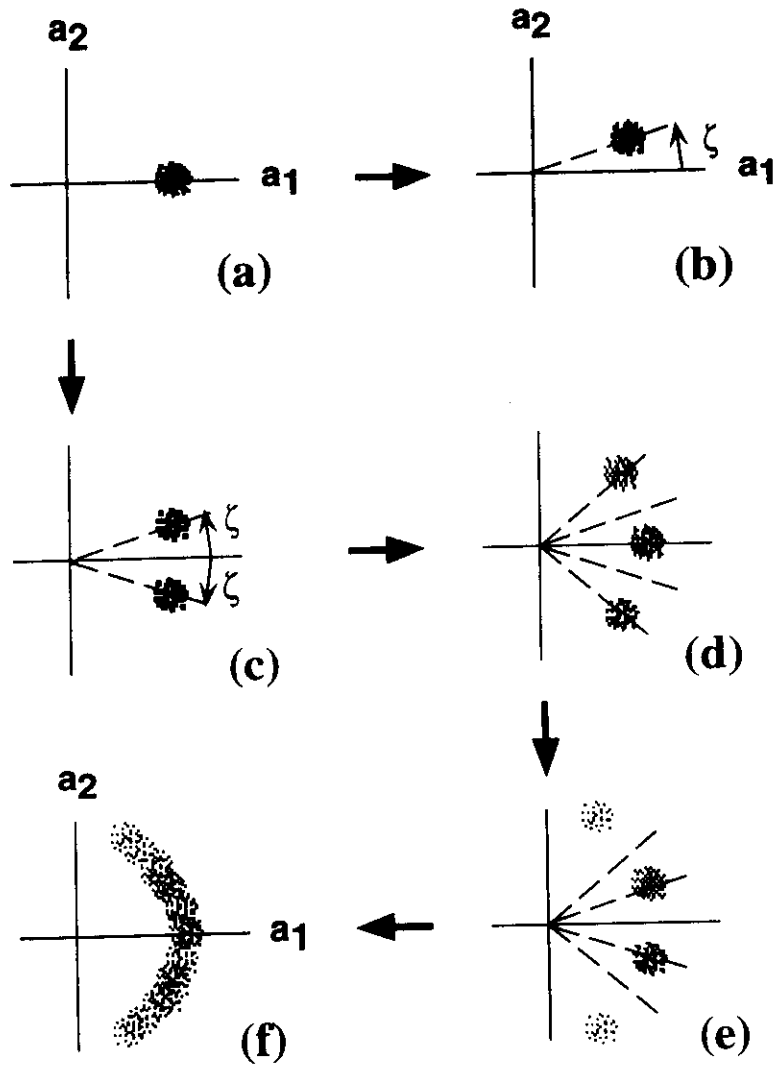

Fig. 2 (a) When the initial photon state is a coherent state, it can be represented as a circular "cloud" in the a_1-a_2 plane. (b) When two quantum wires are identical, the photon state rotates by ζ after the collision with an electron in the wires. (c)-(f) When two quantum wires are non-identical, on the other hand, the photon state is drastically deformed. (c), (d), (e) and (f) represent the photon state after the collision with one, two, three and many electrons, respectively. In (b)-(e) a large value of ζ is assumed in order to make the diagrams vivid, whereas realistic small ζ is assumed in (f).

between (b) and (f) demonstrates that the pair of non-identical wires, for which $\zeta_N \neq \zeta_W$, is the very origin of the backaction noise, $\delta\phi^2_{BA}$.

9. Measurement error

A principal postulate of quantum mechanics is that when "ideal measurement" is performed the state vector of the measured system is reduced to an eigenstate of the measured variable. For photon-number measurement, for example, ideal measurement would lead to the post-measurement density operator of the form,

$$\hat{\rho}_{ph}^{ideal\ meas} = \sum_n |a_n|^2 |n\rangle\langle n|. \tag{29}$$

Actual measuring devices, however, are non-ideal in two points: (i) they would destroy (demolish) the photon state by, say, absorbing photons, and (ii) they have a finite measurement error. Therefore, the density operator (or the state vector) will be reduced to another form. Theory and experiment of such non-ideal measurement have been attracting much attention recently [7, 8, 11].

The present QND photodetector is a good example to understand the physics of non-ideal measurement. Although the QND photodetector does not absorb photons, it may be non-ideal because of a finite measurement error, and the state vector would not be reduced completely. Let us examine this subject, as well as the origin of the measurement error.

Measurement consists of a series of physical interactions which occur among many degrees of freedom in the measured system and the measuring apparatus [12]. In our case, the interactions consist of that between photons and electrons, that between the electrons and ammeters which measure $J_\pm$, that between the ammeters and a recorder which records the values of $J_\pm$, and so on. The key to treat non-ideal measurement is the fact that among these interactions we can (almost always) find an interaction process which can be approximated as ideal measurement— for such a process we can apply the above principal postulate of quantum mechanics, and everything can then be evaluated (at least in principle) [8]. Note that we do not need any additional postulate; *we can treat non-ideal measurement within the standard framework of quantum mechanics* [8].

In our case, we have assumed in section 7 that the measurement of the *electronic current*, $J_\pm$, is ideal. As a result, the state vector of the coupled photon-electron system is reduced to an eigenstate of $J_\pm$. The photon part of the reduced state vector is shown in Eq. (18), and the reduced density operator in Eq. (22). The photon number n is *estimated* from the measured values of $J_\pm$ through Eq. (17). Since we get information on n, the whole process can be called measurement of n. That is, we measure n through ideal measurement of $J_\pm$. This measurement of n is non-ideal because it has a finite measurement error. In fact, since $J_\pm$ are quantum interference currents, they have finite quantum fluctuations [13]–[18], which make the estimation of n ambiguous

[2, 18, 19]. (This is a quite general result for quantum interference devices, as shown in [18, 19].) Namely, the fluctuations of $J_\pm$ give rise to a finite error in measurement of n, and the present QND device works as a ***non-ideal*** measuring device of n. As a result, the post-measurement photon state is ***not completely reduced*** to an eigenstate of n, as explicitly seen from Eq. (22), which shows that $\hat{\rho}''_{ph} \neq \hat{\rho}_{ph}^{ideal\ meas}$ for finite N.

As N is increased $\hat{\rho}''_{ph}$ approaches $\hat{\rho}_{ph}^{ideal\ meas}$. We thus expect that the measurement error decreases with increasing N. This is indeed the case; the measurement error is evaluated to be [2]

$$\delta n_{err}^2 = 1/g^2 N. \tag{30}$$

This result can be understood as follows. As the effective coupling g is increased, the flow of information from the light field to the electrons is increased, hence $\delta n_{err}^2 \propto 1/g^2$. On the other hand, we get to know the photon number by measuring the electron phase shift. To measure the phase shift, however, we need many electrons because of the number-phase uncertainty principle (of electron waves) [13, 18]. This results in $\delta n_{err}^2 \propto 1/N$. It was shown in Refs. [18] that similar discussions can be applied to most quantum interference devices, and their fundamental limits have been derived [19].

Interestingly, if we multiply δn_{err}^2 by the backaction noise $\delta\phi_{BA}^2$, Eq. (28), we get a constant; $\delta n_{err}^2 \delta\phi_{BA}^2 \simeq 1/4$, whereas the number-phase uncertainty principle (of a light field) gives $\delta n_{err}^2 \delta\phi_{BA}^2 \geq 1/4$ [10]. This means that the present device is a very effective measuring device in the sense that it extracts the information on the measured variable n with the minimum cost of the backaction noise in the conjugate variable ϕ.

10. Summary

I have analyzed a quantum non-demolition (QND) photodetector composed of a double quantum-wire electron interferometer, which measures the photon number n without absorbing photons (more precisely, without changing distribution of n). It is shown that (i) If we used an *single*-wire structure, or if we used a double-wire structure composed of two *identical* wires, we could not get information on the photon number. It is therefore essential to use a double-wire structure composed of *non-identical* wires. (ii) Such a double-wire structure, on the other hand, is the very origin of the backaction noise, which appears as an increase of quantum fluctuations of the *phase* of the light field. (iii) The QND photodetector works as a *non-ideal* measuring device because it has a finite measurement error. As a result, the photon state is not completely reduced to an eigenstate of n. (iv) The measurement error, δn_{err}^2, comes from quantum fluctuations of electrical currents in the interferometer. Because of this fluctuation, we need many electrons to measure the phase shift which is induced by the light field. As a result, $\delta n_{err}^2 \propto 1/N$, where N denotes the number of colliding electrons. (v) The error is also inversely proportional to an effective

49

coupling constant g^2 between photons and electrons. The coupling constant is a function of the structural parameters of the quantum wires. (vi) The measurement error and the backaction noise is closely related: $\delta n^2_{err}\delta\phi^2_{BA} \simeq 1/4$. Namely, the backaction noise is proportional to Ng^2 and is also a function (through g^2) of the structural parameters of the wires.

These results demonstrate close relationships between measurement and fluctuations, and not only shed light on the physics of quantum measurement, but also suggest fundamental limitations and possibilities of nanostructure devices.

References

[1] K. K. Likharev, IBM J. Res. Develop. **32**, 144 (1988).

[2] A. Shimizu, Phys. Rev. **A43**, 3819 (1991); A. Shimizu (unpublished).

[3] A. Shimizu, K. Fujii, M. Okuda and M. Yamanishi, Phys. Rev. **B42**, 9248 (1990).

[4] For virtual excitation, see, e.g., B.S. Wherrett, A.C. Walker, and F.A.P. Tooley, *Optical Nonlinearities and Instabilities in Semiconductors*, ed. by H. Haug, (Academic, 1988), Chap.10, Sec.2.

[5] W.G. Unruh, Phys. Rev. **D18**, 1764 (1978); V.B. Braginsky et al., Science **209**, 547 (1980); C.M. Caves et al., Rev. Mod. Phys. **52**, 341 (1980); G.J. Milburn and D.F. Walls, Phys. Rev. **A28**, 2065 (1983); N. Imoto, H.A. Haus, Y. Yamamoto, Phys. Rev. **A32**, 2287 (1985).

[6] See, e.g., R.J. Glauber and M. Lewnstein, Phys. Rev. **A43**, 467 (1991), and references therein.

[7] See, e.g., C.W. Gardiner, *Quantum Noise* (Springer-Verlag, Berlin, 1991). Note that this reference uses SI units, whereas the present paper is working in cgs Gauss units.

[8] A. Shimizu and K. Fujita, *Quantum Control and Measurement* (H. Ezawa and Y. Murayama, eds., Elsevier, 1993), p.191.

[9] More precisely, the relation between the old and new $\hat{a}$'s are expressed as a unitary transformation, and the commutation relations are preserved.

[10] D.F. Walls, nature **306**, 141 (1983); R. Loudon, *The quantum theory of light*, 2nd ed. (Oxford Univ. Press, 1983);

[11] M. Ueda and M. Kitagawa, Phys. Rev. Lett. **68**, 3424 (1992).

[12] J. von Neumann, *Die Mathematishe Grundlangen der Quantenmechanik*, Springer-Verlag, Berlin, 1932.

[13] B. Yurke, S.L. McCall and J.R. Klauder, Phys. Rev. **A33** (1986) 4033; M. Kitagawa and M. Ueda, Phys, Rev, Lett. **67** (1991) 1852.

[14] M.P Silverman: Nuovo Cimento **97**, 200 (1987) ; Phys. Lett. **A120**, 442 (1987); Physica **B151**, 291 (1988).

42

[15] Y.P. Li, D.C. Tsui, J.J. Hermans, J.A. Simmons and G. Weimann, Appl. Phys. Lett. **57**, 774 (1990).

[16] V. A. Khlus, Sov. Phys. JETP **66**, 1243 (1987); G. B. Lesovik, JETP Lett. **49**, 592 (1989); B. Yurke and G. P. Kochanski, Phys. Rev. **B41**, 8184 (1990). M. Büttiker, Phys. Rev. Lett. **65**, 2901 (1990); M. Ueda and A. Shimizu, J. Phys. Soc. Jpn. **62**, 2994 (1993).

[17] A. Shimizu and M. Ueda, Phys. Rev. Lett. **69**, 1403 (1992); A. Shimizu, M. Ueda and H. Sakaki: Proc. 4th Int. Symp. Foundations of Quantum Mechanics (Tokyo, 1992), p.189 (JJAP Series 9, 1993).

[18] A. Shimizu and H. Sakaki, Phys. Rev. **B44**, 13136 (1991).

[19] Reference [18] assumed that the coherence length in reservoirs, ℓ_c^{res}, is short, whereas Refs. [16] assumed that ℓ_c^{res} is long (which was implicitly assumed by assuming the perfect Fermi distribution in reservoirs.) The noise formula in the general case, which interpolates between the two limiting cases, was given in Eq. (21) of Ref. [17], which shows that finite ℓ_c^{res} induces an "emission noise" in addition to the "granularity noise" derived in [16]. However, conserning the fundamental limits of quantum interference devices, which were derived in [18], the limits depend only on the granularity noise, hence *apply to any case* irrespective of the length of ℓ_c^{res}. To break the limits, one must resort to well-designed many-body correlations among electrons, as discussed in [13].

Photon-Energy Dissipation Caused by an External Electric Circuit in "Virtual" Photoexcitation Processes

Akira Shimizu*
Institute of Physics, University of Tokyo, 3-8-1 Komaba, Tokyo 153, Japan

Masamichi Yamanishi
Department of Physical Electronics, Hiroshima University, Higashi-hiroshima 724, Japan
(Received 27 December 1993)

We consider generation of an electrical pulse by an optical pulse in the "virtual excitation" regime. The electronic system, which is any electro-optic material including a quantum well structure biased by a dc electric field, is assumed to be coupled to an external circuit. It is found that the photon *frequency* is subject to an extra redshift in addition to the usual self-phase modulation, whereas the photon *number* is conserved. The Joule energy consumed in the external circuit is supplied only from the extra redshift.

PACS numbers: 42.65.Vh, 03.65.Bz, 78.66.–w

Virtual excitation of electronic systems by optical fields has been attracting much attention recently [1–5]. Here, "virtual" means roughly that the photon energy is lower than the absorption edge by some detuning energy Δ, so that photon absorption does not take place. More precisely, it means that the excitation takes place *adiabatically* so that no real transitions occur and the quantum-mechanical coherence is preserved. For a simple two-level system (with a long dephasing time), for example, the excitation will be virtual if

$$(T_{\rm tr}/\hbar)^2 \gg (\mu\mathcal{E}/\Delta^2)^2, \tag{1}$$

where $T_{\rm tr}$ is the transient time for which the envelope of the optical pulse changes appreciably, μ denotes the transition dipole moment of the two-level system, and $\mathcal{E}$ is the envelope of the electric-field amplitude of the optical pulse. The concept of the virtual excitation has been widely used, for example, to describe ultrafast nonlinear optical responses [1–5]. It was also shown that "quantum nondemolition" (QND) measurement of the photon number N (i.e., measurement of N without changing its statistical distribution) is possible by the use of the virtual excitation of an electron interferometer [6].

On the other hand, many studies have recently been devoted to generation of an electrical pulse by excitation of a material by a short optical pulse [2–5,7]. For the material, we can basically use any materials which possess finite electro-optic (EO) coefficient, $\chi^{(2)} \equiv \chi^{(2)}(0;-\omega,\omega)$. Of particular interest is a quantum well structure (QWS) biased by a dc electric field [2,3]. The dc field is applied to induce large $\chi^{(2)}$, which results in high efficiency for the generation of an electrical pulse. In particular, it was suggested that the ultrafast response would be obtained by working in the "virtual excitation" regime [2,3]. However, present understanding seems quite insufficient to investigate such a fancy combination of the idea of the electrical-pulse generation with the concept of the virtual excitation.

In this paper, we raise and answer the following fundamental questions on the electrical-pulse generation by virtual photoexcitation: (i) What is the state of the optical pulse after it passes through the EO material? In particular, what is the photon energy and photon number? (ii) What role is played by the external electric circuit in determining the photon state? (iii) When the material is a biased QWS, what supplies the energy to the electrical pulse—an external battery (which induces the dc bias field) or the optical field? (iv) Is it possible to perform QND measurement by monitoring the generated electrical pulse?

Let us start with a biased QWS. We suppose that metallic contacts are deposited on both sides of a QWS sample in order to apply the static bias field F_0 (>0) by an external battery V_0 (Fig. 1). The sample thus works as a capacitor, whose capacitance is $\epsilon L \equiv C_0$, where ϵ denotes the linear dielectric constant at low frequencies. Exciton states of the QWS are strongly deformed by F_0, and each exciton acquires a large *static* dipole moment, l [2,3].

It is convenient to describe the exciton dynamics *in terms of such deformed states*. If, for simplicity, we look at the lowest-exciton state only, an effective Hamiltonian in the optical field, $\mathcal{E}\cos\omega t$, may then be written as [8]

$$H = \varepsilon_x a^\dagger a - \mu(a^\dagger + a)\mathcal{E}\cos\omega t - l(F_P + F_1)a^\dagger a, \tag{2}$$

where $a^\dagger$ (a) and ε_x denote the creation (annihilation) operator and the energy, respectively, of the deformed exciton state. When the detuning energy $\Delta \equiv \varepsilon_x - \hbar\omega$ satisfies Eq. (1), the optical field virtually excites the deformed excitons, which induce the static electric field $F_P = -l\langle a^\dagger a\rangle/\epsilon_0$ [9], which is nonzero (<0) only in the well region [2,3]. Since l is large ($= 10^{(1-2)}$ eÅ), $|F_P|$ becomes large, which results in a large EO coefficient $\chi^{(2)}$ [2–5]. On the other hand, to cancel out F_P, current J is induced which alters the surface charge density of the metallic contacts from the equilibrium value $\sigma_0 \equiv \epsilon F_0$

0031-9007/94/72(21)/3343(4)$06.00

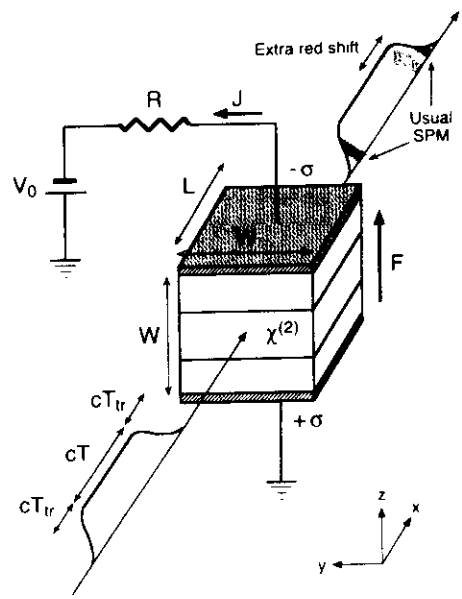

FIG. 1. A schematic diagram of the system under consideration. An optical pulse goes into a capacitor, the center region of which is made of a biased QWS or another EO material. An electrical pulse is generated in the center region, and the current J flows in the external circuit. We find that the optical pulse, after it passes through the capacitor, is subject to an extra redshift, in addition to the usual self-phase modulation which occurs in the initial and final transients.

into $\sigma = \sigma_0 + \sigma_1$, and σ_1 generates the canceling field $F_1 = \sigma_1/\epsilon$. Therefore, the total dc field in the QWS is $F = F_0 + F_P\Theta(z) + F_1$, where Θ is a unit step function which is nonzero only in the well region. The equation of motion of σ_1 may thus be

$$\frac{d\sigma_1}{dt} = -\frac{\sigma_1}{C_0R} - \kappa\frac{F_P}{RL}, \tag{3}$$

where $\kappa \equiv$ well thickness$/W$. The models of the previous work [2,3], which assumed the absence of the external circuit, correspond to the limit of $R \to \infty$ of our model.

It is seen that the optical field $\mathcal{E}$ interacts with the quantum-mechanical excitonic variables a, $a^\dagger$ via the μ term in Eq. (2), and the excitonic variables interact with the classical surface charge σ_1 via the F_P and F_1 terms in Eqs. (2) and (3). The interesting point here is that *only* the motion of σ_1 suffers explicit dissipation [due to the C_0R term in Eq. (3)]. We will show below that this dissipation eventually causes, through a chain of interactions, energy dissipation in the optical field.

We first note that F_0 has not appeared explicitly in Eqs. (2) and (3): all effects of F_0 have been incorporated only in the deformed exciton state which defines a, $a^\dagger$, μ, and l. Consequently, the external battery which produces F_0 supplies *no* net energy: the Joule energy RJ^2 must be supplied by something else—the only possible supplier is the optical field. The role of the battery (and F_0) is just to produce large $\chi^{(2)}$. The absence of energy supply from the battery will be confirmed also in the following calculations.

We are interested in the evolution of the optical field and energy flow. We here evaluate them to $O(\mathcal{E}^2)$, because the analysis [10] which includes the third-order nonlinear effects shows that the second-order effects are essential [11]. We also found [10] that concerning the quantities which we will discuss below the microscopic model of Eq. (2) gives the same results as a phenomenological model in which the excitonic (or electronic) system is phenomenologically treated as a transparent EO material. The only difference is that in the former model $\chi^{(2)}$ is obtained by solving Eq. (2), whereas in the latter $\chi^{(2)}$ is a given parameter. The phenomenological model is therefore applicable to any transparent EO materials including the biased QWS. For this reason, we hereafter present our results in the language of the phenomenological model: for example, F_P is now

$$F_P = -(\epsilon_0/\epsilon)\chi^{(2)}\mathcal{E}^2, \tag{4}$$

where $\chi^{(2)}$ is, as in the case of the biased QWS, the value of $\chi^{(2)}$ *in the presence of* F_0.

To avoid inessential complexities, we assume that the light intensity is almost constant over the cross section of the optical beam, and also that the cross section agrees with that $(W \times W)$ of the capacitor. In the propagating direction x, the optical pulse is assumed to have a portion (of length cT) of constant intensity in between the initial and final transient portions of length cT_{tr}. To focus on new phenomena only, we assume that $T_{tr} \ll C_0R,\ T$; under this condition σ does not change during the transients and thus what happens in the optical field of the transient portions is just the usual self-phase modulation, which is well known and of no interest here. We therefore focus on the constant-intensity portion, and take $t = 0$ as the time at which that portion begins to enter the capacitor. We further assume, for simplicity, that $L \ll cT/n$ (i.e., $\mathcal{E} \approx$ const in the capacitor), where L is the length of the capacitor, c the light velocity in vacuum, and n the refractive index.

Under these conditions, Eq. (3) can be easily solved to give

$$\sigma_1 = \begin{cases} \kappa\epsilon|F_P|(1 - e^{\frac{-t}{C_0R}}) & (0 \le t \le T), \\ \kappa\epsilon|F_P|(1 - e^{\frac{-T}{C_0R}})e^{\frac{T-t}{C_0R}} & (T < t), \end{cases} \tag{5}$$

where F_P is given by Eq. (4), and κ is now $\kappa \equiv$ (thickness of the EO material)$/W$. Associated with the time varying σ_1 is the current $J = \frac{\partial}{\partial t}WL\sigma_1$, which generates the Joule heat in the resistance R [12];

$$U_R = \int_{-\infty}^{\infty} RJ^2dt$$
$$= (\kappa WL\epsilon_0\chi^{(2)}\mathcal{E}^2)^2(1 - e^{-T/C_0R})/C_0. \tag{6}$$

Let us find out the supplier of this energy—the battery or the optical field? The work done by the battery is

$$U_{V_0} = \int_{-\infty}^{\infty} V_0 J dt = V_0 W L[\sigma_1(\infty) - \sigma_1(0)], \quad (7)$$

which is zero because, as seen from Eq. (5), $\sigma_1(\infty) = \sigma_1(0) = 0$. That is, the battery does not supply net energy at all, in agreement with the observation we have drawn above from the microscopic model. Therefore, the only possible supplier of the Joule energy is the optical field, the evolution of which we will investigate now.

We note that the dc field F in the EO material varies from F_0 (for $t < -T_{\rm tr}$) to $F_0 + F_P + F_1$ (for $0 \le t \le T$) and then to $F_0 + F_1$ (for $T + T_{\rm tr} < t$), where $F_1 = \sigma_1/\epsilon$ also varies according to Eq. (5). The time-dependent F produces the time-dependent change of the refractive index n:

$$\delta n = \chi^{(2)}(\omega;\omega,0)(F - F_0)/2n, \quad (8)$$

where n and $\chi^{(2)}(\omega;\omega,0)$ denote their values *in the presence of* F_0. With the help of the symmetric relation, $\chi^{(2)}(\omega;\omega,0) = 4\chi^{(2)}(0;-\omega,\omega)$, Eqs. (5) and (8) yield, for $0 \le t \le T$,

$$\delta n = -(2\epsilon_0/n\epsilon)|\chi^{(2)}|^2\mathcal{E}^2[1 - \kappa(1 - e^{-t/C_0R})]. \quad (9)$$

By this time-dependent δn, the optical field undergoes a frequency shift (chirping) [10]. When $L \ll C_0Rc/n$, the shift is simply given by

$$\delta\omega = -\frac{\partial}{\partial t}\frac{\omega L\kappa\delta n}{c} = -\frac{2\epsilon_0\omega\kappa^2|\chi^{(2)}|^2\mathcal{E}^2 L}{n\epsilon c C_0 R}e^{-t/C_0R}. \quad (10)$$

Here κ in the first line has appeared because δn is large only in the EO material.

We find that (i) the optical field undergoes a redshift, (ii) the shift approaches zero in both limits of $R \to \infty$ and $R \to 0$, and (iii) the shift becomes maximum at the beginning ($0 \le t \ll C_0R$) of the constant-intensity portion of the optical pulse, and decays exponentially after that.

This shift is a kind of a self-phase modulation (SPM) process in the sense that the shift is driven by the optical field *itself*. However, it is totally different from the *usual* SPM, which generally occurs when an optical pulse passes through a nonlinear medium. To distinguish between the two, we hereafter call the shift of Eq. (10) the "extra shift" or "extra redshift." Major differences are as follows: (a) In contrast to Eq. (10), the usual SPM is basically independent of the external circuit—it occurs, for example, even when $R \to \infty$. (b) The *total* energy of the optical pulse is conserved in the usual SPM process (because the frequency shifts occur in the opposite directions at the initial and final transients), whereas the extra shift results in loss of the total energy [Eq. (11) below]. (c) The usual SPM is approximately instantaneous (delay $\approx$ response time of nonlinear processes), whereas the extra shift occurs with a considerable delay ($\sim C_0R$)—the shift takes place during $0 \lesssim t \lesssim C_0R$ in order to compensate for F_P which is established at $t = 0$. These differences arise because the extra shift is a property of the *coupled* system of a nonlinear EO material and an external electric circuit, whereas the usual SPM is a property of a nonlinear material only.

In terms of the microscopic model, the physics of the extra shift may be understood as follows: Photons (virtually) excite excitons of energy $\varepsilon_x - l(F_P + F_1)$, and the excited excitons will emit photons subsequently. Here, the energy of the excitons is decreasing as t goes by because $F_1 = \sigma_1/\epsilon$ is increasing according to Eq. (5). As a result, the emitted photons have lower energies than the (virtually) absorbed photons. Hence the redshift and its magnitude decay exponentially with the same decay constant as that of σ_1.

The magnitude of the extra shift, Eq. (10), depends on many material and structural parameters. For example, for a (100-Å well)/(100-Å barrier) multiple quantum well structure for which $\kappa \approx 1/2$, the redshift is estimated to be of the order of 10^2L MHz when $I \sim 10^2$ MW/cm^2, $F_0 \sim 10^2$ kV/cm, $T \sim C_0R \sim 1$ ps, $\Delta = 10$ meV, and L here is measured in μm,

Our next task is to find out the energy flow. To do this, we for the moment assume that the photon number is conserved (this assumption will be justified soon). In this case, the loss of the light intensity $I = \epsilon_0 cn\mathcal{E}^2/2$ is given by $\delta I = I\delta\omega/\omega$. Therefore, the loss of the total photon energy due to the extra redshift is

$$U_{\rm ERS} = \int_0^T |W^2\delta I|\, dt = W^2 I L\kappa[\delta n(0) - \delta n(T)]/c. \quad (11)$$

Inserting Eq. (9) and $C_0 = \epsilon L$, and comparing with Eq. (6), we find that $U_{\rm ERS} = U_R$. Therefore, *all the Joule energy is supplied by the extra redshift of the optical field.* It also shows that *the photon number N is conserved*, because if it were lost then $U_{\rm ERS} < U_R$. This indicates that the present photon-energy dissipation *cannot be described as a simple dephasing process*, which is accompanied by loss of N.

We have thus found that when an optical pulse excites the electronic system of Fig. 1 "virtually" [in the sense that Eq. (1) is satisfied] then the final state of the optical pulse has the *same* number of photons as the initial state. However, the frequencies of photons are lowered, which are consumed to generate the Joule heat in the external circuit. This is in a marked contrast to the virtual photoexcitation of an electron interferometer which was discussed in [6], where it was shown that *both* the number and frequencies of photons are conserved. Since we can estimate the photon number N by measuring the interference currents, the electron interferometer works as a QND photodetector [6]. We can estimate n also in the present case by, say, monitoring the voltage drop

46

across the resistance. Can we call it QND measurement? The answer clearly depends on the definition of the QND measurement. Kitagawa [13] proposed to accept it as QND measurement in a broad sense. To perform QND measurement in the narrow sense (i.e., both N and frequencies are conserved), one may use the scheme of Ref. [4], in which the generated voltage modulates an electron interference current in an electrostatic Aharonov-Bohm interferometer.

We have thus found that when you try to get information on photons through virtual photoexcitation of an electronic system, the photon energy will or will not be conserved depending on the detailed structures of the electronic system *and* the external circuit (although the circuit is *not* directly connected to the optical field). These findings shed light on the theory of measurement of photons using electronic systems.

Finally, let us comment on the case in which the external circuit of Fig. 1 is a transmission line or something like that, which has a complex impedance Z rather than the pure resistance R. The extension of the present theory to such a general case is straightforward—all we have to do is to modify the last term of Eq. (3). We would then observe, for example, that the extra shift would exhibit an oscillatory behavior which is superposed on the exponential decay. However, the main conclusions do not change because, for example, the irrelevance of the battery in the energy consumption processes relies on the fact that F_0 does not appear explicitly in Eqs. (2) and (3)—this fact remains true when we modify the last term of Eq. (3). For this reason, we believe that the present paper has revealed bare essentials of the electrical-pulse generation by the virtual photoexcitation.

To summarize, we have considered electrical-pulse generation in the "virtual excitation" regime. The electronic system is any electro-optic material including a quantum well structure biased by a dc electric field, which is applied to induce large $\chi^{(2)}$. The energy transfer is analyzed when the electronic system is coupled to an external circuit. It is found that the photon *frequency* is subject to an extra redshift in addition to the usual self-phase modulation, whereas the photon *number* is conserved. The extra redshift approaches zero in both limits of zero and infinite impedance of the circuit. It is also shown that an external battery, which produces the dc bias field in the QWS, supplies *no* net energy, and the Joule energy consumed in the external circuit is supplied only from the extra redshift of the optical field.

* Electronic address: smz@tansei.cc.u-tokyo.ac.jp

[1] For a review, see, e.g., papers in *Optical Nonlinearities and Instabilities in Semiconductors*, edited by H. Haug (Academic Press, Boston, 1988).

[2] M. Yamanishi, Phys. Rev. Lett. **59**, 1014 (1987).

[3] D. S. Chemla, D. A. B. Miller, and S. Schmitt-Rink, Phys. Rev. Lett. **59**, 1018 (1987).

[4] M. Yamanishi, K. Kurosaki, Y. Osaka, and S. Datta, in *Proceedings of the Sixth International Conference Ultrafast Phenomena*, edited by T. Yajima *et al.* (Springer-Verlag, Berlin, 1988), p. 334.

[5] E. Yablonovitchi, J. P. Heritage, D. E. Aspnes, and Y. Yafet, Phys. Rev. Lett. **63**, 976 (1989). They showed that $\chi^{(2)} = \chi^{(3)}(0;0,-\omega,\omega)F_0$ is larger in a bulk crystal than in a QWS. However, this relation is valid only for small F_0: in F_0 of the order of 10^2 kV/cm a QWS has larger $\chi^{(2)}$.

[6] A. Shimizu, Phys. Rev. A **43**, 3819 (1991).

[7] D. H. Auston, K. P. Cheung, J. A. Valdmanis, and D. A. Kleinman, Phys. Rev. Lett. **53**, 1555 (1984); H. G. Roskos, M. C. Nuss, J. Shah, K. Lee, D. A. B. Miller, A. M. Fox, S. Schmitt-Rink, and K. Kohler, *ibid.* **68**, 2216 (1992); X.-C. Zhang, Y. Jin, K. Yang, and L. J. Schowalter, *ibid.* **69**, 2303 (1992); P. C. M. Planken, M. C. Nuss, I. Brener, K. W. Goossen, M. S. C. Luo, S. L. Chuang, and L. Pfeiffer, *ibid.* **69**, 3800 (1992).

[8] Neither the multilevel effect nor the exciton-exciton interaction alter the main conclusions of the present paper.

[9] We are working in the SI units, and ϵ_0 denotes the vacuum dielectric constant.

[10] M. Yamanishi, S. Kodama, and A. Shimizu (unpublished).

[11] The third-order effects, for example, modify the decay constant C_0R in Eqs. (5)–(11). This, however, does not alter the main conclusions such as $U_R = U_{ERS}$ and $U_{V_0} = 0$.

[12] We include in R the internal resistance of the external battery.

[13] M. Kitagawa (unpublished).